Engineering of Microbial Fuel Cells technology: Materials, Modelling and Architecture

(Article begins on next page)

04 August 2020

Doctoral Dissertation
Doctoral Program in Electronic Engineering (29th Cycle)

Engineering of Microbial Fuel Cells technology: Materials, Modelling and Architecture

By

Matteo Gerosa

Supervisor:
Prof. C.F. Pirri

Doctoral Examination Committee:
Prof. Sabato D'Auria, CNR Centro ISA, Salerno
Prof.ssa Silvia Giordani, IIT Central Research Lab, Genova
Prof.ssa Federica Cappelluti, Politecnico di Torino, Torino
Prof. Simone Marasso, CNR IMEM, Parma
Prof.ssa Elena Maria Tresso, Politecnico di Torino, Torino

Politecnico di Torino
2016

Declaration

I hereby declare that, the contents and organization of this dissertation constitute my own original work and does not compromise in any way the rights of third parties, including those relating to the security of personal data.

Matteo Gerosa

2016

* This dissertation is presented in partial fulfillment of the requirements for **Ph.D. degree** in the Graduate School of Politecnico di Torino (ScuDo).

La magia è credere in noi stessi.

Se riusciamo a farlo, allora possiamo far accadere qualsiasi cosa.

J.W. von Goethe

Acknowledgment

At the end of this hard work, I would like to thank everyone who helped me in writing this thesis.

First of all, I'd desire to thank Prof. Pirri, that allowed me to perform the PhD career. I must say a big thank you also to all the IIT research group (Marzia, Gian Paolo, Giulia, Adriano, Nadia, Valentina, Valeria, Simona, Stefano, Angelica and Micaela) that followed me in my activity and allowed the "happy ending" of this long work.

This work has never been the same also without my "break's friends", especially Michela, Giulia e Alain, with whom I spent together many breaks, lunches and laughs;

A special thank goes to my special friend Giulia, that was always present in every moment.

The last important thank goes to my wife Elena, who has always been by my side and agreed to spend our life together.

Without all these important aids, the last three years would not have been possible. For this reason, a big thanks to everybody!

Abstract

A Microbial fuel cell (MFC) is a bio-electrochemical reactor, able to convert chemical energy, contained in organic substrate, in electrical energy, thanks to the metabolic activity of microorganisms.

Firstly, a fluid-dynamic modelling of different Microbial Fuel Cell configurations to study trajectories and concentration profile of the liquid containing the organic substrate during operation of the device was developed. The study of the device was joined with the study and the synthesis of carbon based aerogels to be used as new electrode materials, both for the anode and the cathode.

The aim of the modelling was to understand what happen, from a fluid-dynamic point of view, inside the cell during operation. It was based on the application of equations from fluid-dynamics in order to study both the particle trajectories (using Navier-Stokes equations) and diffusion of substrate inside the reactor (using Fick's laws).

Three different MFC architecture were investigated, starting from a circular shape. To increase the area of the reactor interested by flux exchange with respect to the one in the circular configuration, a new a squared MFC, with a non-alignment of the inlet and the outlet was proposed.

Starting from results obtained during the simulation for the squared reactor, to accommodate the flux distribution, a further improvement in architecture was introduced: a drop-shape MFC, with a percentage of fluid area exchanged, higher than 96%.

Another possibility to improve MFC performances, is the optimization of materials used as electrodes. To be an efficient electrode, a material must satisfy some important

condition: biocompatibility, good electrically conductivity, resistance to electrolytic solutions and high surface area together with high porosity to allow the formation of the biofilm. Carbon based aerogels can satisfy all these properties.

Organic aerogels were synthetized following a green approach, starting from marine polysaccharides, like agar and starch and then transformed in carbon based, thanks to a thermal process. The synthesis procedure is the sol-gel technique, followed by a drying process that can extract the liquid part of the gel, leaving the solid structure, without collapse the material. Synthetized materials were analyzed both structurally and morphologically in order to understand if porosity, surface area and chemical composition were appropriate. To enhance some of these properties, a post synthesis treatment was performed: the surface of the aerogel was treated with a KOH solution in order to enlarge pores and increase the porosity of the overall material. The optimized aerogel was tested, as anode, into the square shape MFC and compared with commercial carbon material having the same function. Due to their high surface area, high porosity and good interaction with microorganisms, aerogels presented better performances of commercial materials if used as anode in MFC.

Considering, instead, the addition of amino acids as nitrogen source to the previous material, it allowed the used of polysaccharide aerogel, as cathode electrode able to catalyze the oxygen reduction reaction (ORR). They were tested in MFC, compared with the most used catalyst material in literature, that is platinum.

Another alternative to platinum in the catalysis of the ORR, is represented by the metal oxide aerogels.

In this work, aerogels based on Mn_xO_y were tested. The synthesis of this material is similar to the previous one, with the difference of the addition of the manganese oxide directly between initial precursors.

Through the thermal process, the organic part of the material is burned, leaving an oxide structure that is active from a catalytic point of view. After the morphological,

structural and chemical analysis of the sample, the catalytic activity of the material was tested, as in the previous case, using the Rotating Ring Disk Electrode (RRDE) technique, in order to investigate its catalytic properties.

Contents

List of Figures

List of Tables

Chapter 1
Introduction

The global energy problem raised from the need to satisfy the constantly growing world energy demand, accompanied with a gradual depletion of the fossil fuels. The elevated amount of energy required should be produced by low environmental impact methods, not to further damage the world atmosphere [1].

More the world becomes advanced in technology and economy, more the energy demand increases. The International Energy Outlook 2016 reported that the worldwide energy demand from 2014 to 2040 should increase dramatically, passing from 549 quadrillion British thermal units (Btu) in 2012 to 815 quadrillion Btu in 2040, with an increase of 48% [2]. In the map reported in Figure 1, the worldwide energy consumption is reported.
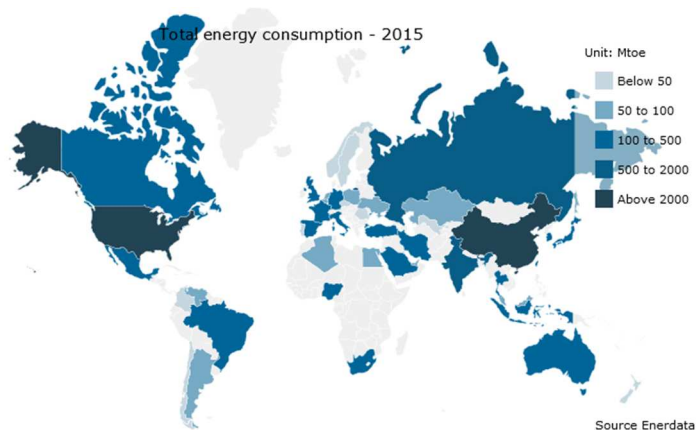
Figure 1 Worldwide energy consumption in 2015 [3]

Actual energy production is mainly based on fossil fuels, in particular oil, natural gasses and coal, representing more than 80% of the total energy production [4]. One of the major drawbacks of the fossil fuel output, is the production and the release in the atmosphere of CO_2, that is connected to a continuous increase of the temperature over global land and ocean surfaces: this problem is known as "global warming", responsible for the greenhouse effect.

Introduction

Primary Energy Overview (Quadrillion Btu)

Overview, 1949–2015
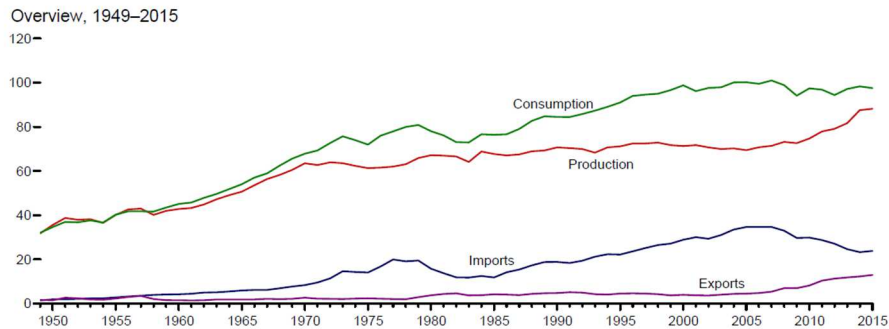
World energy production (Quadrillion Btu)

By Source, 1949–2015
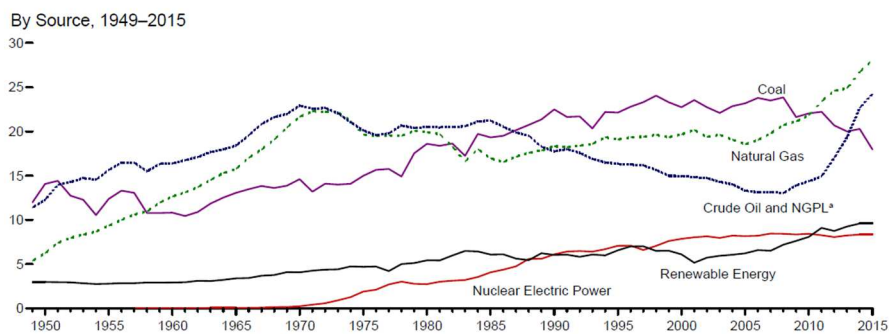
Figure 2 Worldwide energy overview and worldwide energy production from 1950 to 2015 [4]

From the graph presented in Figure 2, it is possible to notice how, in the world, from 1950 to the present, the energy consumption was quite always greater than the production, and this discrepancy increases, with the increase of the population and technology level. Analyzing, then, the production of energy, the monthly U.S. report for November 2016 underlines how the energy obtained from fossil fuels continues dominating the market [4]. Renewable energy, instead, depicted in black in the bottom graph of Figure 2, remains practically constant all over the considered period, with a slight increase only in the last decade, being a promising trend for the research on this topic. The consequence of this is a demand of renewable energy sources that becomes much more important. The "renewable energy" concept identifies all those energy production sources that are self-renewing without any

undesired consequences for the environment. Examples are sunlight, flowing water, biomass, wind and a lot of new discovered sources, such as energy produced by bio-electrochemical systems.

To be economically attractive and competitive, they must be efficient and inexpensive at the same time, joining the sustainability and the environmental friendliness.

Among all the available technologies producing renewable energy, photovoltaics and fuel cells represent two of the most intensively studied and promising alternatives to fossil fuels.

Both of them are electrochemical cells that, starting from different energy sources, solar radiation for solar cells and chemical energy for fuel cells, are able to convert it into electrical power in a green and renewable way.

Dye-sensitized solar cells (DSSC) are devices belonging to the third generation of solar generators. They are based on the use of low cost and organic materials to fabricate cheap devices. A typical DSSC is made of a photoelectrode, on which a photosensible dye is adsorbed in order to collect solar radiation, a counter electrode and an electrolyte with the function of electrically connect the anode and the cathode and to allow charge movement between the two electrodes [5]. One of the key research topic on this cell, is the anode, typically made by a porous nanostructured material: the most used one is TiO_2. Here, the nanostructuration of the supporting material is fundamental for the dye absorbance: higher is the amount of organic dye that is possible to insert in the cell, higher is the amount of absorbed solar energy and so higher could be the energy production. The structuration of the anode to guarantee high performances, must be also accompanied by the durability in time of the performances above a certain value.

To do this, in my work, I studied the possibility to modify the commercial electrolytic solution inserted in the cell (Iodolyte Z150, Solaronix based on the I^-/I_3^- redox couple), creating a dispersion of γ-Al_2O_3 nanoparticles (5 wt%) [6]. The addition of nanoparticles increased the viscosity of the electrolyte, creating a quasi-solid state device.

Effects of the quasi-solid electrolyte on performances of the device are appreciable analyzing the cell operation over time. While electrical performances are not variable too much with the addition of nanoparticles, the durability in time increases

in a significant way: after more than 5 months, overall performance were unchanged, while the cell using commercial liquid electrolyte, after less than 2 months, presented a considerable decrease in efficiency.

The study of solar devices, apart from the material optimization, was also conducted on the architecture of the device itself. Depending on the end use of the device, a different aspect of the architecture was analyzed: if the aim is to fabricate a portable and with low dimensions device, a totally flexible architecture was developed [7], while if the final target was the production of a high power production with a low cost device, a solar concentration using DSSC was realized [8].

In [7], a completely flexible DSSC was obtained to achieve portability, down-scalability of dimensions and lightening of the device. Starting from the first rigid device proposed by its inventor, Grätzel [9], the glass support was substituted by PET films. They were used as packaging system for a totally flexible electrode structure made of titanium grids constituting both the anode and cathode, separated by a polymeric membrane acting as electrolyte. Performances of the flexible device are comparable with the ones of the rigid configuration, with a small decrease due to a non-optimal contact area at the counter electrode/electrolyte interface.

In [8], instead, the architecture was optimized for a power generation system. The aim of the work was to verify that performances of a DSSC working in connection with a solar concentrator system, characterized by a high concentration ratio, were on the same order of magnitude of the ones of traditional systems. The realized prototype was tested both in outdoor and indoor conditions using both monochromatic and large bandwidth radiations. Tests show a good sensitivity to the visible radiation presenting a significant peak in the green region, while a global decrease was observed if cells were illuminated with a blue and red light. Good results also under real outdoor conditions for a prolonged time give the possibility to consider the DSSC, coupled with this setup, as a possible solution for an efficient and green solar concentrator.

The other emerging technology in the last years is the one regarding Fuel Cells. A Fuel Cell is a device able to convert chemical energy, contained in a fuel, in electrical energy by a chemical reaction between positively charged ions and oxygen. It requires that a continuous source of fuel and oxygen must be guaranteed.

A particular type, among all the Fuel Cells, is represented by Microbial Fuel Cells (MFC) that uses selected microorganisms able to produce electrons to oxidize the

fuel inserted in the reactor, converting it into electrical energy. As for the previously presented technology, also this one requires an optimization both on used material and on the architecture. To perform this optimization, both nanotechnology and porous structures of materials are good supporters. Electrodes structure inside electrochemical cells can increase, in a significant way, the total device performances if they are optimally designed. If, for example, the porous material, acting as electrode, has the function of supporting material for additional composites or organisms, higher is the surface area and the porosity of the structure with well-defined properties, higher will be the possibility to host the additional species, needed for energy production: in MFC, in particular, microorganisms are the hosted species on the porous material.

The aim of this thesis is the study and the optimization of the MFC technology both considering the design and architecture of the device and the use of innovative materials as electrodes. Firstly, being a MFC a fluidic device, the study of the fluid behavior inside the reactor and the subsequent development of an optimized shape are the first fundamental step to further increase performances. Using a finite element method (FEM) analysis, particle trajectories and the evolution of the concentration of carbon source in three different cell configurations were studied and analyzed, analyzing the role of fluid dynamics on the real operation of a single chamber MFC. Thanks to results obtained from the modelling, a MFC test cell, with a square shape, was realized.

Together with the optimization of the architecture, helpful to find the best fluidic conditions for MFC operation, a development of an innovative material with high surface area and elevated porosity was performed. The chosen material to do this, is the aerogel. An aerogel is an ultralight porous material derived from a gel, in which the liquid component has been replaced with air, leaving a self-standing structure. During the thesis, carbon aerogels obtained from marine polysaccharides on one side, and metal-oxide based ones, on the other one, will be studied.

The thesis is arranged into Five Chapters. In the first one, a general introduction on energy demand and production problems, together with the need of renewable energy sources is presented, showing two particular renewable technologies: the dye-sensitized solar cells and microbial fuel cells.

Chapter 2 is an introduction of Microbial Fuel Cells, with the aim to contextualize the device in terms of key operating principles, materials, architectures and possible applications of the device itself.

Chapter 3, instead, introduces the basis of the aerogel synthesis and characterization. After a brief history remark of the material, most important groups in which aerogels are divided, are presented. Depending on the chosen material, they can have different properties, that allow the use of the material in different applications.

Chapter 4 has the aim to introduce the basics of the modelling analysis with main results obtained for the development of the new geometry.

Chapter 5 summarizes all the obtained results, combining the new synthetized material with the designed improve geometry.

Chapter 2
Microbial Fuel Cell as emerging technology for energy supply

Microbial Fuel Cells (MFC) are an emerging technology able to overcome energy problems facing the current society combining the energy production and the wastewater treatment using the catalytic activity of microorganisms.

The ability of a particular kind of microorganisms to produce current from organic matter and wastewater was demonstrated for the first time by Potter in 1910 [10]. Some studies on bio-fuel cells and Microbial Fuel Cells were performed until 1980s, but only in the last decade, the attention to this technology has become significantly important ([11],[12],[13]).

2.1 Brief history review on MFC

The first MFCs were based on living cultures of _Escherichia coli_ and _Saccharomyces_ microorganisms [10]. In 1980s was discovered that power generation and performances of MFC could be improved by adding electron mediator species inside the initial inoculum [14], to allow the electrons transfer from the microbe to the anode. Mediators can improve performances of the device capturing electron from the membrane of the microbe and, moving on the membrane itself, reaching the anode and oxidizing and release the electron to the anode [15].

Good synthetic mediators must have some important characteristics: they can cross easily the membrane; they must possess high electrode reaction rate; they should

have good solubility in anodic solution; they must be bio-compatible and low cost [16].

The drawbacks of these synthetic mediators consist in toxicity and instability of the response, limiting the MFC applications.

An important progress in MFC operation was made in the early 2000s, when Chaudhuri and Lovely [17] found that some microorganisms can transfer electron directly to the anode, without the presence of external mediators. They also demonstrated that these microbes, such as *Shewanella putrefaciens, Geobacteraceae sulfureducens* [18] and *Rhodoferax ferrireducens* [17], are bioelectrochemically active. They are able to create a biofilm directly on the anode, transferring the electrical charges to the anode itself by their membrane, eliminating the need of synthetic mediators, and using the anode as final electrode acceptor in the respiratory chain of microbes.

Initially MFCs were developed as a method for wastewater treatment, combined to power production ([19]–[21]), but the big problem of MFCs, at that early stage of development, was that the energy produced, with this technology, was not so competitive as the one produced by other renewable sources, from an economical point of view.

Because of this problem, the application range of this type of device was enlarged from the power generation, purifying wastewater, to several specialized applications which provide for the integration of the MFC with other processes; examples are the monitoring and sensing of the amount of organic matter and toxicity of different types of environments, the bioremediation of sediments in lakes, marine environments and desalination with an electrodialysis process [19], [22]–[26].

To overcome limitations and classify MFCs as a promising renewable energy source, fuel cells are in continuous upgrade to improve the device performances and reduce production and operation costs.

2.2 Working principle of a MFC

A typical microbial fuel cell is constituted by an anaerobic and an aerobic chamber, usually separated by a membrane. The anaerobic one is the anodic compartment, while the one with the presence of air constitutes the cathodic region.

The resulting device is named two chambers MFC (2C-MFC), and different shapes can be designed for this setup ([27],[28],[29]). A general scheme of a double chamber MFC is reported in Figure 3.
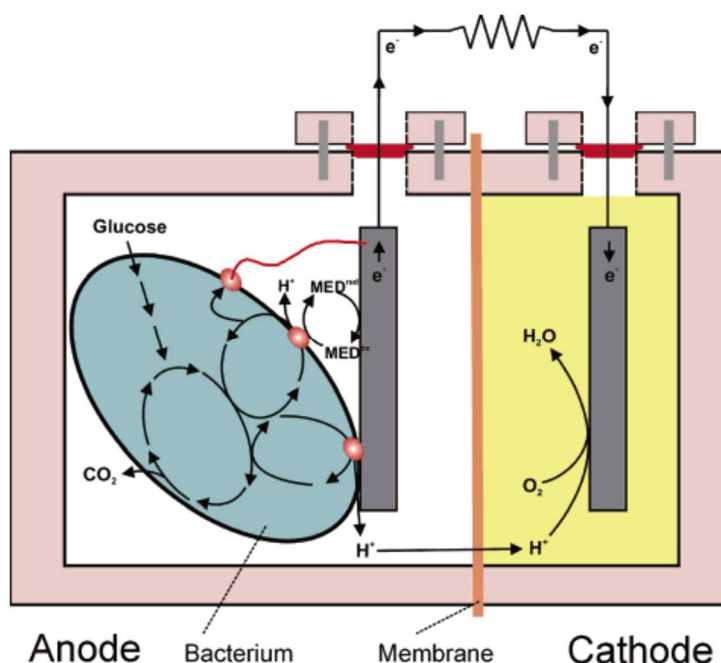
Figure 3 A scheme of operation principles of a double chamber Microbial Fuel Cell

The bioelectrochemical cell is based on the catalytic activity of exoelectrogen microorganisms, that are able to produce and release electrons from the substrate oxidation: to do this, strictly anaerobic conditions are needed.

During the oxidation of the organic matter at the anode, carbon dioxide, electrons and protons are produced, since oxygen is not present to react with electrons. Generated protons flow through the membrane up to the cathode; electrons produced at the anode, instead, to be useful for power generation, must be transferred from the cell to the electrode and then via an external circuit to the cathode. Here they recombine with protons in order to close the electrochemical circuit.

A wide range of organic compound can be used in MFC as nutrient for microorganisms, such as organic matter contained in wastewater, acetate, glucose, glycerol, citrate, etc. [30].

At the cathode, instead, a reduction reaction occurs. Also in this case a variety of final electron acceptor can be used, such as oxygen, ferricyanide, iron, manganese dioxide, etc. [27].

Each reaction, both at the anode and at the cathode, has a proper redox potential, that is different depending on the organic substrate and the final electron acceptor used. The difference between these two potentials is the driven force for charges inside the reactor.

In this work, the anodic chamber was filled with an electrolyte containing sodium acetate as carbon source (nutrient) for bacteria, ammonium chloride to guarantee anaerobic conditions and phosphate-buffered saline (PBS) to maintain a constant neutral pH.

As cited before, the main activity of bacteria is to oxidize the substrate to generate power: the reduction reaction of sodium acetate is reported in Eqn. (1) generating a OCV potential $E_{an}^0 = -0.3\ V$ vs SHE with a concentration of 1g/l with a neutral pH.

$$2HCO_3^- + 9H^+ + 8e^- \Rightarrow CH_3COO^- + 4H_2O \qquad (1)$$
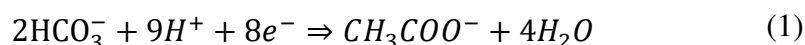
SHE is the standard hydrogen electrode and represents the absolute electrode potential, assumed to be zero at all temperature. For this reason, it is used as reference in electrochemical devices to measure potentials of any other electrode [31].

A typical cathode of double chamber MFC, instead, is based on ferricyanide as final electron acceptor, and, in particular, on potassium hexacyanoferrate $Fe(CN)_6^{3-}$. It is chemically stable, with a good solubility in water and does not require any catalyst. The reduction reaction is reported in Eqn.(2) and its standard reduction potential is $E_{cat}^0 = 0.613\ V$ Vs SHE.

$$Fe(CN)_6^{3-} + e^- \Rightarrow Fe(CN)_6^{4-} \qquad (2)$$
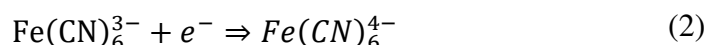
However, the use of potassium hexacyanoferrate in the cathode chamber has also some drawbacks: the need of a continuous exchange of the reduced chemicals with

fresh ones, the toxicity and nonrenewable property, and a not so high redox potential.

2.3 Exoelectrogens microorganisms and charge transfer mechanisms in MFC

One of the most important component, affecting MFC performances, is the biological aspect, in particular the type and source of the inoculum, that is the initial microorganisms' colony inserted in the MFC.

When the inoculum is inserted in the anodic chamber, microorganisms interact with the electrode and form on it the biofilm. A biofilm is an aggregate of microorganisms in which cells can attach to each other and, in turn, adhere to a surface, while microorganisms not attached to the surface remain in the planktonic solution.

Among all the available microorganisms in nature, the most interesting ones to be used in MFC for power production are the exoelectrogens. Their name is the sum of "exo" for exocellular and "electrogens" for their ability to directly transfer electrons outside the cell to a material that is not the immediate electron acceptor: it is this important ability that distinguish exoelectrogens from strictly anaerobic microorganisms, and permit their use in MFC. Most known and used exoelectrogens are Geobacter and Shewanella species.

Electrons generated by bacteria must be transferred to the electrode to be collected by the external circuit.

Bacteria can transfer electrons in two different ways: electron shuttling through mediators, and through nanowires or re-oxidizing primary metabolites, as summarized in Figure 4.

The presence of nanowires was discovered by Gorby in the first decade of 2000s. He observed that some bacteria produce a conductive appendage. Its conductivity was investigated with several techniques, and at the end it was confirmed that this wires were conductive on x-y plane, having so the function of electron transfer from the cell to a surface [32]. The transport of charges through conductive pili can be

substitute by a direct contact between the microorganism and the surface, to which the electron is transferred. These direct mechanisms are illustrated in Figure 4-A.
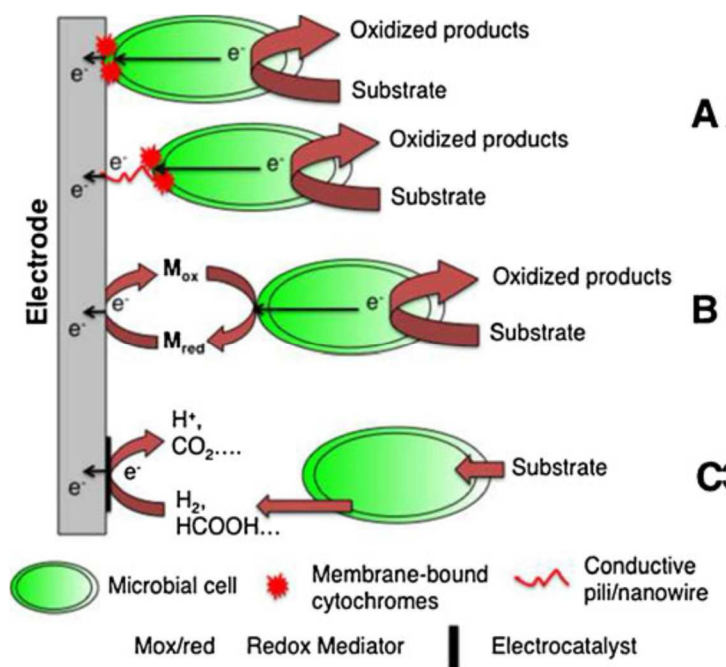
Figure 4 Summary of extracellular electron transfer mechanisms: through conductive pili or nanowires (A), through mediators (B) and through re-oxidation of primary metabolites (C) [33]

The other charge transfer mechanism, is the one involving mediators. Some microorganisms, in fact, to transfer produced electrons from the cell to the electrodic surface, need the presence of mediators. In some cases, external mediators, like thionin, methyl blue, methyl viologen, potassium ferricyanide, etc. are added to the MFC to allow the shuttle of electrons. External mediators are needed for those microorganisms that not possess electrochemically active surface proteins able to transfer charges.

Rabaey, instead, found that, in some cases, certain electrochemically active bacteria can produce endogenous chemical mediators (i.e. pyocyanine) able to shuttle electrons from the cell to the electrode surface. This charge transfer mechanism is summarized in Figure 4-B.

The last possibility to transfer electrons from the cell to the electrode is reported in Figure 4-C and it is based on the oxidation of reduced primary metabolites. This mechanism is typical only of fermentative microorganisms and yeasts [33].

More efficient is these transfer mechanisms from the bacterium to the electrode, higher will be the performances of the total device.

2.4 Single Chamber MFC

A good possibility to overcome drawbacks rising from the use of chemical cathodes is the single chamber microbial fuel cell (SC-MFC). The transition from the double chamber configuration to the single one has some important advantages: firstly, avoiding the use of chemical cathode, the idea of a green device producing sustainable energy is realized. Moreover, using a single chamber reactor, the use of a charge separation membrane is avoided, and, being one of the more expensive part of the 2C-MFC, production costs of the device are reduced. In this configuration, the anode and the cathode share the same electrolyte.
The most important advantage in using this new configuration, is the possibility of use oxygen present in the environment, as final electron acceptor.

In Figure 5, a scheme of a single chamber MFC is reported.
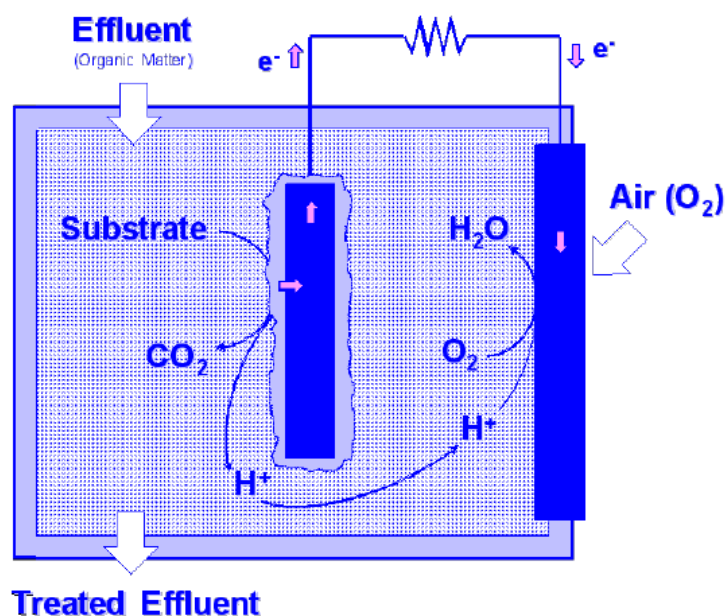
Figure 5 A scheme of a Single Chamber Microbial Fuel Cell [34]

Initially, in early configurations, the use of charge transfer membrane was maintained both to prevent the contamination of the cathode with the electrolyte containing microorganisms, both to preserve the anodic biofilm from the oxygen flux coming from the cathode. To further reduce costs and complexity of the device, Liu et al. developed a SC-MFC without the PEM, observing an increase in performance of the device, due to a better charge movement between the two electrodes and a decrease of internal resistances due to the presence of the membrane [35].

Sharing the same electrolyte, the cathode is in front of the anode, with one side directly in contact with air. To prevent the loss of electrolyte from the cathode, a diffusion layer (DL) is added. Commonly the DL is made of a quite cheap fluorinated-based material, such as Polytetrafluoroethylene (PTFE) [36], because this category of materials has the particularity to be permeable to the Oxygen, but non-permeable to the water.

As introduced for the double chamber configuration, using sodium acetate as the organic substrate in both the MFC configurations ($E_{an}^0 = -0.3\ V\ vs\ SHE$), the maximum achievable potential with a double chamber setup, using potassium hexacyanoferrate as chemical cathode, is

$$E_{2C-cell} = \big(0.613 - (-0.300)\big)V = 0.913V \tag{3}$$

while the one reachable using oxygen as electron acceptor is

$$E_{SC-cell} = \big(0.805 - (-0.300)\big)V = 1.105V \tag{4}$$

The big advantage of use a SC-MFC with respect to the double chamber one, is the possibility to reach a higher maximum voltage production thanks to the use of oxygen as final electron acceptor, together with the removal of a chemical species in a reactor allowing the use of oxygen directly from the environment.

In a single chamber MFC oxygen is directly used as the reducing agent. Oxygen reduction reaction can occur following two different pathways: the two electron reaction (Eqn. (5) and (6)) and the four electrons pathway (Eqn. (7)). For each equation, the correspondent potential is reported.

$$O_2 + 2H^+ + 2e^- \Rightarrow H_2O_2 \qquad E = 0.69\ V\ vs\ SHE \qquad (5)$$

$$H_2O_2 + 2H^+ + 2e^- \Rightarrow 2H_2O \qquad E = 1.76\ V\ vs\ SHE \qquad (6)$$

$$O_2 + 4H^+ + 4e^- \Rightarrow 2H_2O \qquad E = 0.8\ V\ vs\ SHE \qquad (7)$$

Depending on the number of electron involved into the reaction, oxygen can be reduced to hydrogen peroxide or to water. As appreciable in Eqn. (5), the first pathway is favored because its activation energy is lower; the problem is that, the second reaction associated to this one, that transform hydrogen peroxide in water (Eqn. (6)), requires a high amount of energy, and so it is not favored. It results into the presence of hydrogen peroxide into the electrolyte, that is poisonous for bacteria. The aim of the catalyst is to avoid the formation of toxic H_2O_2, promoting water production, following the direct four electrons reactions, reported in Eqn. (7).

2.5 Main parameters of a Microbial Fuel Cell

To study and compare MFCs, some important electrochemical parameters, able to classify device performances, must be defined [27].

Generally, a Microbial Fuel Cell is able to produce a maximum voltage during its activity of 0.3 – 0.7 V [27]. Following the Ohm's law, the voltage (reported in Eqn. (8)) is a function of the external load applied R_{ext} and the current flowing between the electrodes.

$$E = I \cdot R_{ext} \qquad (8)$$

Because the current is very small, in laboratory, instead of derive the potential from Eqn. (**8**), it is directly measured. Depending on the inoculum type, the metabolic activity of microorganisms and the quality of the formed biofilm, the voltage trend

of a MFC can vary, both in profile and in characteristic times: the time needed to reach the maximum voltage value, in fact, changes from cell to cell.

The potential generated by a MFC may not overcome a certain value, that is defined as the maximum electromotive force E_{emf} generated by an electrochemical cell. It is given by

$$E_{emf} = E^0 - \frac{RT}{n\,F}\,\ln(\Pi) \tag{9}$$

where E^0 is the standard electromotive force, R is the gas constant, T the absolute temperature, n the number of electron transported and F the Faraday constant. Π is the reaction rate, defined as the ratio between the activity rate of the products that are reduced and the activity rate of reactants that are oxidized, raised to their respective stoichiometric coefficients.

The maximum potential generated by a MFC is obtained in open circuit mode, disconnecting the device from any external load; the corresponding potential is named *open circuit voltage (OCV)*.

Connecting, instead, a load (R_{ext}), the output power (Eqn. (10)) of a MFC can be calculated as a function of the voltage drop across the two electrodes (E_{MFC}) and the current (I) flowing through them.

$$P = I \cdot E_{MFC} = I^2 R_{ext} = \frac{E_{MFC}^2}{R_{ext}} \tag{10}$$

In order to generally compare devices with different shapes and different materials used for electrodes, the main output parameters (i.e. current and power) were normalized as a function of the active surface area of the electrode (A_{el}), giving to this new parameter the name of *density*. The active area can be calculated as the projected geometric area exposed to the electrolyte, or calculated using a gas adsorption analysis considering the porosity of the material. Output parameter adapted with surface areas are reported in Eqn.(11) and (12).

$$J = \frac{I}{A_{el}} \tag{11}$$

$$P_{el} = J \cdot E_{MFC} = J^2 R_{ext} \tag{12}$$

The expression reported in Eqn. (10) represents the theoretical power generated by the device, without considering internal parameters. To obtain the real produced power, also the internal resistance of the device must be considered (R_{int}): this topic will be explained in paragraph 2.6. Finally, the ***theoretical maximum power generated*** by the MFC, based on the measured OCV, can be summarized as reported in Eqn. (13)

$$P = \frac{OCV^2}{(R_{int} + R_{ext})} \tag{13}$$

This is the power generated by the cell itself. More important for the study is the output power, that is the effectively usable one, and it is reported in Eqn. (14).

$$P = \frac{OCV^2 \, R_{ext}}{(R_{int} + R_{ext})^2} \tag{14}$$

2.6 Factors affecting performances of MFCs

As well as the internal resistance, also other contributions affect the performances of the device. The OCV value produced by the cell, in fact, is always lower with respect to the predicted one, due to some internal losses. Analyzing a polarization curve of a MFC, described in 5.4.1, (Figure 6) it is possible to identify three different regions, associated to three different losses mechanisms: a rapid voltage losses when current when current flows in the external circuit (1); a linear region (2) and a second rapid decrease corresponding to high current densities (3).
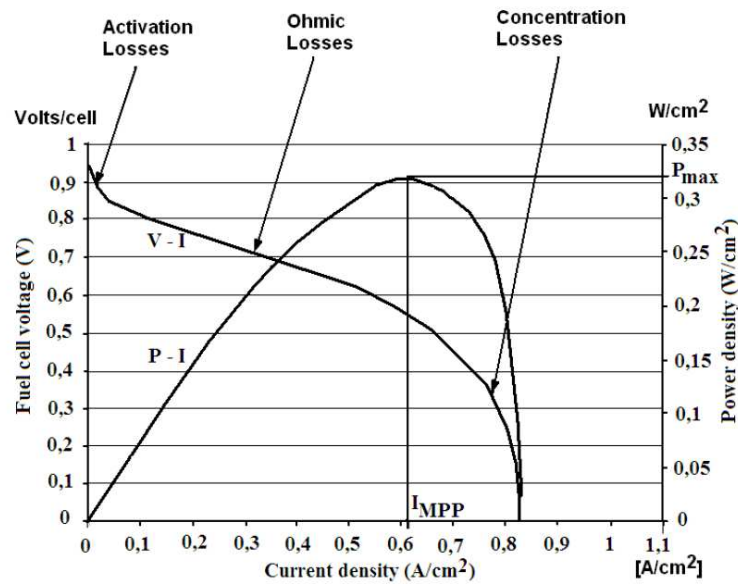
Figure 6 Characteristics of a polarization curve, in which the three losses types are reported [37]

The total voltage generated by the cell, taking into account all the previous factors, can be summarized in Eqn. (15)

$$E_{cell} = E^0 - \left(\sum OP_{An} + \left| \sum OP_{cat} \right| + IR_{\Omega} \right) \tag{15}$$

Where $\sum OP_{An}$ and $\sum OP_{Cat}$ are the anodic and cathodic overpotentials, and R_{Ω} is the Ohmic resistance.

Voltage losses of a MFC derived from internal parameters (i.e. internal resistances), can be generally classified in three groups: *Activation losses; Bacterial Metabolic losses* and *Mass transport losses*.

- *Activation losses* are generated when an oxidation or reduction reaction occurs, because this type of performance loss is connected to electron transfer from the cell terminal compound (i.e. nanowire) to the electrode surface. This contribution occurs at low current densities. Activation losses can be reduced modifying the electrode, increasing the surface area, improving the catalytic

- properties of the cathode or improving the electron transfer between bacteria and the electrode.
- *Bacterial metabolism losses* occur when bacteria oxidize the organic substrate. Here, bacteria, to generate electrical power, transfer electrons from a substrate with a low potential, to the final electron acceptor at a higher potential. In a Microbial Fuel Cell, the anode is the final electron acceptor, whose potential determines the energy gain for microorganisms. Higher is the difference between the anode potential, and the redox potential of the substrate, higher is the metabolic energy for microorganisms, but lower is the maximum voltage achievable. In order to maximize the cell potential, the potential of the anode must be maintained at a value as low as possible to allow electron transfer.
- *Mass transfer losses* are present when the current production is limited by the mass transport rate to or from an electrode. At the anode they are generated by a limited discharge of oxidized species through the electrode, leading to an increase of the anodic potential; at the cathode the opposite situation happens: a lowering of cathodic potential can occur.

In Eqn. (15), in addition to the overpotential contributions, also the losses due to Ohmic part are present.

Ohmic losses are the most important losses that must be mostly reduced in MFC optimization. The nature of this type of losses is the resistance of ion conduction due to the solution and the membrane (when present), and the flow of electrons to the connection point between the electrode itself and any electrical internal connection. These types of losses can be reduced shortening the electrode distance, using electrode coating with low internal resistances or engineering the contact point between the material and the external electron connection to reduce losses due to the contact itself.

2.7 MFC applications

2.7.1 Power generation

As mentioned above, the Microbial Fuel Cell is a device able to convert chemical energy into electrical power; under specific conditions, this type of device can reach

conversion efficiencies above 70%, theoretical Carnot cycle limit. It is possible because chemical energy obtained by oxidation of the organic matter is directly transformed into electrical one, instead of heat, avoiding Carnot cycle.

Using, for example, a sediment MFC, Tender et al. in 2008 powered a meteorological buoy with a MFC in a marine environment. To successfully power the device, the energy produce by the MFC was, firstly, stored in a capacitor and then transferred to the buoy [38].

Another application, using sediment MFCs, is the powering of small wireless sensors requiring a small power to communicate in remote locations, like the one powered by Donovan et al. [39]

An additional example of the application of MFC as power generator is the robot named EcoBot-I, able to accumulate energy and work in a pulsed way [40].

2.7.2   Biosensors

Another application of Microbial Fuel Cells is the in situ detection of pollutant in wastewater [41]. The main parameters to be detected by a MFC if used as biosensor, are the amount of biodegradable organic substance content, present in the waste water, expressed in terms of the amount of oxygen needed by microorganisms to break down organic matter present in water in a certain time, called Biological Oxygen Demand (BOD) or the Chemical Oxygen demand (COD), that is the amount of organic and inorganic content present in water, considered pollutant The working principle of the detection is a proportional correlation between the COD/BOD value and the current generated by the cell: higher is the amount of BOD/COD, higher will be the current generated. The way to correlate the current with the amount of BOD is to analyze the Coulombic yield: a high BOD/COD concentration in water requires a longer response time for the MFC to be calculated, instead a quite low quantity of BOD/COD can be immediately calculated thanks to a linear correlation with the current [42], [43].
The advantage of using MFC as bio-detector, is that this biological device has a better stability and reproducibility in time with respect to other types of sensors.

Based on the same principle, also the detection of chemical toxicants can be performed by MFC [42] [44]. In this application, the detection is based on the inhibition of the oxidizing activity of the microorganisms due to the presence of chemicals into the inflow liquid. Since the oxidation of the substrate is inhibited,

also the efficiency in transport of electrons from the bacteria to the electrode is not more efficient, resulting in a decrease in current generation.

The main drawback in using MFC as biosensors, is the non-selectivity of the device. Differently from chemical sensors, able to identify specific toxicant, microorganisms are not able to select or produce different output power values depending on the type of contaminant is present in the wastewater to be analyzed.

2.7.3   Wastewater treatment

Most common wastewater treatment setups are based on the aerobic degradation of domestic and industrial wastes. These configurations require energy and resource consumption: only aeration requires 0.5 kWhm^{-3}. Habermann and Pommer in 1991 [45] firstly discovered the possibility to use bio-electrochemical reactors, as Microbial Fuel Cells, for water treatment. The use of MFC instead of classical aerobic systems, leads to a series of benefits that enhance the microbial fuel cell technology: they are able to transform the chemical energy present in the wastewater into electrical power, while purifying.

Also the amount of sludge, produced by the depuration, is lower with respect to classical configurations, up to 90% less. During the aerobic process, bacteria use all the chemical energy present into the pollutants, but only a small fraction is used for the biofilm growth; in MFC, instead, most of the chemical energy is used and transformed.

This system can be further improved with the usage of the produced current from the purification of wastewater, in the same wastewater purification process, or with the addition, together with the ones naturally present in nature, of more efficient exogenous bacteria to increase efficiency in water treatment and power production.

2.8 A key point in MFC performances: the electrode.

2.8.1   Anode

During MFC operation, the output power depends on a lot of internal parameters, such as the rate of degradation of the nutrients, the efficiency in the electron

transport from the bacteria to the electrode, the mass transfer in the electrolyte, the circuit resistance, the operating conditions and, mostly, from electrode efficiency.

The electrode itself, in particular the anode, must have some physical and chemical properties that can support and enhance all the biological and electrical processes cited above; some of the key properties of a good anodic material are a good electrical conductivity, low resistance, biocompatibility, non-corrosive interaction and chemically stability, large surface area, easy scalable and also be inexpensive in order to be competitive with MFC evolutions.

To optimize the electrode, one of the main objective is to find and develop a suitable material to enhance performances of the Microbial Fuel Cell, keeping costs low.

Although different materials have been tested as anode electrode, carbon based materials remains the mostly used and studied in recent works [46]; they are present in different forms, such as graphite rods, plates or fiber brush or fibrous materials that include carbon felt, carbon paper, carbon felt or, still, glassy carbon.

Considering graphite rods, felt, plates and so on, they were used in several studies, especially in electrochemical ones, due to their conductivity and their well-defined surface area. Chaudhuri et al. [17] tested performances of some of these materials, and they found that increasing the available surface area of the material, also the performances of the MFC increased. The most illustrative work in which graphite rods were used, is the one of Liu et al. [47]. In this work a single chamber MFC was used and 26 mW/m^2 as maximum generated power.

The limiting factor in using this material is its low porosity and limited surface area; Lovley et al. [17] overcame this problem, substituting the graphite rod with graphite felts, having an higher porosity accessible by microorganisms.

To further improve surface area and porosity, a 3-D assembly made of graphite fibers, called brush, was used. It is made of carbon fibers arranged in a 3-D structure around a conductive wire using a brushing machine. Ahn and Logan [48] used an anode made with this structure, obtaining a maximum power of 422 mW/m^2.

Lately, the most used materials became carbon cloth and carbon paper [49]. They present a good affinity in bacterial growth, together with a good electrical conductivity. Carbon paper, in particular, is stiff and very brittle, but it is not a problem for wiring the electrode: the electrical connection is joined to the material

using an epoxy resin, able to fix the wire and isolate it from bacterial growth. The carbon cloth, instead, appears more flexible with a higher porosity with respect to carbon paper, leading a higher maximum power density (483 mW/m^2 with respect to 40 mW/m^2 obtained with carbon paper) [50], [51].

2.8.2   Cathode

The cathode, especially in a single chamber MFC, is the most complicated interface because here electrons, protons and oxygen interact with the catalyst in a three-phase reaction, and, if air-cathode is used, it must also guarantee the not exit of the electrolyte contained in the reactor. The design and optimization of the electrode material, in fact, is a big challenge to make the Microbial Fuel Cell a scalable and usable device.

The catalyst layer must be supported on a conductive material that is exposed at the same time to both aqueous electrolyte and air, and it must be able to be reach both from electrons and protons.

Because of all the characteristics explained for anode are sharable also for cathode, all the cited material in paragraph 2.8.1, can also be used as cathode with the difference of the application of a catalyst layer, on the electrolyte side, to speed up the cathodic reaction. The presence of a catalyst (Platinum in general), in fact, is needed to reduce the cathodic reaction activation energy and increase the reaction rate, increasing performances of the device.

The main problem that limits application of the Platinum as catalyst is its elevate cost. Research has moved so, to the attempt to reduce platinum content in the cathode, or to find new catalytic materials Platinum-free based on transition-metals (Iron and Cobalt are the mostly used) [52].

If catalyst is used at the cathode, it must be held to the surface of the electrode, using a material permeable to both the oxygen, the electrons and protons. The mostly used binder is nafion, that allows the oxygen flux, together with a good proton permeability. Also other materials, in alternative to nafion, were used, for example a suspension of polytetrafluoroethylene (PTFE) was found to have the same role of its competitor. Testing the two materials in air-cathode SC-MFC, has been found that nafion produced higher power (480 ± 20 mW/m^2) with respect to PTFE suspension used as binder (360 ± 10 mW/m^2) [27].

At the side exposed to air, a diffusion layer is required. The most used and the most efficient one is represented by polytetrafluoroethylene (PTFE).

The membrane used in MFC has also the ability to control and limit the flux of oxygen flowing in the reactor. If the membrane is not present in the cell, a too high amount of oxygen can enter in the chamber, reaching anodic biofilm, reducing the efficiency of the device and generating important water losses at the air-side of the cathode. Overall performance of the device is reduced due to a gas headspace, generated by a too high permeability through the electrode, that can increase too much the redox potential in the anode, reducing so power generation efficiency [27]. To overcome this problem, a hydrophobic layer was added by Cheng et al. [36] at the air side to control the gas flux, preventing water losses. Not to reduce too much permeability and so performances, the loading of fluorinated material must be investigated and optimized.

A great improvement in satisfying important properties of materials to be used as electrodes can be reached using nanotechnology. Through this technology, it is possible to modify the surface of the material, or directly synthetize a new one with desired properties in order to enhance the exposed surface area or to adapt and increase catalytic activity of the electrode.

An example of the use of nanotechnology to improve electrode properties is introduced in the next chapter, where a new type of nanostructured electrode realized with aerogels, is explained.

2.9 Technological improvements in Microbial Fuel Cells

To improve Microbial Fuel Cell performances, a deep study and an optimization of all the characteristic parameters must be taken into account.

Applications of MFC require a design of the reactor, that is not only able to produce high efficiencies associated to high output power, but also it must be cheap, and easily scalable on large scale. To do this a study both on materials and on architectures must be considered.

As introduced before, the material used as electrode in a fuel cell must satisfy some important parameters, such as porosity, high surface area, electrical conductivity and, moreover, have low costs.

Most of these characteristics can be found in commercial carbon materials, such as carbon felt and carbon paper: they have a good electrical conductivity, good stability in biological solutions and a high porosity to improve the available area for biofilm formation, increasing so performances.

The development of a three-dimensional structure of the electrode can overcome these limitations allowing also the reduction of the overall dimensions of the reactor, not reducing the electrode area available by microorganisms.

Using nanotechnology this achievement can be reached. Nanotechnology found a great importance in different fields [53]: it was used for water remediation, pollutants removal, coatings, ceramics, personal care products, water decontamination, but also to fabricate electrodes for batteries, super capacitors and biosensors.

Engineering of the electrode material, in my PhD activity, was obtained developing a high porosity material with good electrical conductivity called aerogel with a high surface area values, good electrical conductivity, good stability and relatively low cost. This material will be discussed in the following Chapter.

To further improve MFC performances, reducing so losses inside the reactor, some optimization on the architecture must be also done.

A big challenge in reducing mass transport losses, is the reduction of the distance between electrodes, reducing so the distance that charges have to travel. In addition of the reciprocal distance, also dimensions of the electrode itself are very important. Also the study of the liquid movement inside the reactor chamber is fundamental for power generation. Developing, in fact, a chamber with a bigger region in which the fluid is effectively moved during operation is a key point in biofilm activity efficiency.

To do this, in my work, a new architecture was developed to overcome these problems. Starting from a 2C-MFC [54], a square-shape SC-MFC was introduced. The new cell was designed with a modular approach and then fabricated by a polymeric additive manufacturing technique that allows a lot of degrees of freedom.

Using a 3D-printer, the reactor is build layer by layer using a photo-curable polymer, able to get hard thanks to a UV lamp located near the printer tip. Using

this technique, through a CAD project, it is possible to obtain many geometries also with miniaturized features.

The device that I developed in my PhD period, is a modular square-shape reactor optimized both for characterization of materials used as electrode and biosensing analysis. This device can be operated both in fed batch mode and continuous mode. In the fed batch mode, the reactor works in a cycling way: it is firstly filled with the solution containing the organic substrate, and it is then left without any external contribution, until bacteria have completely oxidized all the organic matter. Once the organic nutrient is finished a new amount of fresh substrate is inserted. The voltage corresponding to this operation mode has a cycling trend too, similar to that of the concentration of nutrient into the cell [55]. In Figure 7 an example of output voltage of a MFC working in fed-batch mode is reported.
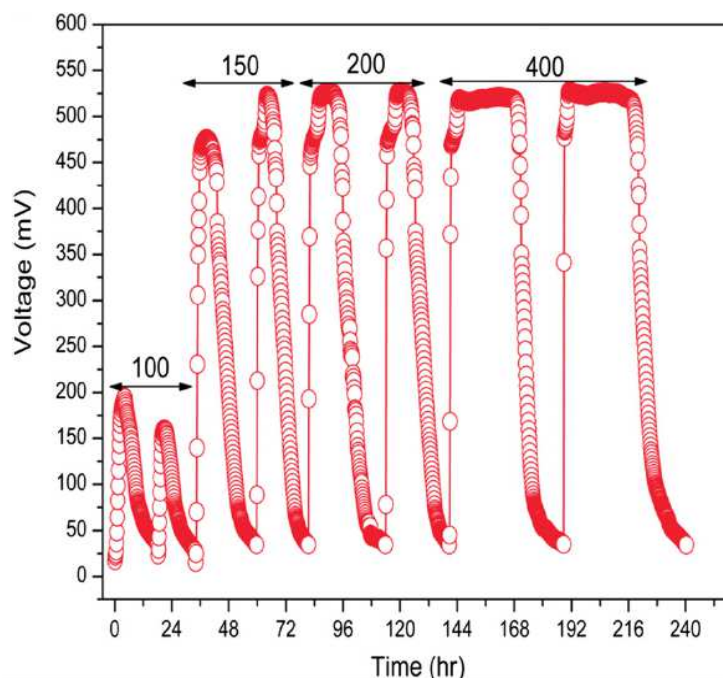
Figure 7 Example of voltage trend during fed-batch mode operation [56]

In the continuous flow, instead, the cell is connected to an external pumping system able to supply fresh nutrient continuously to the reactor at the selected flow rate, so varying the hydraulic retention time (HRT) of the liquid [55].

This parameter is important because it defines the mean time during which organic substrate remains inside the reactor, that is indirectly connected to the time during which bacteria are in contact with the fresh medium. This time influences the

sensitivity of the device if used as a bio-sensor or the amount of maximum power produced if working in power production mode.

To increase the efficiency of the MFC reactor, considering these contribution (maximize exchanged area and allow good performances in both operational modes), the new squared cell presents inlet and outlet connections not aligned on the x-y plane. This geometrical configuration increases the path that nutrients particles have to travel from the inlet to the outlet, increasing the volume over which the fluid directly moves when operating in continuous mode. A detailed investigation on this cell and the corresponding simulations are reported in Chapter 4.

Chapter 3
The aerogel: materials, synthesis and characterization

An aerogel is a gel in which the liquid was replaced with a gas, without collapsing the structure.

Different procedures and techniques were used to obtain this material, but a general scheme and process flow, common to this entire class of material, can be defined. All the aerogels start from precursors that, sometimes using chemical gelling agent or sometimes independently, under particular conditions, were transformed in gels. The process that distinguishes aerogels from all other porous materials, is the drying process, during which the liquid part is removed by the gel. After this step, the aerogel is synthetized and, in order to improve or modify its surface properties, some post drying processes can be performed.

Generally, a porous material can be defined as aerogel if two fundamental conditions are satisfied: no collapse of the bone structure during drying, and a total shrinkage less than 15 % of the initial volume [57].

Before to start the aerogel discussion, also the concept of porosity and pore dimensions must be introduced to uniformly describe its properties. IUPAC defines porosity as a texture property, referred to the pore space inside the material [58]. More generally, porosity is a measure of the empty spaces in the structured material, expressed as the fraction of voids over the total volume. Its value can range from 0 to 1, or, in percentage, from 0% to 100%.

Depending on the pore dimensions, they can be classified in micropores (diameter less than 2 nm [59]), mesopores (diameter greater than 2 nm but lower than 50 nm [60]) and macropores (diameter greater than 50 nm [61]).

Aerogels have the particularity and the possibility to contain all of these pore diameters, and the needed porosity class can be enhanced by means of particular synthesis procedures or post-synthesis treatments.

3.1 Brief history of aerogel

The concept was firstly introduced by Kistler in 1931, who invented the term *aerogel*, as the sum of "air" and "gel", well summarizing the main characteristic of the material [62].

The main component of an aerogel is the air, that is enclosed by a thin network; the amount of present framework must be controlled, to have the aerogel density only three times higher with respect to the one of air.

The particularity of this structure is the ability to combine several physical properties with different chemical compositions that can be enhanced depending on the end use of the material.

The first produced aerogel was a silica-based one, during which the first supercritical drying was performed.

From their invention, the interest for aerogels in the scientific communities did not rise too much: in the first years, few papers were published on this matter, and most of them regarding the preparation of silica-based materials. The drawback of this early stage research was the time-consuming procedure, that avoid the widely use of the material in the experimental work.

In the early stage, in fact, the aerogel was prepared by an acid-catalysed reaction that required waterglass/water system to remove chloride ions, followed by the solvent exchange from water to ethanol, necessary for supercritical drying [62].

From first aerogel synthesis to the present, the research on this topic was subjected to three main upsurges. The first one, between 1970s and 1980s, consisted into the substitution of waterglass/water system with organic precursors with their correspondent organic solvents, reducing the preparation time. Representative materials of this period were the tetramethyorthosilicate (TMOS) and tetraethylorthosilicate (TEOS)-based aerogels [63]–[66]

In the 1990s, the second improvement in the research consisted into the birth of organic and carbon aerogels and the introduction of the ambient pressure drying.

These innovations made increasingly important the aerogel, making it a competitive material both in properties and costs [67],[68],[69].

The last upturn is the one occurred from 21st century to the present and it is the most significant one, because new types of aerogels, based for example on chalcogenides, oxides carbon nanotubes, graphene, etc. were developed [70], [71].

During the last decade, the synthesis techniques, become much more refined by means of the introduction of the rapid supercritical extraction, in which precursors forming the gel are brought to their supercritical conditions directly in a pressurized mold, for example. The research on precursors and synthesis techniques was also accompanied by the better knowledge of aerogel properties, such as porosity, mechanical and electrical properties, density, etc.

3.2 Different types of synthetized aerogels

Among all the studied materials and the new ones still under investigation, aerogels can be divided into three main groups, depending on their precursors: purely inorganic aerogels, purely organic ones and composite aerogels.

3.2.1   Inorganic aerogels

Historically, inorganic aerogels are the oldest: as cited before, the first aerogel, in fact, was based on silica. From its born, it became the most studied and diffused material. Before considering some of the most important properties of the silica based aerogels, a more general overview must be considered.

Almost all metal and semimetal oxides are able to form a gel, that is why a lot of materials were tested and studied. Considering, for example, metal oxides aerogels, different possibilities can be synthetized. Aqueous solutions of salts, molecular precursors in organic solvents, or some alkoxides, are suitable for sol-gel processing. Thanks to their lower electronegativity and higher Lewis acidity with respect to alkoxysilanes, metal alkoxides (such as titanium, zirconium, tin or aluminum) are much more reactive towards water. Their high water reactivity allows, in some cases, the spontaneous formation of a precipitate [72]. While in the case of alkoxysilanes, the addition of a chemical catalyst is needed to promote the gelation process, alkoxides, instead, require the addition of a moderator agent, in

order to obtain a gel instead of a precipitate: the most common moderate agent is the acetic acid.

The large water excess in the hydrolysis reaction allows the formation of a crystalline portion inside the material, that was not possible in aerogels based on silicate network. From most popular metal oxides aerogels, alumina, titania and zirconia are the most studied ones. In Table 1, a summary of the principal properties of the most diffused metal oxide aerogels are reported.

Table 1 Most important properties of some metal oxide aerogels [72]

Aerogel	Density	Porosity	Pore radii	Surface area
TiO_2	0.3-1 g/cm^3	78-90 %	1-25 nm	316-690 m^2/g
ZrO_2	0.2-0.3 g/cm^3	84-96 %	10 nm	81-480 m^2/g
Al_2O_3	0.13-0.18 g/cm^3		5 nm	123-616 m^2/g
Al_2O_3/SiO_2	0.06-0.21 g/cm^3		12 nm	

Among all the inorganic gels, the most studied ones are silica-gels. The first synthesis consisted into the mixing of an aqueous solution of sodium silicate and hydrochloric acid, from which, Kistler, demonstrated the possibility to remove the liquid without destroying the structure.

The nanostructured network is formed in a liquid medium as a result of a polymerization process, that creates siloxane bridges between Si atoms. At the beginning of the sol-gel process, silica particles are arranged in linear oligomers. They can link to each other creating a 3D open network structure named gel. During the entire synthesis, the two driving reactions are the hydrolysis and water/alcohol condensation. The obtained gel, after an aging time to reinforce the solid skeleton of the material, is dried using one of the typical drying procedures for aerogels, described afterwards. A scheme of the synthesis process of silica based aerogels is reported in Figure 8.
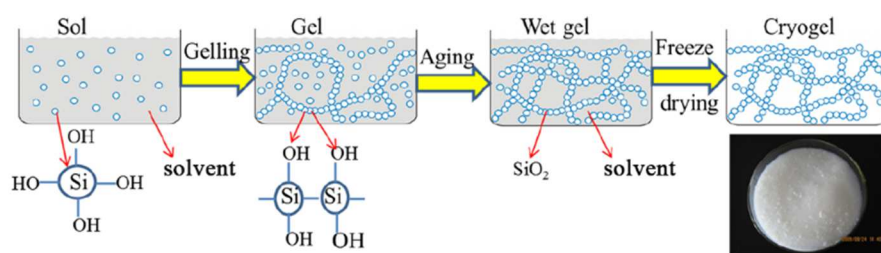
Figure 8 A scheme of the synthesis procedure of silica based aerogels [73]

The synthetized material presents a variety of physical-chemical properties, starting from the texture. Silica aerogels are amorphous materials with a skeletal density that is of the same order of magnitude of the amorphous silica, and a typical pore volume above 90%; with a particular synthesis process, also an ultra-light material, with a density 0.003 g/cm^3 can be obtained [74].

The porosity that the silica aerogel has is typically meso and macroporous with pores up to 100 nm and an average diameter of 40 nm. This porous structure leads to a specific surface area that can range from 250 m^2/g, up to above 1000 m^2/g.

All these properties can be controlled by sol-gel, drying and/or post drying treatments conditions in order to set the material for the target application.

As concerns the physical properties, they can be divided in thermal conductivity, optical and mechanic properties.

The most important characteristic that identifies silica aerogels, is their very low thermal conductivity, typically on the order of 0.015 Wm^{-1}K^{-1}, that identifies these materials as the best known insulating products [75]. This property leads the use of silica aerogels in various applications: from electronic, for example, to space and military ones.
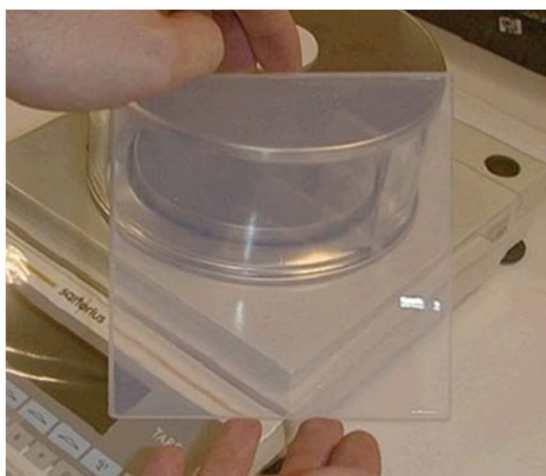
Figure 9 Silica aerogel after supercritical drying [76]

Regarding optical characteristics, silica aerogels have the particularity to be transparent; property that, if combined with thermal conduction, can allow the use of this particular porous material for windows production, and, more in general, in architectural applications.

Mechanical properties of these class of materials are various, because, depending on the synthesis and precursors, they can change dramatically: compressive strength, tensile strength, and elastic modulus depends on the density and the network structure of the aerogel. They can, in fact, be elastically compressed mirroring rubber-like flexibility, but can also be very brittle, depending on the internal porous structure [76]. Silica aerogels are, in fact, good candidates for shock impedance materials to confine plasmas, or support materials for the study of mixing of fluids that requires X-rays-induced shocks. In Table 2 all the most important structural properties of silica-based aerogels are reported.

Table 2 Summary of important properties of SiO$_2$ aerogels [72]

Property	Range	Typical value
Bulk density [g/cm^3]	0.003-0.500	0.1
Skeletal density [g/cm^3]	1.700-2.100	
Porosity [%]	80-99.8	
Mean pore diameter [nm]	20-150	
Specific surface area [m^2/g]	100-1600	600

3.2.2 Organic aerogels

The most interesting alternative to purely inorganic aerogels is the porous material firstly developed by Pekala in 1987: a completely organic aerogel based on resorcinol and formaldehyde (RF aerogels). The main process of the synthesis is the polymerization of multifunctional organic monomers in a dilute solution, treated then with a supercritical drying.

RF aerogels were synthetized by polycondensation of resorcinol and formaldehyde in aqueous solution using a basic or acid catalyst. Initially the two precursors are mixed together with an appropriate molar ratio with the addition of the catalyst (generally a basic, and rarely an acid one). The obtained solution is heated to form a wet stable and cross-linked gel. It was, subsequently, solvent exchanged with a desired organic solvent suitable both for the removal of the gelling agent from the pores, and for the drying in supercritical conditions or by means of ambient pressure drying.

One of the key points in the RF aerogel synthesis is the pH of the initial solution, easy determined by the use of a basic or acid catalyst. Considering the base-catalyzed solution, it occurs in aqueous media with the addition of sodium carbonate or another similar reagent, whose gelation requires elevated temperatures for long times. The effect of the basic catalyst is to deprotonate the resorcinol anion, leading to a very reactive and unstable resorcinol monomer, that is able to react with another resorcinol molecule to form stable methylene bridge linkage, producing water/formaldehyde or water. After the gel formation, the liquid part is removed using one of the technique described later in this chapter and, then, a thermal process is done to obtain a carbon material. A summary of these reactions is depicted in Figure 10.
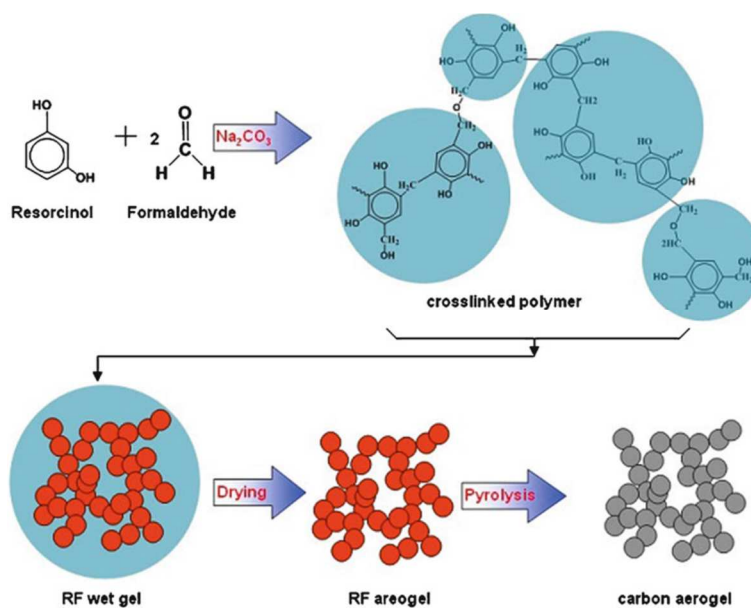
Figure 10 Reaction mechanisms occurring during RF aerogel synthesis.

The resorcinol-to-catalyst ration (R/C) is, in fact, a fundamental parameter for the structure and morphology of the final material. The ratio R/C typically varies from 50 to 300 if aqueous solutions are considered, and this influences in a significant way the final structure: if low R/C are used, particles with large empty regions for each other are formed, while, if the R/C is elevated, cross-linked microsphere can be synthetized. The pore size of base-catalyzed RF aerogels vary as a function of the R/C ratio in the range of 5-20 nm [76].

Also the pH of the solution characterizes the final pore structure and gelation time of the gel: lower is the pH, more important is the precipitation of precursors instead of the gel formation presenting particle sizing and voids between them.

Considering, instead, the rarely used acid-catalyzed reaction, one of the main reasons of its implementation, was the attempt to speed up the reaction more and more [77], [78]. While, during the base-catalyzed reaction the process time can extend from few days to weeks, using an acid catalyst, this time can be significantly reduced. Despite of this, few reports and few studies are present on this topic. From performed studies, the most important aerogel characteristic that changes, varying the pH nature of the catalyst, is the morphology. The specific surface area of aerogels synthetized via basic materials is relatively high (about 800m^2/g), while

their competitors present a value around 300 m^2/g. The pore diameters, instead, are not so interested by the catalyst change: in both cases it is on the order of 10-20 nm.

Because of the RF aerogels were the first synthetized, they became the symbol of the organic aerogels, but, more the research advances, more the types of used materials increased. Subsequently, formaldehyde resins, such as phenol-formaldehyde, melamine-formaldehyde, were accompanied with polyimides, polyacrylamides, polystyrenes, etc. for preparing organic aerogels [79]

RF aerogels, and more generally organic based aerogels, are attractive as precursors for carbon aerogels.

Carbon aerogels are obtained from the pyrolysis of organic aerogels under inert atmosphere at temperatures above 500 °C, in order to generate an electrically conductive network. Processes occurring during the pyrolysis are essentially the preservation of the high specific surface area and the large specific mesopore volume, together with a shrinkage in the volume. Carbon aerogels can be applied as electrodes for super-capacitors, fuel cells or batteries, for example.

3.2.3   Composite aerogels

When molecules or fundamental block of organic aerogels are combined with structural elements typical of ceramic materials, composite aerogels are derived. Motivations that prompted researchers to modify oxide materials with organic groups are several, but they can be summarized in the amplification of the properties spectrum of the obtained material, and in the limitation of the shrinkage and cracking occurring during drying of wet inorganic gels.

There are different techniques to synthetize composite aerogels, but the more general route is the integration of the organic compounds directly in the sol-gel process, even if it is not always a simple way. If organic molecules are embedded into the inorganic matrix without any chemicals, achieved by dissolving molecules in the precursor solution, they can be washed out from the gel, during the supercritical drying process. The only success was observed when, using poly(2-vinylpyridine) for example, the inorganic matrix and the organic compound remained mixed thanks to the formation of hydrogen bonds on the surface of the inorganic compound [80].

Considering that the most studied inorganic aerogel is the silica based, also in the composite field, silica remains the most investigated ones.

Schwertfeger et al. [81], [82] modified the silica aerogels with the addition, during the sol-gel synthesis of an organic compound. They modified the inner surface of the aerogel without modifying the characteristic properties of the starting material: the performed process was a sort of core-shell structure formation around the aerogel. This process, confirmed by Raman spectroscopy, increases the application possibilities of silica aerogels, because their chemical properties can be properly tuned, choosing the organic compound or simply its amount.

Organic modifications of silica aerogels can change the optical properties of the porous material, allowing the improvement of sol-gel glasses, the use of the material as abrasive-resistant coating, dielectric material, or a chemical or biochemical sensor [83] [84] [85].

3.3 Aerogel synthesis technique: the sol-gel process

The most used technique for the aerogel preparation is the sol-gel process, that involves a solid material synthesis performed in liquid solutions at low temperatures (typically lower than 100°C) [79].

The process can be divided into three main sub-processes: the preparation of the sol; the evolution of the sol, the transition to the gel and, at least, the gel aging.

- **Sol preparation:** "A sol is a stable suspension of colloidal solid particles within a liquid" [86]. In this way, the chemistry defines the starting point of the aerogel production.
  The sol preparation consists in the dispersion of precursors, that are starting compounds of the final material, into a solvent, typically water, with the addition of the catalyst. The solvent has also the function of the reaction media of the entire process, in which all the reactions occurs. The catalyst addition, trigger the sol-gel reaction between precursors, even if not always it is fundamental: in some cases, such as in the synthesis of natural aerogel discussed in this work, gelation occurs directly thanks to some properties of the precursors; in other cases, an external catalyst, that will be removed at the end of the synthesis, is necessary.

In a sol, in order to be stable, the solid particles, denser with respect to the surrounding liquid, must be small enough to guarantee that dispersion forces remain greater than the gravity one; only in this case the precipitate formation is avoided.

- **Sol-gel transition:** inside the sol, some chemical reactions occur leading to reactions between the inserted precursors. Depending on the nature of the precursors, different reactions take place: hydrolysis and condensation for mineral gels, and only condensation for organic ones.

  When chemical reactions are concluded, a gel is formed. It is "a porous 3-dimensionally interconnected solid network that expands in a stable fashion throughout a liquid medium and is only limited by the size of the container" [86].
  If the process occurred in a proper way, the viscosity of the sol increases, until it tends to infinite, forming the gel. The solvent is present all inside the mesh, composing the gel, and does not flow out spontaneously because it is in a thermodynamic equilibrium with the network.
  This moment at which the gel is formed, is called sol-gel transition.

- **Ageing:** during this process, four different processes can occur: polycondensation, syneresis, coarsening and phase transformation. Even if the viscosity of the sol increases a lot, up to the formation of the gel, polycondensation reactions continue as long as functional groups, involved in the process, remain accessible and un-reacted. Together with polycondensation, also syneresis occurs. This phenomenon is the spontaneous shrinkage of the gel and the expulsion of the liquid from pores. Coarsening, instead, is the decrease in surface area of the gel by dissolution and precipitation processes: precipitate can fill small pores, resulting in an increase in average pore size, but a decrease in surface area. Finally, a change in microstructure of the gel occurs when a phase transformation happens.

In Figure 11, a simplified chart of a typical sol-gel process is reported. Both the chemical and the natural paths are represented: they depend on the nature of the chosen precursors and from the possible addition of a chemical catalyst.
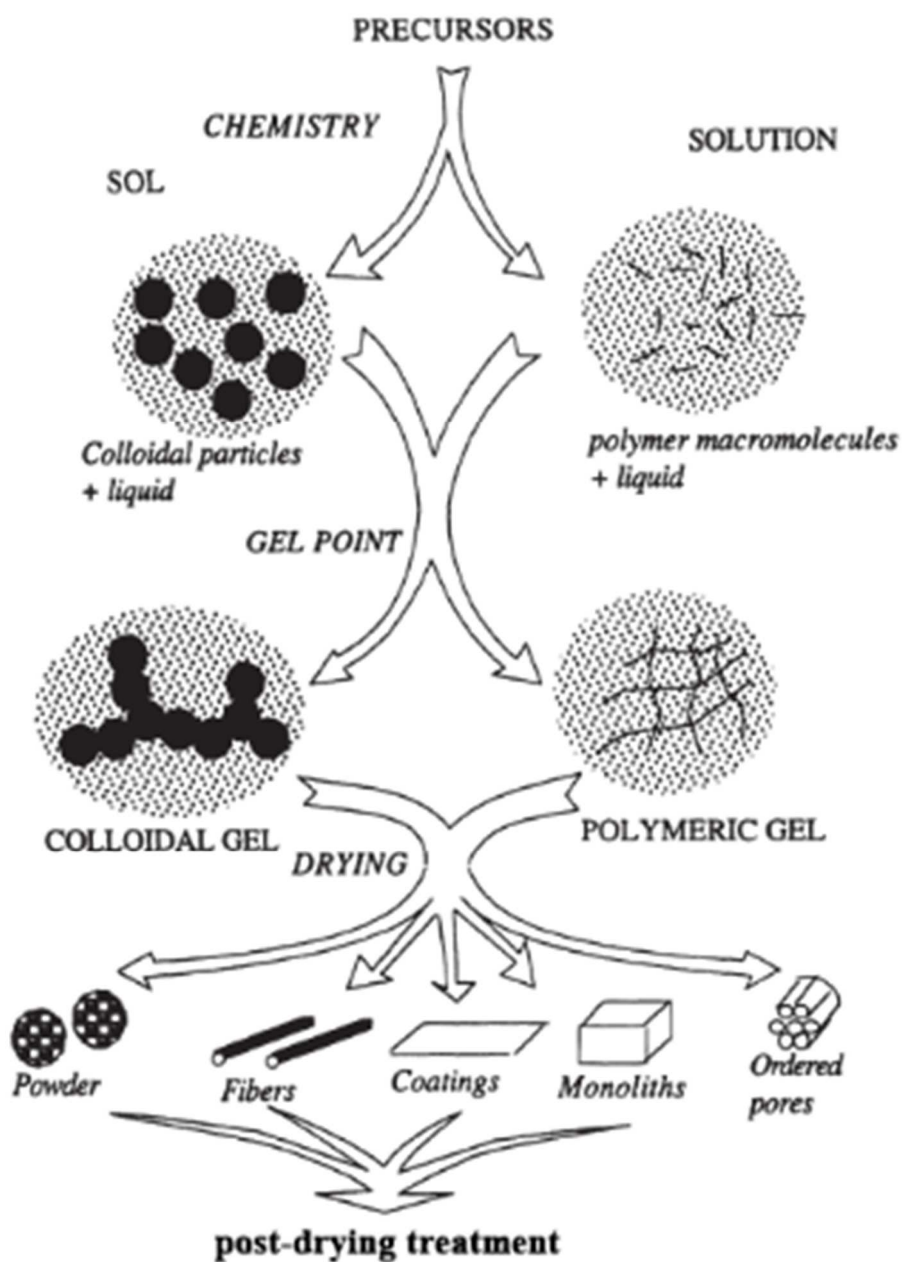
Figure 11 Simplified chart of the typical sol-gel process. Adapted from [86]

The structure of the gel obtained depends on some parameters that can be divided in intrinsic and extrinsic. Intrinsic parameters contain the choice of precursors of the synthesis, the nature of atoms and the complexity of molecules; extrinsic ones,

instead, are the processing conditions, such as the choice of the catalyst, the solvent, the concentration of precursors, pH, etc.

All these parameters vary the kinetic of the sol-gel process, changing the resulting properties of the porous material.

3.4 Liquid removal from gel: the drying process

The aerogel preparation step immediately following the sol-gel, is the drying. It is the process in which the liquid part, contained in the gel, is removed without collapsing the bone structure, leaving so the porosity of the material.

The extraction of the liquid from a wet gel is a complicated process and it is divided in some steps: firstly, the gel shrinks of a quantity equivalent to the amount of liquid contained in pores, that is moved from the inside to the surface. During this step, the structure of the gel becomes stiffer, but the surface tension increases due to the reduction of pore radius.

When the surface tension reaches its maximum value, the second step begins: it is the critical point. Here, the tension in the gel is so high that cracking and collapsing of the structure are possible and most of the liquid evaporates from the surface of the gel.
At the end, this liquid film on the surface is removed.

This process can be performed with different techniques: supercritical, freeze and ambient drying.

3.4.1   Supercritical drying

This is the most used drying technique and it was firstly exploited by Kistler for the first synthetized aerogel. This method prevents the formation of the liquid-vapour meniscus, responsible for possible collapsing and cracking of the structure during liquid removal. Supercritical drying is the best technique for gel drying, able to reduce surface tensions, leading to the recovery of the solid image of the wet gel.

The process consists in the heating of the wet gel in a closed autoclave, to overcome critical temperature (T_C) and critical pressure (p_c) of the liquid inside pores and maintained at these conditions for a certain time. The fluid is then vented, resulting

in a pressure drop. Supercritical conditions vary a lot depending on the chosen fluid, and most important values are summarized in Table 3.

Table 3 Critical values for most used fluid [72].

Solvent	T_C	p_c
Methanol	240 °C	7.9 Mpa
Ethanol	243 °C	6.3 Mpa
Acetone	235 °C	4.7 Mpa
2-propanol	235 °C	4.7 Mpa
H_2O	374 °C	22.1 Mpa
CO_2	31°C	7.3 Mpa
N_2O	37 °C	7.3 Mpa

From values reported in the above table, two different conditions can be identified. A hot process and a cold one.

Some of the cited fluids require, in order to reach their supercritical conditions, temperatures and pressure that are quite elevated. This bring to some problems due to high temperatures (above 250 °C), high pressures (5-8 Mpa) and flammability of the compound involved. The resulting materials from this process are generally hydrophobic, due to the coverage of the surface with alkoxy groups.

The opposite process, the cold one, is the most used, because it requires lower temperatures and lower pressures, leading to more safety operation conditions, and advantages in energy production balance. The most used fluid for this process is the liquid CO_2, because it combines low critical temperatures together with a not so high p_c. The supercritical drying path for this fluid is reported in Figure 12.
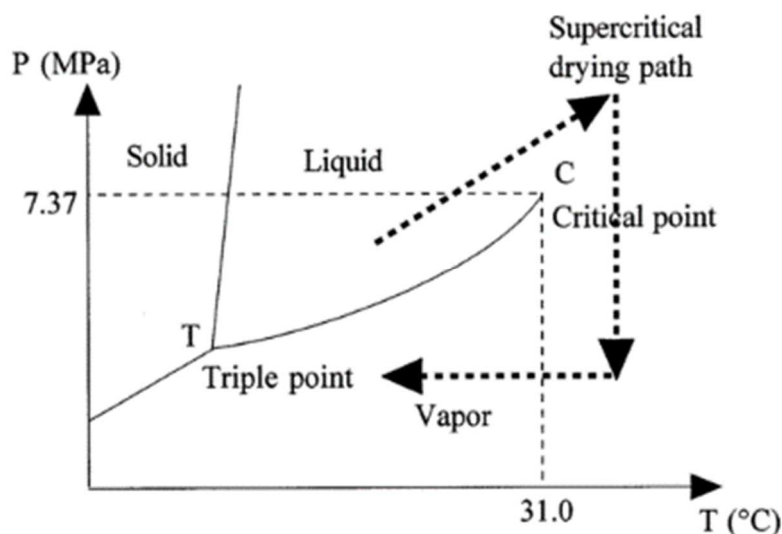
Figure 12 Supercritical drying path using CO_2 as extracting fluid [79]

The drawback of this technique is the time consuming solvent exchange: the substitution of the liquid inside pores of the structure with the CO_2 is a quite slow process, and it depends on the solubility of the fluid in the liquid solvent used for the synthesis and from the structure dimensions. Sometimes, the solvent exchange is compulsory to perform supercritical extraction using CO_2: the miscibility of the solvent with the used fluid is required; if water, for example, is used for the synthesis this step must be performed, because CO_2 is not soluble in water.

3.4.2 Freeze-drying

Another possibility largely used to avoid liquid-phase tension is the freeze-drying process.

This process requires the freezing of the liquid solvent used during the synthesis, that is subsequently sublimed by a vacuum pump. The most important requirement for this technique is the choice of the liquid solvent in the sol-gel process: it must have a freeze temperature not too low, otherwise the freezing is not reached. The solvent exchange is also required both to stabilize the gel structure, and to use a liquid having a low expansion coefficient and a high sublimation pressure. If the chosen liquid is not the correct one, the destruction of the 3D network may occur due to the crystallization of the liquid inside the pores.

Materials obtained with this technique can also be named cryogels.

3.4.3   Ambient pressure drying

The last possibility for the removal of the liquid part from wet gels is the ambient pressure drying. This process allows the creation of a xerogel, that is the other name of an aerogel in which the liquid component is removed by evaporation.

Considering that a gel consists of a solid network in which a liquid phase is entrapped in small pores, gas liquid interface is created if the material is leaved to air. Due to the presence of high surface tensions, in order to use this type of drying, the solid network of the gel must be strengthened, using a chemical modification of the surface during the initial synthesis of the gel. The critical aspects of the technique are the formation of capillary tensions inside pores that cause the collapse of the entire structure, and the elevate shrinkage. If the collapse can be avoided, the solid structure is maintained and large scale aerogel production can take rise, due to the simplicity of the process. In Figure 13 is reported a comparison between the material obtain through supercritical drying, called aerogel, and the one obtained through ambient drying, called xerogel: the shrinkage is elevated and the structure collapsed, reducing porosity and surface area.
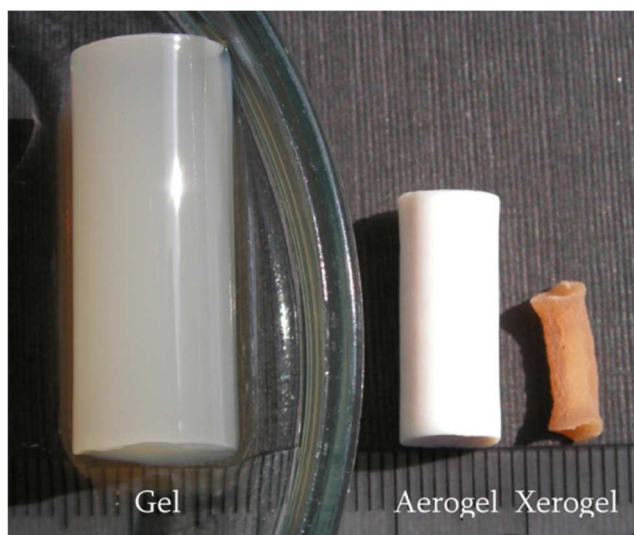
Figure 13 Comparison between a supercritical drying (aerogel) and ambient pressure drying (xerogel) [87]

3.5 Main properties of aerogels

Aerogels have a lot of different properties, that can also be tuned depending on the final target of the material.

Among all properties, such as optical, thermal, electrical and mechanical, there are some structural properties (e.g. porosity and specific surface area) of the material that are fundamental for having the material as an aerogel.

Concerning the porosity and the surface area of the material, some restrictions must be applied. Porosity, in fact, must be higher than 85% with a connected density lower than 0.8 g/cm^3 for carbon aerogels [72], that is why they are defined as lighter materials in the world. These interesting properties, allow the use of aerogels as filters, absorbing media for desiccation, waste absorbent or fuel storage [88].

Besides these structural properties, aerogels have a lot of other properties, depending on the type of aerogel synthetized, leading to the use of them in many fields.

As regards the thermal properties, silica aerogels, for example, are the best insulating materials due to their extremely low thermal conductivity [76]. This allows a variety of application of the material, including architectural purposes, piping automotive exhaust pipes.

Their transparency and their low refractive index values, among all the optical properties, allow their application in detectors, lightguides or special optical application due to the possibility to synthetize an aerogel with multiple compositions inside of it.

Carbon aerogels, instead, due to their synthesis process that requires a thermal treatment at high temperatures, are good candidate for electrical applications, because they are electrically conductive allowing the use as electrodes in batteries and capacitors. Considering, instead, metal oxide materials, they are excellent dielectrics, and they can be used in microwave electronics, in high voltage insulators and also in integrated circuit technology.

3.6 Post-drying treatments

After the complete removal of the liquid part from the wet gel, the obtained material is, definitely, called aerogel, if all the conditions previously described are satisfied. Some of its properties can be modified thanks to a series of post drying treatments: they can include both thermal and chemical processes.

3.6.1   Thermal treatments

The thermal treatment, depending on the organic or inorganic nature of the aerogel, is named in two different ways: calcination or pyrolysis.

From organic precursors, it is possible to obtain carbon aerogels by means of a thermal treatment in an inert atmosphere called pyrolysis or carbonization. During this step, the organic structure of the aerogel is transformed into a relatively pure carbon structure. Typically, a carbonization treatment is conducted under flow of inert gas (N_2, Ar or He) in a tubular furnace. At the beginning, the temperature is maintained at the room one, in order to ensure the complete substitution of the air present in the tube, with the inert atmosphere. After this, the temperature is raised up to values higher than 600 °C to complete the carbonization [89]. The final desired temperature is reached gradually, in order not to modify the aerogel structure.

Variations in pyrolysis conditions modify in a significant way structure and properties of the final carbon aerogel. Higher is the pyrolysis temperature, lower will be the surface area of carbon aerogel, for instance. This trend was observed for temperatures above 600°C; for temperatures lower that this value, the surface area increases increasing the temperature. Also the pore volume and the related density are strongly dependent from temperature: the pore volume decreases slightly, increasing the temperature, while the skeletal density (being the reciprocal of the pore volume) increases up to reach the one of graphite, if the treated temperature is above 1050 °C [90]. The main drawback of using a low pyrolysis temperature, is the electrical conductivity: carbon aerogels are not electrically conductive for temperatures below 750 °C, and so they are not usable as electrode in electrochemical cells, for example [67]. A good compromise must be found between high surface areas and good electrical properties.
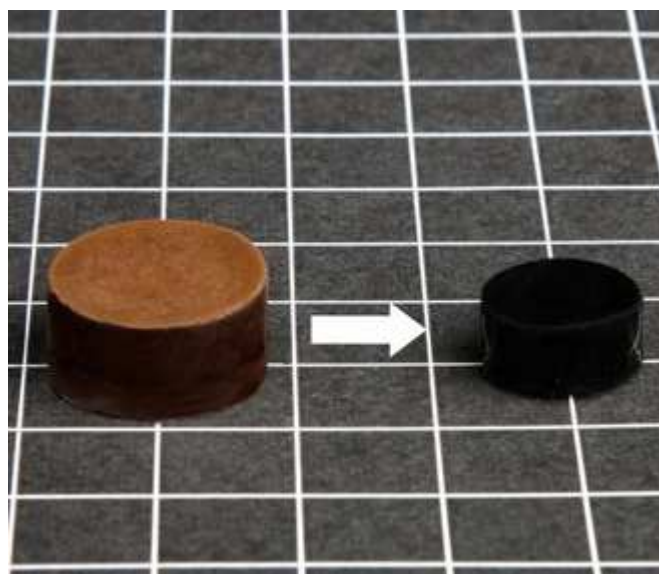
Figure 14 Example of RF aerogel, before and after the thermal treatment in inert condition. The result of the process is a carbon aerogel. Adapted from [91]

The other important process occurring during the pyrolysis is the weight loss connected to the shrinkage of the sample. The most significant weight decrease occurs only in the first part of the process: after a certain temperature, that varies from synthesis to synthesis, the loss of organic matter remains constant, and it is at this time that the real structural change takes place. The first endothermic reaction, occurring for temperatures lower than 250 °C, is the release of absorbed water, and correspond to a weight loss of about 3%. The other, more consistent, weight losses are attributed to the release of organic compound inserted during the synthesis, but not necessary for the final carbon structure. After these losses, only secondary reactions can occur, without a significant modification of the structure [76].

On the other hand, if the starting gel is an inorganic one, the thermal process is called calcination. In this case, the final aim of the treatment, is not the transformation of the aerogel in a carbon material, reaching graphitization, but it is the conversion of the metal precursor to a metal oxide aerogel. During the thermal process, performed in an air or oxygen flow, the organic content, if present, of the dried aerogel is burned, allowing the metal oxide precursor to transform in its final oxide. Also in this case, a first weight loss due to water content is present, like in the previous case, but here the most consistent loss is due to the burn of the organic part, acting only as a support material for the oxide structure.

3.6.2 Chemical activation

Due to the widely use of aerogels in technologies thanks to their high surface area and high porosity, a post drying process able to increase and control the porosity of the final material is necessary and it is applied, especially, on carbon aerogels. The activation can be performed both physically and chemically. The physical one consists into the pyrolysis of carbon precursors in inert atmosphere, in order to remove all non-carbon compounds, followed by the activation in presence of oxidizing agents in a temperature range 600°C-1200°C.

Chemical activation, instead, is made by mixing carbon materials with chemical activation agents, followed by a carbonization at 400°C-900°C [92]. The result of this thermal process is a carbonaceous material with a much more ordered structure, with a more developed porosity, leading, in some cases, to values of specific surface areas over 3000m^2/g, and to large pore volumes constituted by a mix of micropores and mesopores.

This activation type is one of the most used techniques to increase the microporosity of the aerogel; final properties given to the resulting material depend on several process parameters, including the nature of the carbonaceous precursor, the activating agent, its concentration, pyrolysis temperature, gas flow rate, etc.

Several activating chemical agents were presented in literature [92], such as phosphoric acid, zinc chloride, alkaline metal compounds, and so on, but the most interesting one is a thermal process, driven by KOH.

The KOH activation treatment is one of the most known technique to open the pore network in carbon materials; despite of this, it is not completely clear how it works due to the large number and complexity of chemical reactions occurring in the process. At the beginning of the treatment, the KOH present in the solution reacts with a solid-solid reaction with the carbon material; later, the reaction is transformed into a solid-liquid interaction, resulting in the reduction of the potassium to metallic one and the oxidation of carbon into carbon oxide and carbonate.

Studying deeply the reaction, all the reactions occurring between the KOH solution and the carbon material [92]–[94] result into three main mechanisms:
1. etching of the carbon material thanks to redox reactions occurring between potassium compounds and the carbon framework;

2. formation of H_2O during the activation, that is useful for the development of the porosity through the gasification of carbon;
3. intercalation of metallic potassium into the carbon matrix, resulting into an expansion of matrix dimensions.

Chemical activation has some important advantages with respect to the physical one, such as a lower activation temperature, less process time, higher yields and high specific surface areas.

Together with advantages, also some important disadvantages must be considered. The use of chemical compounds, in fact, requires an important washing step because of the incorporation of chemical impurities in the structure that can modify chemical properties of the final activated aerogel, such as pH. Repeated washes are compulsory to restore a neutral pH to the material.

3.7 Polysaccharides based aerogels

Even if the most studied aerogel is the silica one, the biodegradability requirement for an increasingly number of applications, limits the use of this class of aerogels. A good alternative to overcome this problem is the synthesis of organic aerogels starting from biodegradable polymers, such as polysaccharides. The use of these natural compounds and their derivatives showed a lot of interest, due to their non-toxicity, stability, abundance in nature and renewability [95]. They can be used as solid matrices with different structures, such as monoliths or beads.

Polysaccharides are polymeric carbohydrate molecules composed of long chains of monosaccharide units bound together by glycosidic linkages.
Among all the polysaccharides present in nature, some of them were intensively studied: marine polysaccharides are one of the most attractive bio precursor for the synthesis of organic aerogels. Alginate, starch and agar are the most interesting, whose structural formula are reported in Figure 15.
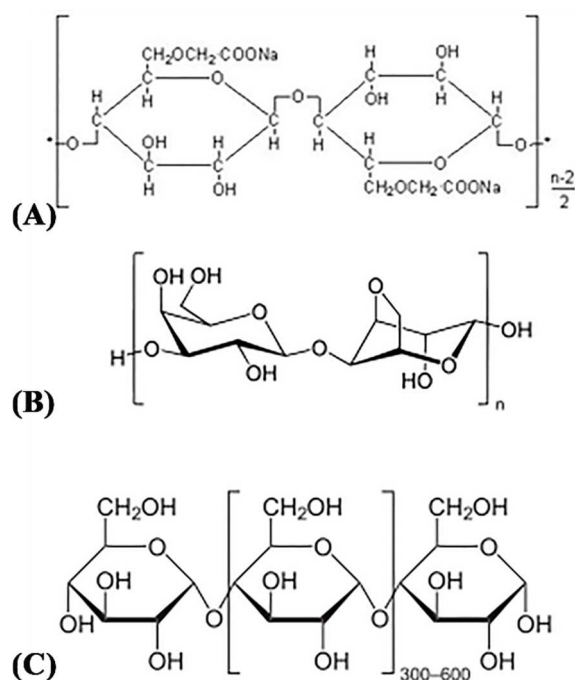
Figure 15 Structural formula of most used marine polysaccharides: (A) alginate, (B) agar and (C) starch

The synthesis of the aerogel starting from marine polysaccharides, follows the typical sol-gel process described in paragraph 3.3. In some cases, under certain conditions, depending on the precursors, the gelation process is induced directly by the polysaccharide molecules which interact through hydrogen bonds, leading a green and biodegradable synthesis: agar and starch are two of these.

The chosen marine compound is mixed with all necessary compounds, and then added to water to form the sol, thanks to its good solubility in this solvent. The formation of the gel occurs by heating the sol to spontaneously trigger the gelation process, or adding an external catalyst [87].

Alginate, for instance, produced by marine brown algae, is made of anionic uronic acids, which enable to cross-linking by the addition of cations. During the sol-gel process, in fact, the addition of bivalent cations (normally Ca^{2+}) allows the gelation of the sol [96].

Starch, instead, follows a gelation process divided into three main steps: swelling, characterized by water absorption in starch granules, gelatinization, that occurs when the previous solution is heated and, finally, the retrogradation step, in which the gel is cooled down and aged; in this step the aerogel structure is formed and it is followed by the reorganization and the partial recrystallization of polysaccharides molecules. Gelatinization temperature is the most important parameter which gives the structure to the final material: increasing the temperature, also the crystallinity, the rigidity and the density of the gel increases. If supercritical drying is chosen for this type of aerogel, the solvent exchange is needed to prevent the collapse of the structure and to increase the solubility of the CO_2 into the liquid solvent.

Agar aerogel preparation is similar to the starch one. Also in this case, the gelation of the sol is spontaneously activated by the heating of the solution to temperatures higher than 85°C. It occurs because, at T>85°C, agarose (one of the components of the agar) exists in a disordered random coil, that results, after cooling down, in a strong gel arranged in a double helix state. The heating of the solution is also needed to ensure the complete dissolution of the precursor in water.
A pyrolysis step, as described in paragraph 3.6 is required for all these organic aerogels based on polysaccharides.

Main properties of this biodegradable class of materials obtained with the most used polysaccharides as precursors are summarized in Table 4.

Table 4 Summary of most important properties of some examples of polysaccharide based aerogels [87]

Aerogel type	Density	Porosity	Surface area	Pore volume
Starch (from potato)	0.46 g/cm^3		72 m^2/g	0.47 cm^3/g
Starch (from corn)	0.34 g/cm^3		90 m^2/g	0.37 cm^3/g
Alginate monolith	0.13 g/cm^3		150-300 m^2/g	1.9 cm^3/g
Alginate beads		99%	300-580 m^2/g	1.1-1.2 cm^3/g
Agar		89%	320 m^2/g	0.3 cm^3/g

Chapter 4
Fluid dynamic modelling for MFC architecture optimization

4.1 Introduction

Understanding what really happens inside a Microbial Fuel Cell during operating is one of the key points for the development of new architectures and for the optimization of the device. To achieve this aim, modelling is a good instrument to study MFC in all its parts, trying to predict its performances.

To completely describe a MFC, an operational building block scheme must be considered (Figure 16). Due to the complexity of the device, it can be summarized in four different processes and contributions: the movement of fluids inside the reactor chamber, governed by laminar flow; the diffusion of the entering chemicals and nutrients; all the processes occurring in contact with the porous electrode and all the biological reactions leading the operation of the MFC.
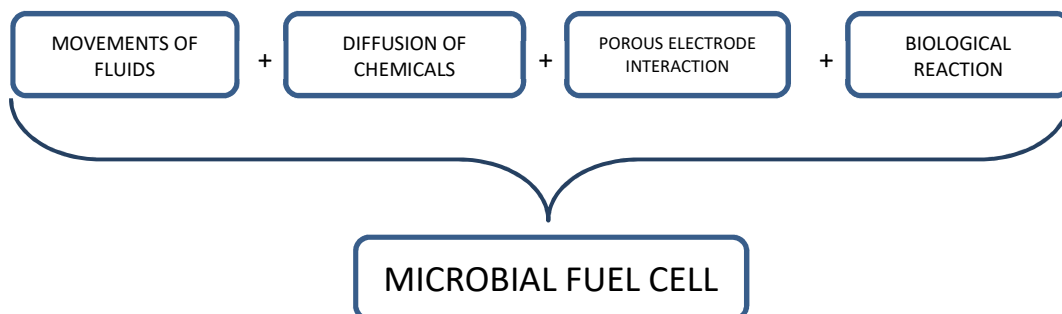
Figure 16 Building block of a MFC

There is a substantial lack of information about the effective role of fluidics in determining the final behavior of MFCs. It is well known in the literature that the device architecture deeply influences the performance of the device. Nevertheless, a systematic investigation of the importance of basic fluidic processes as the substrate drift and diffusion on the processes occurring inside the MFCs is completely missing. For this reason, in this work, the attention has been focused only on the fluidic aspect of the entire reactor, studying the first and the second contributes in the building block. The electrical interface of the electrode, and in particular the interaction between microorganisms and the external surface of the electrode need to be described by an electronic approach, which is not treatable with a fluidic study. Biological mechanisms were already treated and simulated in other works in the literature [97][98].

4.2 Fluid distribution

The MFC can be considered a fluidic device, because its internal regions are filled with an aqueous solution, containing all the substrates and nutrients needed for biofilm formation and maintenance.

A preliminary consideration about some important parameters describing the fluid, is necessary to build up the entire study: these parameters are the Reynolds number (R_e) and the Mach number.[99]

The Reynolds number is a dimensionless quantity very important for fluid-dynamics, because it is used to predict the characteristic of the studied flow. It is a good criterion to distinct the laminar flow from the turbulent one, depending on its value: laminar flow occurs for low Reynolds numbers ($R_e<2300$) and the resulting flow is smooth and constant without mixing of particles of neighboring fluid, if present; turbulent flux, instead, occurs for high values of R_e ($R_e >4000$) and it is characterized by a chaotic and whirling fluid movement with instabilities due to random variation of the velocity and pressure [100]. The transition value from one flow to the other is defined critical Reynolds number, and varies depending on some experimental parameter, such as the geometry of the flow region.

The Reynolds number, whose expression is reported in Eqn. (16), is defined as the ratio between inertial forces and viscous ones present in the fluid.

$$R_e = \frac{\rho \cdot v \cdot D_e}{\mu} \qquad (16)$$

where ρ is the density of the fluid $(\frac{kg}{m^3})$, v is the fluid velocity $(\frac{m}{s})$, D_e is the equivalent fluidic diameter or the characteristic fluid length (m), and μ is the dynamic viscosity of the fluid $(Pa \cdot s)$.

When the fluid region is not a tubular channel, in which the characteristic length is simple to be defined, the equivalent characteristic diameter D_e is introduced. For a rectangular cavity, as in the case of MFCs, it is defined as

$$D_e = \frac{2 \cdot a \cdot b}{a + b} \qquad (17)$$

where a and b are the dimensions of the cross-section area of the region.

In our case, considering the typical values of flow rates used in experiments, the typical dimensions of lab-scale MFC and fluid velocity, the Reynolds number is very smaller than 1, ensuring the laminar characteristic of the flow.

The other important parameter to fully describe a fluid, is the Mach number, that defines the incompressibility of the flow. An incompressible flow is defined as a flow in which the density of each fluid particle remains constant in time. If this condition is not satisfied, the flow is defined compressible. The Mach number is the discrimination parameter to distinct the two conditions. Liquids, due to their intrinsic properties, are generally considered incompressible [99], [101].

Considering these fluid characteristics, the general description of the movement of incompressible fluid inside a square cavity, with very small variation in the fluid temperature, can be studied by the Newton second law. Exploiting this relation using a vector form, the Navier-Stokes equation for a three-dimensional fluid is obtained, and it is reported in Eqn. (18) [102].

$$\rho \left(\frac{\partial v}{\partial t} + v \cdot \nabla v \right) = -\nabla p + \nabla \cdot \left(\mu (\nabla v + (\nabla v)^T) - \frac{2}{3} \mu (\nabla \cdot v) I \right) + F \qquad (18)$$

where v is the flow velocity of the fluid, indirectly dependent on the external pump, p is the pressure of the fluid, ρ is the fluid density and μ the fluid viscosity.

The left-term corresponds to the momentum balance and in particular to the change of momentum $\rho \frac{Dv}{Dt}$ of the particles. The right side of Eqn. (18) is the sum of the contribution of the pressure $(-\nabla p)$, the viscous forces $\left[\nabla \cdot \left(\mu(\nabla v + (\nabla v)^T) - \frac{2}{3}\mu(\nabla \cdot v)I \right) \right]$ and all the external forces applied to the system (F).

The Navier-Stokes equation, representing the conservation of the momentum, in order to be solved, must be coupled with its boundary condition, representing the conservation of mass, and expressed as:

$$\frac{\partial \rho}{\partial t} + \nabla \cdot (\rho v) = 0 \tag{19}$$

In our case, a simplification of the equation can be done considering the flow regime. Considering that, as introduced before, the liquid is incompressible, the boundary equation (Eqn.(19)) can be simplified as follow:

$$\nabla \cdot v = 0 \tag{20}$$

Inserting the boundary condition in the Navier-Stokes equation, the term $\left[-\frac{2}{3}\mu(\nabla \cdot v)I \right]$ can be neglected.

Considering also the low Reynolds number associated to our setup, the contribution of inertial forces is very small compared to the one of viscous one, and so can be excluded.

Therefore, not considering the gravity force contribution contained in the F term into Eqn.(18), the reduced Navier-Stokes equation to be solved for the study of fluid motion inside the cell, results in:

$$0 = -\nabla p + \mu\nabla^2 v \tag{21}$$

4.3 Diffusion of species in the reactor chamber

When two liquids with different concentrations of miscible species are put in contact, a diffusion process takes place, and the concentration of the species evolves following the Fick's law [103].

Considering, primarily, a steady-state condition, the molar flux of species into the solution is proportional to the concentration gradient present along one considered direction inside the chamber. In mathematical form, this may be written as:

$$J_i = -D_i \nabla c_i \qquad (22)$$

where, J_i is the molar flux for species i, D_i is its diffusion coefficient and c_i is its concentration.

Moreover, considering continuity equations for the mass balance, expressed as $\frac{\partial c_i}{\partial t} + \nabla \cdot N_i = 0$, the second Fick's law can be derived. This equation considers, in a more specific way, the evolution of the concentration of the analyzed species, taking into account volume variations due to an in-out flow.

To ensure the linearity of the mass transport equation, the independence of the diffusion coefficient from several parameters, especially the temperature and pressure, must be assumed.

Considering all the assumptions described, the second Fick's law can be written as:

$$\frac{\partial c_i}{\partial t} = D_i \nabla^2 c_i \qquad (23)$$

If a moving fluid is also present, also the advection contribute becomes much more important. Therefore, the classical diffusion equations to be solved, to predict diffusion of interested species, become a combination of both advection and diffusion contribution. The governing equations are:

$$J_i = -D_i \nabla c_i + c_i v \qquad (24)$$

$$\frac{\partial c_i}{\partial t} + \nabla \cdot N_i = R_i \qquad (25)$$

where the term R_i is a reaction rate expression, taking into account all the chemical reactions occurring inside the reactor.

Combining equation (24) and (25), the general equation for advection-diffusion becomes

$$\frac{\partial c_i}{\partial t} = \nabla \cdot (D_i \nabla c_i) - \nabla \cdot (v c) + R_i \qquad (26)$$

The term on the left corresponds to the variation in time of the concentration of the interested species, and it is a sort of accumulation term; in the right part of the mass balance equation (Eqn (26)), the term $[\nabla \cdot (D_i \nabla c_i)]$ describes the diffusion transport of the species taking into account interactions between the dilute species and the solvent: where the concentration is higher with respect to the surroundings areas, the substance will diffuse out, and the concentration will decrease, and vice versa.

The term $\nabla \cdot (v c)$ describes advection (or convection) due to the flux velocity v, obtained from the fluid flow simulation. The last contribution R_i takes into account the creation or the destruction of a quantity of species due to a chemical reaction.

Because of the Navier Stokes equation (Eqn. (18)) is the algebraic sum of coupled nonlinear partial derivatives, and for the presence of nonlinear terms, analytical methods are not able to give appropriate solutions.

The system was implemented in an iterative numerical model using the COMSOL™ multiphysics software, and, in particular, the Computational Fluid Dynamics (CFD) module.

The geometry was developed using Solidworks® software and, then, imported into the COMSOL™ environment and used for the simulation.

To build up the simulation, the mesh and boundary conditions are needed. To better discretize the geometry, a tetrahedral grid was generated, with a maximum element

size of 1.15 mm, optimized for fluid-dynamics applications for the inner part, where the fluid really flows, while the external geometry, not involved in fluid simulation, was meshed with a less fine grid.

Because of the governing equations form a partial differential system, in order to find an appropriate solution, a set of boundary condition was needed. First of all, a condition at the walls of the geometry must be considered. In particular, in our case, a no-slip condition was applied: it means that the fluid at the wall generally assumes the same velocity of the wall itself; fixing the wall velocity to zero, also the fluid velocity in that point is zero. In the equations system this condition is identified by Eqn. (20).

The second parameter on which a boundary condition must be applied is the pressure: in our case, the atmospheric pressure, equal to 1 atm, was applied both at the inlet and at the outlet.

The last one to be taken into account is the temperature: for the entire geometry and setup, the temperature was fixed equal to 25°C, in order to avoid properties variation during the simulation due to temperature oscillations.

In order to use the same parameters for all the simulated flow rates, a time step of 0.01 s was used to be sure that, even in the case of high values of inflow velocity, the time discretization was the right one to be able to study the real particle trajectories, without loose some parts of the movement due to a too high time step.

4.4 Results and discussion

Up to now, our research group used a double chamber MFC based on a circular shape [54]. From a fluidic point of view, the circular shape is not optimized for fluid movements or for the maximization of the exchanged area of fluid in contact with the electrode.
Circular cells were used in continuous operation mode, ensured using a peristaltic pump, to guarantee fluid movement both in the anodic and in the cathodic chamber. Even if the inlet and the outlet were placed one on the top and the other on the bottom of the device, both along the diameter of the chamber, in order to maximize the fluid path, the exchanged area using this geometry is just above the 50% of the entire exposed planar surface of the electrode.

To try to improve performances of the device, increasing the effective exchanged area, a new geometry was implemented. The proposed geometry is a squared reacting chamber, with both the inlet and the outlet on the same plane if considering the z-direction (where the z axes is the one describing the thickness of the chamber), but not symmetric in the x-y plane. This asymmetry creates a bigger area inside the chamber in which the fluid is moving, because the minimum fluidic path that particles have to tread is bigger with respect to the previous geometry or, in general, with respect to a geometry in which the fluidic connections are aligned.

A summary of the used geometry in this work is reported in Figure 17.
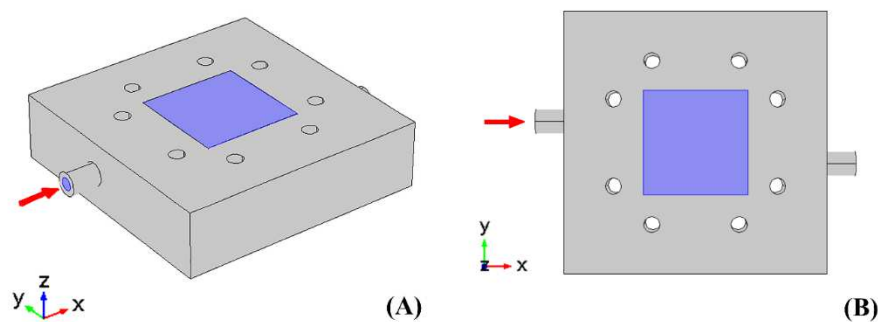
Figure 17 Geometry of the intermediate part of the square shape MFC used in the simulation. Orthogonal view (A) and x-y plane (B)

Considering this new geometry, simulations were implemented using different values of flow rates to compare fluid distributions inside the reactor, to correlate this parameter with the output of the device. Values of the tested flow rates were chosen considering the total volume of the internal chamber of the cell (12.5 ml, in our case), and a representative operation time of the device fixed at 1 hour. Subsequent flow rate values were chosen as multiple of the internal volume of the cell, in order to have a fixed number of total fluid exchange in the chosen operation time.

Tested flow rates were: $12.5 \frac{ml}{h}$, $25 \frac{ml}{h}$, $50 \frac{ml}{h}$ and $100 \frac{ml}{h}$. Results obtained using Navier-Stokes equation, were used as input parameters for the concentration gradient evaluation inside the MFC reaction chamber, using a diffusion coefficient of sodium acetate in water of $1.2 \cdot 10^{-9} \frac{m^2}{s}$. [104]

The geometry model used in this work represents only the real volume in which the liquid can move (excluding the two regions occupied by electrodes); on the top and on the bottom of the geometry reported in Figure 17, the cathodic and the anodic chamber, respectively, were placed. Here it is possible to appreciate the inlet and the outlet of the volume, representing the inlet and the outlet of the total MFC device tested in laboratory, with an inner diameter of 3 mm.

The used mesh for fluid simulation, instead, is reported in Figure 18
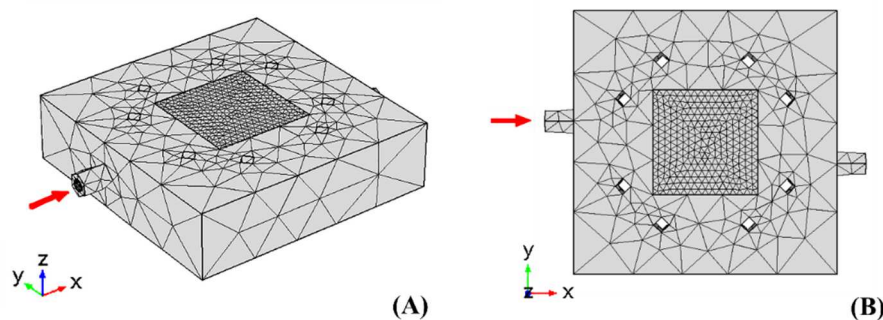
Figure 18 Used mesh during simulation in COMSOL. Orthogonal view (A) and planar view (B)

In order to gain quantitative information from the simulation, some important parameters, such as the particle trajectory, the effective area interested in the liquid replacement, the concentration gradient profile and the value of the concentration in some key-points of the chamber were taken into account.

4.4.1 Trajectories profile and areas analysis

To compare the effects of different flow rates, plots of the effective regions in which particles are moving are compared, and results are reported in Figure 19.

The cell, at time t=0 (Figure 19-A), is initially filled with water.
The figure also shows how the fluid particles are distributed after a complete fluid replacement for each flow rate. The analysis was carried out considering the top view of the cell, from which it is possible to appreciate the maximum exchanged area. From the considered trajectories picture, it is possible to evaluate how the

particle velocity changes, not only in the two channels, that is connected to the imposed input flow rate, but, more significantly, inside the chamber. The main flux occurs on the diagonal between the inlet and the output, but all around this direction, the velocity profile changes, leading differences in occupied areas.

Also the area of the chamber interested by the fluid exchange varies changing the flow rate. The fluid distribution, increasing the inlet velocity, moves towards the right of the chamber, reducing the effective area interested by the fluid turnover.

So, the fluid distribution inside the cell depends both on the geometry of the reactor, both on the inlet flow rate.
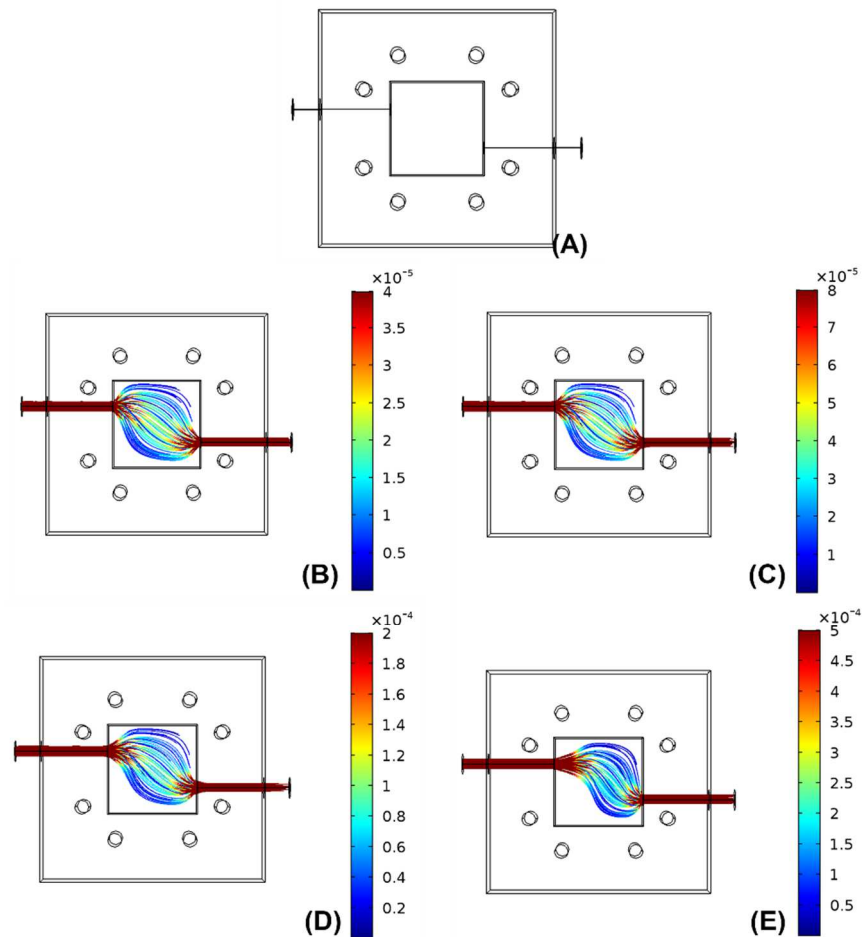
Figure 19 Trajectories profiles inside the cell at time zero (A) and after one complete fluid exchange for each flow rate: 12.5 ml/h (B), 25 ml/h (C), 50 ml/h (D) and 100 ml/h (E)

Fluid dynamic modelling for MFC architecture optimization

As said before, from the above images it is possible to appreciate the percentage of area variation as a function of the flow rate. In order to quantify the areas occupation, a numerical analysis must be performed, and results are reported in the graph in Figure 20.
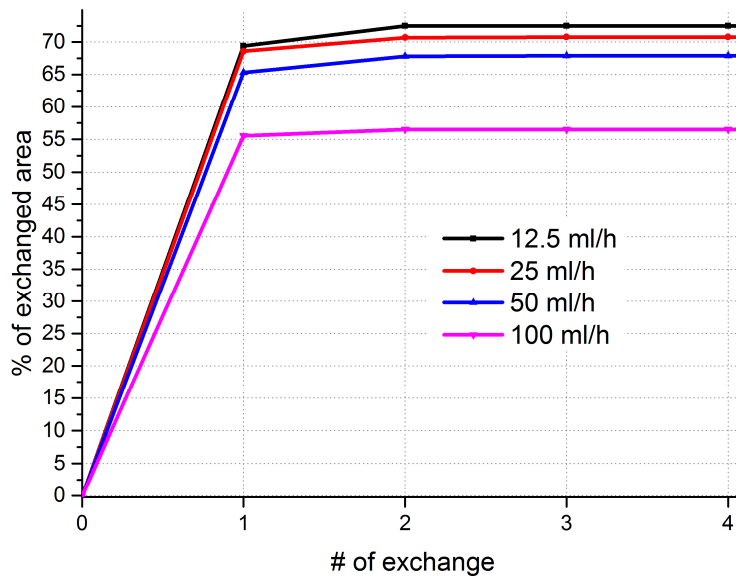
Figure 20 Percentage of exchanged area as a function of the number of compete fluid exchange in the chamber for each tested flow rate

The interesting event, appreciable from the above graph, is that the percentage of the area interested by the fluid motion, after 3 complete exchanges, remains constant to its saturated value, above 65% for all the three slower flow rates (12.5 ml/h, 25 ml/h, 50 ml/h). Considering, instead, the highest flow rate (100 ml/h), the total exchanged area saturates to a percentage value lower with respect to all the others, around 55%. It is due to the high inlet velocity that produces a big asymmetry with respect to the inlet/outlet direction of the fluid distribution. The consequence of a smaller area exchanged is the presence of bigger regions in which the fluid does not move, or it moves with a very slow velocity.

If the attention of the study is focused only after 1 exchange, areas exchanged for flow rates bigger than 25 ml/h vary in the same way, reaching around 65% of the total area. Considering the slowest flow rate, instead, the slope of the associated

curve is a little bit smaller, due to a smaller percentage of area value reached. Percentages of area exchanged are summarized in Table 5.

Table 5 Percentages of exchanged area of the cell after one complete fluid exchange for the simulated flow rates

	12.5 ml/h	25 ml/h	50 ml/h	100 ml/h
% of exchanged area after 1 complete fluid exchange	69.4 %	68.6 %	65.3 %	55.6 %

After having studied the distribution after 1 complete exchange, the analysis was extended up to 1 hour of continuous operation of the device, in order to do some consideration about the area. Images reporting particle trajectories for all the simulated flow rates are summarized in Figure 21

Fluid dynamic modelling for MFC architecture optimization
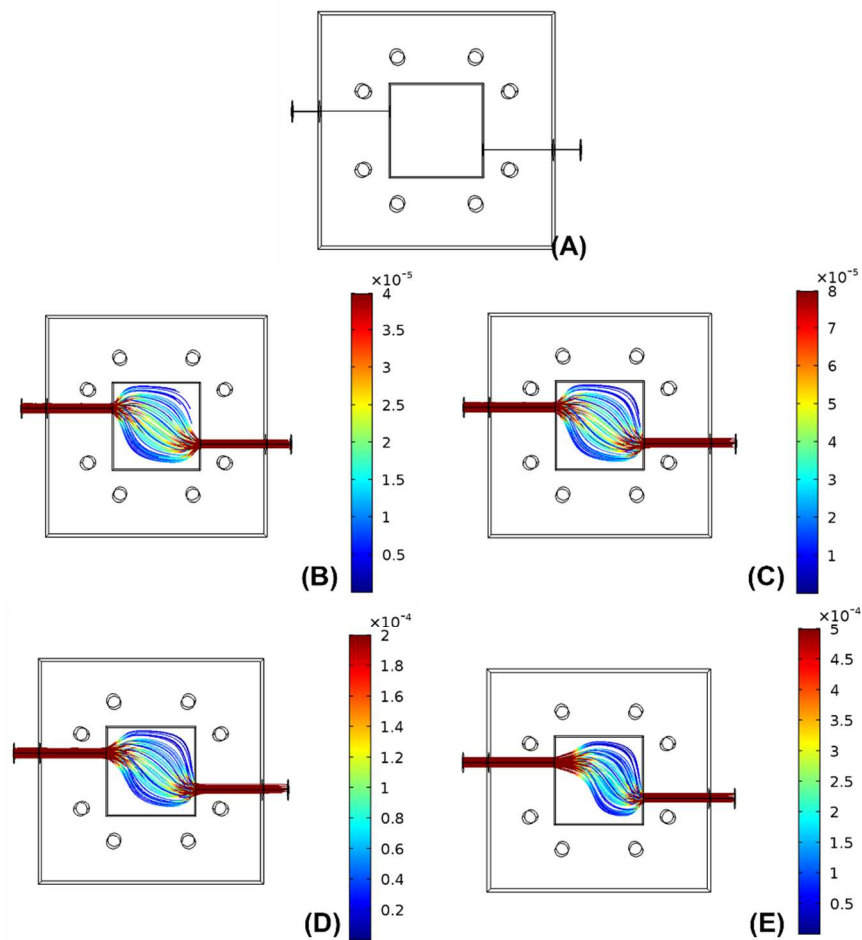
Figure 21 Trajectories profiles inside the cell at time zero (A) and after 1 hour for each flow rate: 12.5 ml/h (B), 25 ml/h (C), 50 ml/h (D) and 100 ml/h (E)

The above figure shows the particle profile after 1 hour of flux, simulating the real operation of the MFC. Also in this case, only looking at the images, the behavior of the exchanged region is similar to the previous case: increasing the flow velocity at the input, the turnover area decreases. Also in this case, as previously done, a numerical evaluation of regions affected by fluid movement was performed, and reported in the Figure 22. Results are reported for a time up to 4 hours to better understand the behavior.
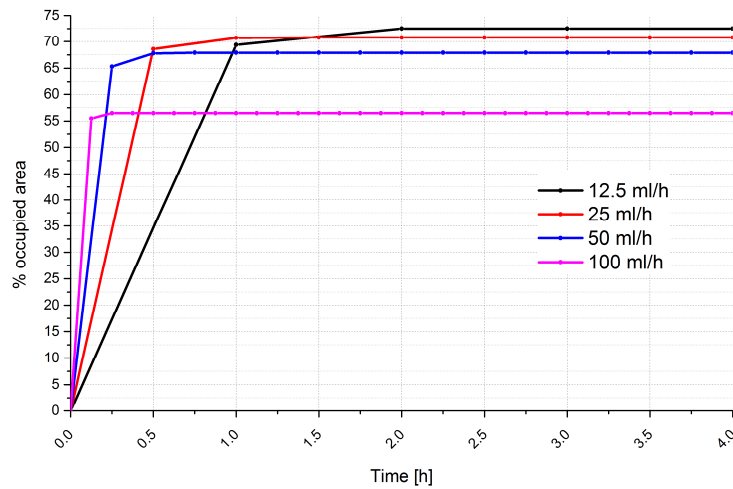
Figure 22 Percentage of exchanged area as a function of the simulation time for each tested flow rate

In this case, considering the percentage of area as a function of the simulation time, the behavior is different from the previous graph.

Increasing the flow rate, the time needed to reach the saturation value decreases significantly: 2 hours for the 12.5 ml/h case, compared to 30 minutes for the fastest flow rate.

Graph in Figure 22 confirms that, increasing the flow rate, the amount of area interested by the fluid turnover decreases, passing from 72% to 56%.

This result permits to distinct different application of the SC-MFC. Faster is the reaching of the saturation of the concentration, faster could be the detection of the nutrient's concentration, useful if the aim of the device is the COD detection, in which the detection of small quantity of the new concentration is required as fast as possible.

If power maximization, instead, is the target application, a maximization of the exchanged area must be reached.

4.4.2 Concentration profile inside the SC-MFC

The simulation of the concentration behavior was set up using the "Transport of Diluted Species" module of the COMSOL® software. Simulation parameters such as flow rates, boundary conditions, mesh parameters, etc., were maintained fixed as for the trajectory study presented in the previous paragraph. New parameters that were added for this study are all the properties of the fluid used in SCMFC: a water based solution containing sodium acetate as the nutrient for microorganisms. The diffusion coefficient of the sodium acetate was fixed at $1.2 \cdot 10^{-9} \, m^2/s$ [104].

To better investigate how the solution is distributed inside the fluidic chamber as a function of the position and time, some planes were defined inside the reactor.

Considering the fluidic asymmetry of the cell geometry in the x-y plane with respect to position of the inlet and the outlet, and the actual distribution of the solution, 5 monitoring points were selected. In particular, as shown in Figure 23, one monitoring point is placed just after the inlet, another one just before the outlet, two are at corner regions where the flow is minimum and the last one is placed at the center of the chamber.

In the z direction, the cell is symmetric, with the inlet/outlet plane coinciding with the midsection of the reactor. As illustrated in the lateral view of the cell in Figure 23, naming h the total height of the chamber, z=h/2 is the midsection plane, z=0 is the interface between the liquid electrolyte and the biofilm, and z=h is the interface between the electrolyte and the cathode. The symmetry of the devices permits to simplify the fluidic model of the concentration trend since from a fluid dynamic point of view the two interfaces, at z=0 and z=h, are equivalent. Therefore, along z, two monitoring planes were chosen: the one at z=0 and the one at z=h/2. On both the considered two planes at different z values, all the five points were studied.

Fluid dynamic modelling for MFC architecture optimization
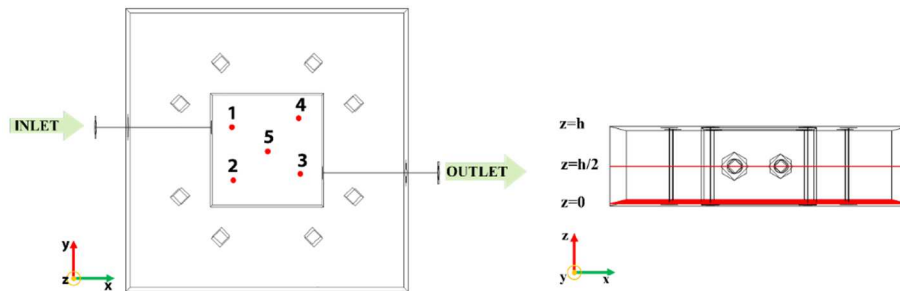
Figure 23 A map of the considered point during the study of concentration evolution in a square-shape SC-MFC, both in the x-y plane and along z direction

To better understand the diffusion of sodium acetate concentration into the SC-MFC, the concentration was analyzed at time frames relevant for the experiment: after 1 fluid turnover and after 1 hour of operation of the cell

A color map of the evolution of the concentration was exported both at the level located at *z=h/2* and at the interface between the electrolyte and the anode (*z=0*); results are reported in Figure 24 and Figure 25, respectively.
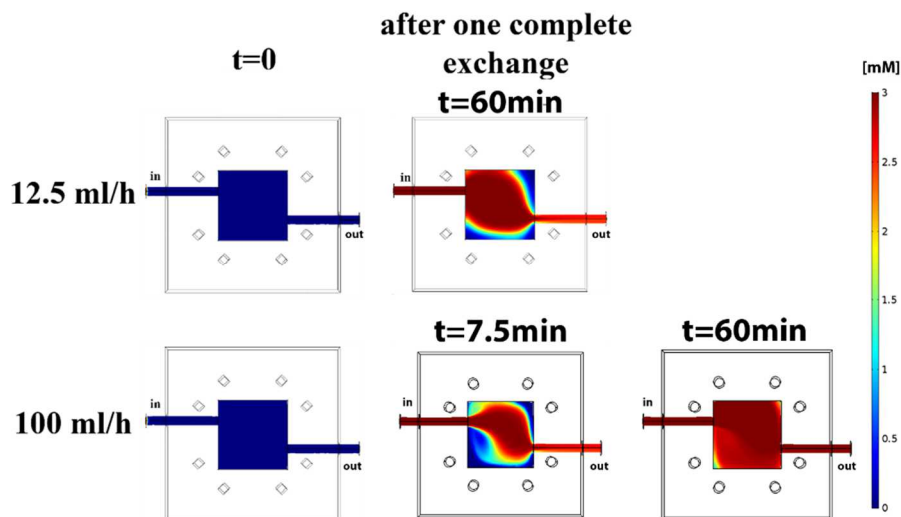
Figure 24 Concentration distribution at the beginning of the simulation, after 1 complete fluid exchange and after 1 hour of operation, evaluated at z=h/2

In Figure 24, the simulation for the middle plane is proposed. As expected the fresh solution enters the reactor chamber following the particle trajectories discussed in the previous paragraph (see Figure 19).

Being the particle trajectories very different for the two flow rates, also the distribution of sodium acetate concentration is quite different, both for the concentration values, both for the position.

The concentration of sodium acetate at the electrolyte/biofilm interface (i.e., z=0), is analyzed in Figure 25. Sodium acetate, entering at z=h/2, can reach the bottom interface by a drift process plus a diffusion one during the pumping phase that last one hour, and after that time only diffusion can occur: the concentration profile is therefore deeply influenced by the flow rate: higher is the flow rate, slower will be the diffusion, overshadowed by the drift contribution.
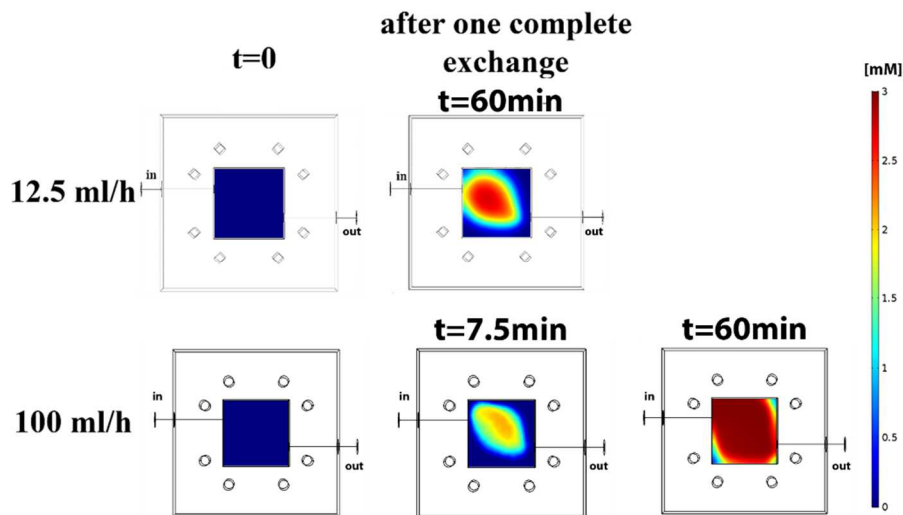
Figure 25 Concentration distribution at the beginning of the simulation, after 1 complete fluid exchange and after 1 hour of operation, evaluated at z=0

The concentration profile in all the analyzed points is reported in Figure 26 for 12.5 ml/h flow rate, and in Figure 27 for the 100 ml/h one. As it is possible to observe from the graphs, the effective concentration value is different among the selected points: considering the plane located at z=h/2, independently from the flow rate, the first region that saturates at the concentration of the fresh nutrient, is the one located in front of the input, while the slowest regions are a little bit different if the two

flow rates are considered. While in the 12.5 ml/h case, the regions where the concentration is lower are both the corners far away from the inlet/outlet characterized by a turnover process very slow, in the 100 ml/h case the slowest region is represented by only one of the two corners, confirming the asymmetry in the particle trajectory profile.

At the bottom interface, z=0, despite sodium acetate reaches its maximum value quite slower than in the midsection, the trend, is the same of the middle plane: the point in front of the input is the first that reaches the inlet concentration, and the remaining area of the chamber reaches a maximum concentration value, following particle trajectories.
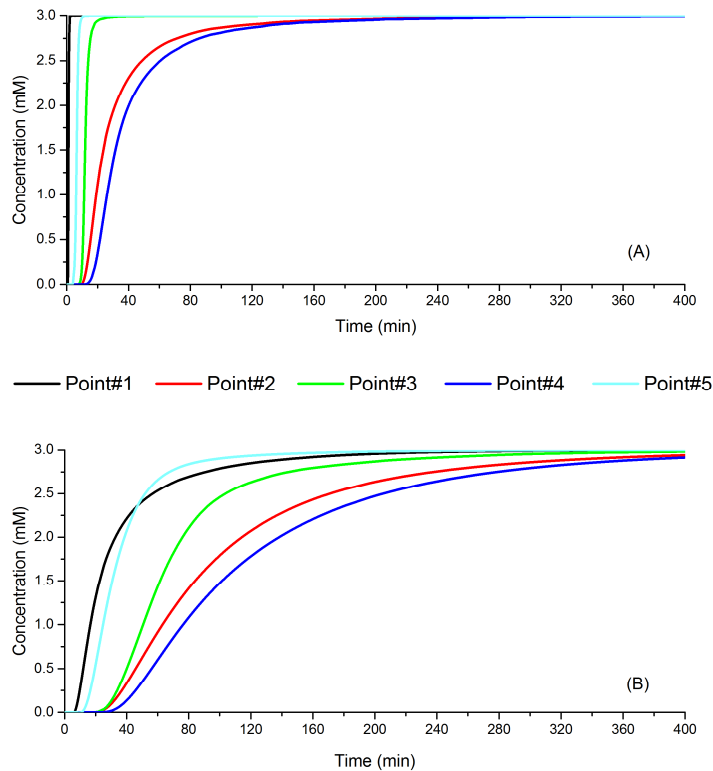
Figure 26 Concentration trend evaluated for a flow rate of 12.5 ml/h in 5 different points at the middle plane (A) and at the anode interface at z=0 (B)
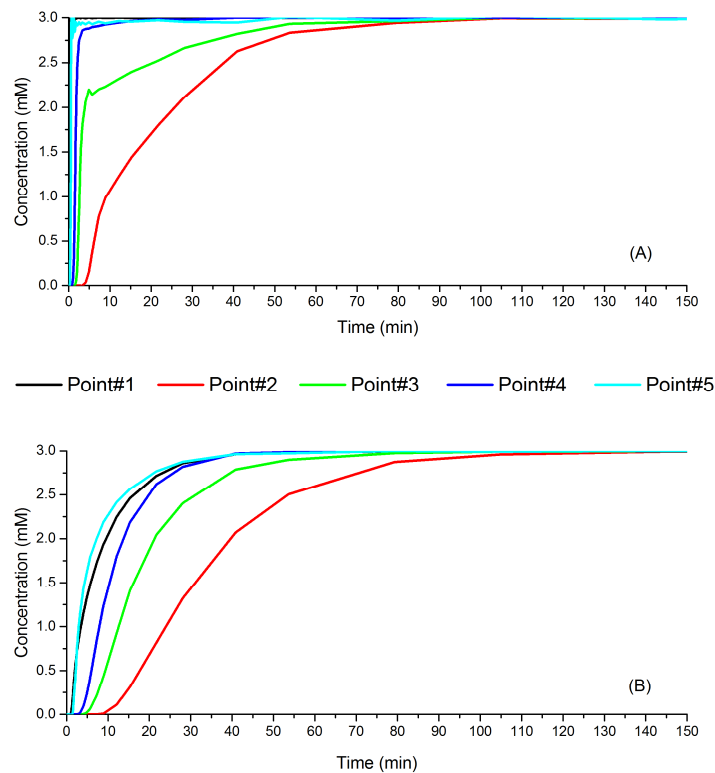
Figure 27 Concentration trend evaluated for a flow rate of 100 ml/h in 5 different points at the middle plane (A) and at the anode interface at z=0 (B)

4.5 Improved geometry for performance maximization

Starting from previous results, another possibility of application of MFC can be taken into account. If the aim of the MFC is, for example, the power production, higher is the exchanged area, bigger is the amount of microorganisms able to use the fresh nutrient, and higher will be the power produced. The best way to do this, is to improve the geometry, favoring the real shape that fluid creates while is moving. Analyzing trajectories reported in Figure 19, it is possible to notice that the internal region in which the particle velocity is significant, is only the one along the diagonal between the inlet and the outlet, forming a sort of drop shape. Exploiting this consideration, a new geometry was proposed to maximize the percentage of exchanged area: a drop like SC-MFC.

Cell dimensions and fluid volumes are comparable with the squared cell. Also for the drop like one, the total internal liquid volume is about 20 ml when the cell is completely empty without electrodes, while presents a volume of 10 ml of the intermediate fluid region in presence of electrode materials.
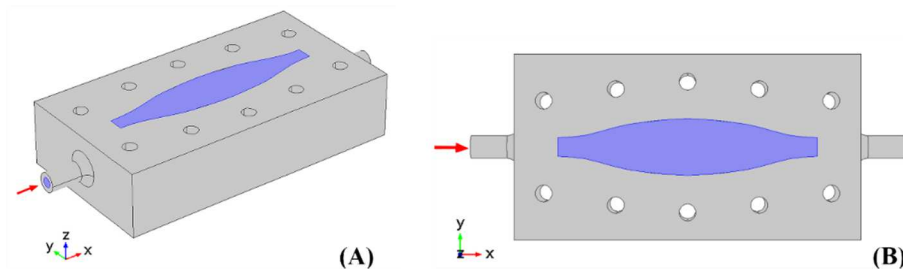
Figure 28 Geometry of the intermediate part of the drop shape MFC used in the simulation. Orthogonal view (A) and x-y plane (B)

Figure 28 shows the geometry developed and used during simulation in both orthogonal view and top view. All the conditions and equations used for the previous configuration are still valid, because, also in this case, the flow is laminar, the temperature is the ambient one and the applied pressure is the atmospheric one. Also boundary conditions, satisfied by no-slip condition of walls, are maintained and mesh, illustrated in Figure 29 is the same as in the square geometry.
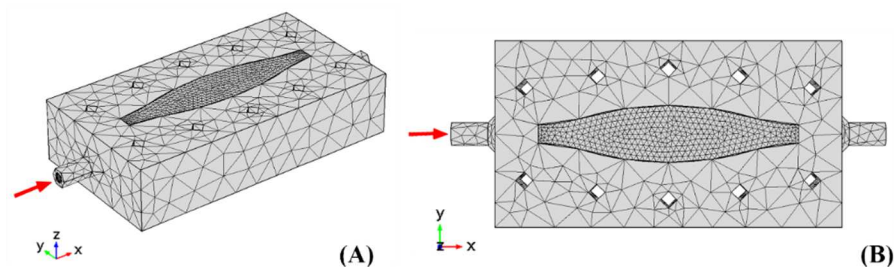
Figure 29 Used mesh during simulation in COMSOL. Orthogonal view (A) and planar view (B)

Following the same reasoning of the previous case, the analysis of particle trajectories, both visually and numerically was performed. For this new cell configuration, only two flow rates were tested, that are the slowest and the faster one, slightly adapted to the geometry, in order to have an integer number of fluid exchange in 1 hour of operation.

Results of the particle trajectories obtained from the simulation are reported in Figure 30, in which both the cases, after 1 complete exchange and after 1 hour, are presented. Differently from the previous case, the region dedicated to the fluid exchange is completely interested by the movement of particles, ensuring the maximization of moved volume.
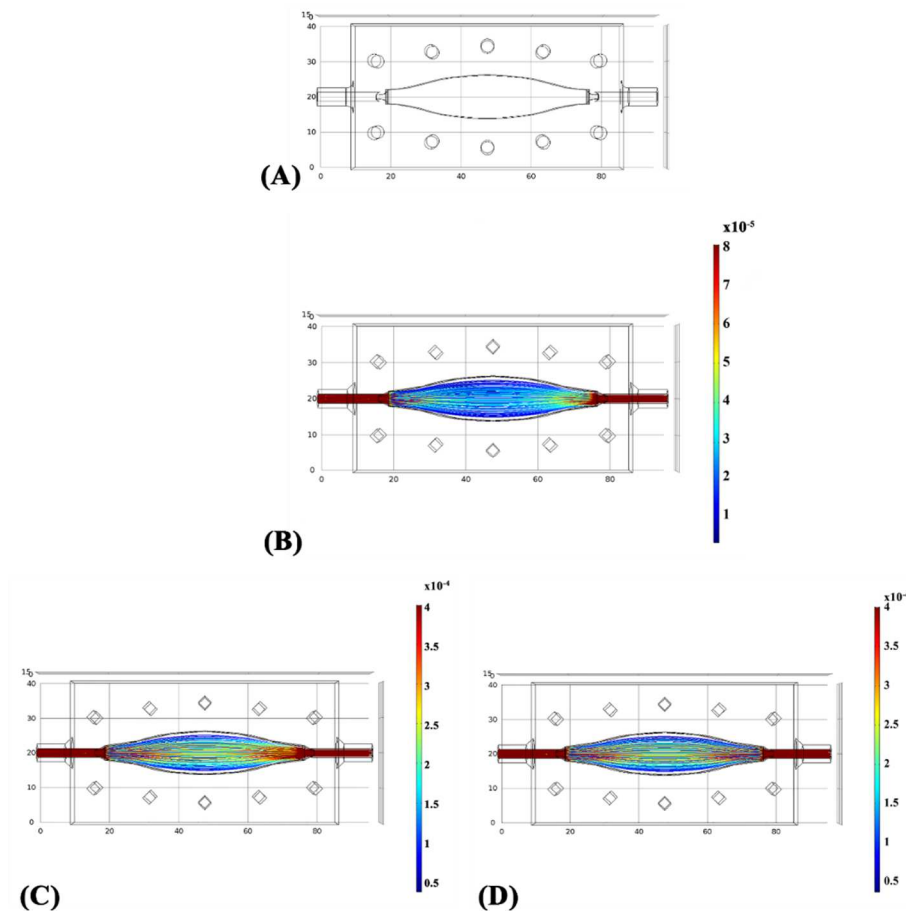
Figure 30 Trajectories profiles inside the drop shaped cell at time zero (A), after 1 hour (coincident with 1 complete exchange) for 10 ml/h (B), after 1 complete exchange for 100 ml/h (C) and after 1 hour for 100 ml/h (D)

Numerically analyzing the images in the above figure, a value of percentage of exchanged area can be obtained: also in this case the area does not change

significantly with the flow rates, but reaches important values with respect to the previous geometries.

Finally, analyzing all the considered geometries and starting from the circular shape, previously used, up to the drop-like one, the region interested by fluid flow increases dramatically.

While in the circular one, the area was about 50%, a quite big improvement was performed introducing the square-shape Microbial Fuel Cell: around 70 % of the fluid contained in the reaction chamber is exchanged, leading to improved performances of the device and to a multiple application of the MFC device, just varying the velocity of the inflow containing the microorganisms' nutrient.

The amount of exchanged volume is further improved introducing the drop shape, developed favoring the natural shape of the fluid in a chamber, passing from 70% to above 96%, value that represents to totality of the available volume.

For this new geometry, only simulation results are available without any test of the device in laboratory.

Future work is the fabrication and the test of the new geometry directly in laboratory using the same operation conditions of the square cells, in order to compare performances and study correlations between the percentage of exchanged areas and real performances of the device.

Chapter 5
Results

5.1 Characterization of the new squared Microbial Fuel Cell

Starting from the simulation study, presented in the previous chapter, a good compromise between a good fluid exchange and reduced dimensions of the final device is a square–shaped single chamber microbial fuel cell, with dimensions of both the electrodes of 9 cm^2. The proposed device has a modular architecture with a 6 ml fluidic chamber placed between two modules hosting the electrodes. The inner total volume the cell, without any material inside, is about 20 ml. A sketch of the device is reported in Figure 31.

(A)   **(B)**
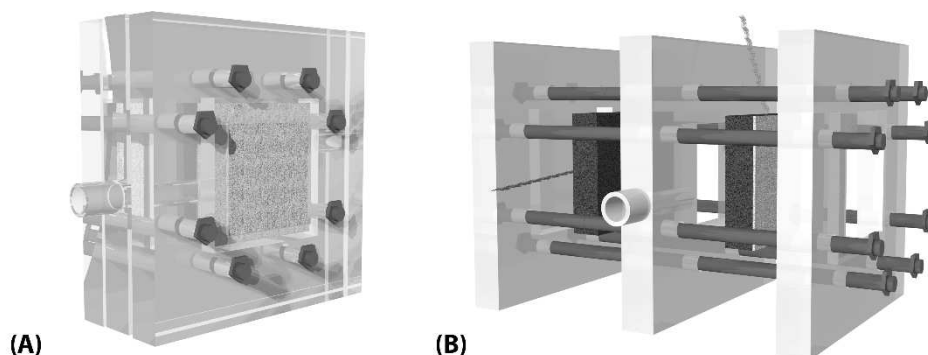
Figure 31 Sketch of the assembled squared MFC (A) and the exploded view (B). In the exploded image, from left to right there are the anode, the intermediate spacing and the cathode

The setup was designed with a 3D software (Solidworks®) and then the CAD was layered by layered fabricated using a 3D printing technology (Objet30, Stratasys), equipped with a photocurable polymer (VEROWHITE PLUS).

Being an air-cathode configuration, the cathodic material directly exposed to air, was treated with a gas diffusion layer to guarantee a controlled oxygen flux, together with the impermeability to water.

On the air-side of the electrode, several films of Polytetrafluoroethylene (PTFE) were realized following the standard procedure reported in literature. On the inner side of commercial materials, a layer of catalyzer was applied; the most used catalytic material is Platinum, applied to the material with a paste made of platinum particles supported on carbon powder, water, isopropanol and Nafion®, used both as a binder material, both as a membrane to reduce the formation of biofilm at the inner side of the electrode.

Fluid is allowed to flow through tube-exiting connections placed in the intermediate module, with an inner diameter of 3 mm. Flexible tubes can be used to insert the fluid, containing the substrate supplying, during operation of the device. The three parts were maintained sealed through bolts all around the fluidic chamber.

Since this cell is made up of three different parts, there is the possibility to use the reactor in different configurations, depending on the selected modules: in this work a single chamber reactor with an air cathode, directly exposed to the atmosphere was used.

In this chapter, the test of the new designed squared SC-MFC is reported and the performance of the device discussed. During the test, commercial carbon paper was used as anode, while commercial carbon felt was adopted as cathode.

The new cell setup has been designed to optimize electrical connections too. This result has been achieved by a polymeric squared frame in which a small size titanium wire can be inserted. The frame and the electrode are mounted in optimal mechanical contact, granting so optimal electrical conductivity. Regarding the cathode, this frame has also the function to press the cathode material to avoid liquid losses on the air side.

To ensure the impermeability of the material from the water, while keeping high the oxygen permeability, a gas diffusion layer (GDL) was applied, as described in Chapter 2. The material used to realize it was polytetrafluoroethylene (PTFE), that is the same reported in the literature [36], [105]. At the inner surface, instead, a platinum based catalyst layer was prepared to ensure the ORR, as reported in literature [2].

To apply results obtained during the simulation step, an experiment using SC-MFC was built up with the lowest (12.5ml/h) and the highest (100 ml/h) flow rates already tested computationally (see Chapter 4), with a substrate concentration of 3mM.

The experiment was conducted in a "controlled batch mode", meaning that the substrate for the microorganisms was supplied by a peristaltic pump for 1 hour, to guarantee a controlled flux equivalent to the one set during the simulations. When feeding was stopped, the drop of the performances was waited before starting with a new concentration. A typical performances trend of a batch mode operating MFC is shown in Figure 32. In the graph, it is possible to observe an increase of performances when the fresh substrate reaches the reactor chamber, followed by a decrease that is the consequence of the stop of the feeding system and the oxidation of the organic substrate by microorganisms. Before starting a new cycle, a complete drop and stabilization of performances is waited.
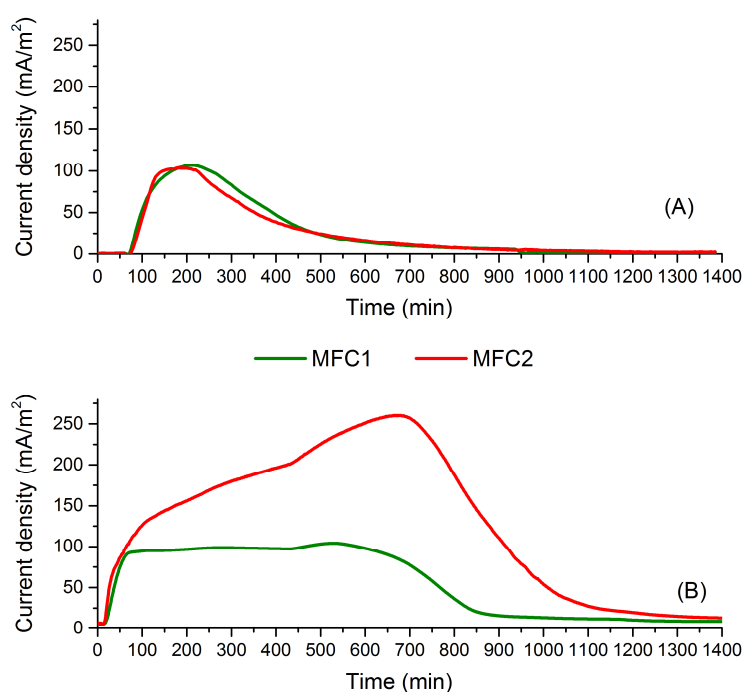
Figure 32 Current density profile of cells considering 3 mM of sodium acetate as organic substrate, compared with two different flow rates: 12.5 ml/h (A) and 100 ml/h (B)

To try to compare results of the concentration profile inside the cell, obtained through simulation and presented in the previous chapter (Figure 24 and Figure 25), with the real performances, the overlapping between current density curves and concentration in the five different points is considered and reported in Figure 33.

Results

Being the microorganisms responsible for the electrons production, and being located at the lower interface of the simulated volume (corresponding to z=0), only concentration curves corresponding to points located at this interface are reported.
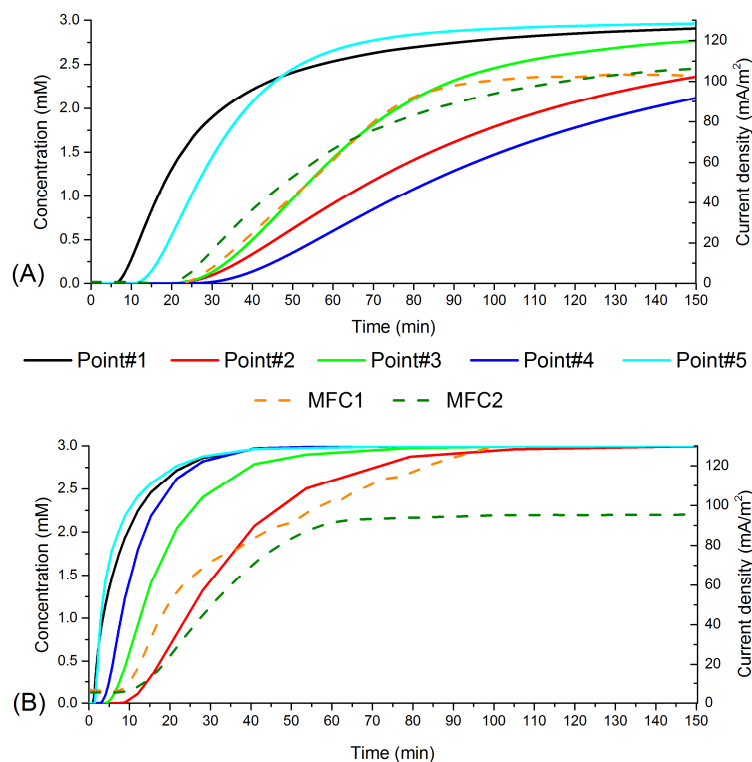
Figure 33 Comparison between concentration evaluated in points inside the cell, and performance of SC-MFC considered at 12.5ml/h (A) and at 100 ml/h (B). Solid lines are the concentration trends, while dashed lines are the current density profiles

Both the concentration curves and the current density profiles were fitted with a linear regression, in order to study the slope of single curves and correlate position dependency of the concentration, with real device performance.

Table 6 Analysis of the slope of the concentration profiles compared with the slope of current density curves of MFC

	Slope of the concentration profile at z=0, flow rate **12.5 ml/h**	Slope of the concentration profile at z=0, flow rate **100 ml/h**
Point #1	0.077	0.165
Point #2	0.023	0.065
Point #3	0.043	0.114
Point #4	0.019	0.178
Point #5	0.082	0.218
MFC 1	0.035	0.081
MFC 2	0.034	0.078

Analyzing the slope of the linear regions of curves (reported in Table 6), it is possible to find a correlation between simulations and experiments: depending on the velocity of the inflow, the most significant point inside the reactor chamber, in terms of prediction ability of the cell performance, changes. When the velocity is quite low (i.e., flow rate of 12.5 ml/h) the concentration curve with the most similar slope is the one close to the outlet. The explanation of this is related to the diffusion process: diffusion is the dominant process in this case, but it is coupled with a "drift" component, imposed by external pump. Due to the low velocity, however, it does not modify the diffusion profile connected to particle trajectories. Not considering the acetate consumption from microorganisms, but only its movement, it diffuses from the plane on z, on which the inlet/outlet are located, to the bottom interface, following trajectories proposed by the drift model: the result is a non-orthogonal diffusion path from the inlet/outlet plane to the bottom interface along the z axes.

Considering, instead, the faster flow rate, the most significant point is the one placed at the corner, where the concentration is lower. Indeed, increasing the flow rate, the drift process becomes the dominant one with respect to the diffusion, and sodium acetate is moved too fast by the fluid carrier to be the limiting factor for current production. For this reason, the points placed at the corner, experiencing diffusion as the main process, exhibit curves with the most significant correspondence to the one of the current density.

Results obtained using a "controlled batch mode" can be extended to a continuous operation of the device, if needed.

Starting from concentration profiles reported up to now, two different applications of the SC-MFCs can be proposed: power generation (if used in a continuous mode) and bio-sensor both for COD and toxicants, such as heavy metals present in wastewater (if the device is used in batch mode).

For power production application, in which all the inserted substrate must be consumed, in order to obtain high power values, a slow flow rate is the appropriate one, because, in this case, the organic matter enters the reactor in a slow way allowing a complete oxidation.

Even if the aim of the operation is a detection of the COD of the substrate the slow flow rate is the correct choice, because the slope of the current density of the cell is higher with respect to the one obtained with faster flow rates, meaning that the COD value is detected in a faster way.

If a contaminant sensor is the end use of the device, faster flow rates are useful because the toxicant is identified by the microorganisms, performance response is present, but, at the same time, being the flux fast, the biofilm is not contaminated by the toxicant, being rapidly exchanged.

5.2 Polysaccharides based aerogels

One of the aims of my PhD activity was the design and fabrication of innovative electrode for Microbial Fuel Cells. The proposed alternative to commercial materials are carbon based aerogels synthetized using polysaccharides as precursors.

Among all possible polysaccharides available in nature I focused my attention on agar and starch compounds.

The synthesis procedure of the material is the sol-gel process, described in Chapter 3.

The polysaccharide (agar 4 %wt or starch 15 %wt), was stirred with 4 %wt of glucose, to obtain a homogeneous powder mixing.

The function of the addition of glucose is to modify the aerogel networking structure. Glucose works as the cross-linker agent, reducing the size of the junction zone and helix aggregation. As a result, a more elastic structure with a more controlled porosity is obtained, reducing so the shrinkage of the gel occurring during the synthesis, especially after drying and after pyrolysis [106]. This mix was added to hot water and was left for 2 hours at 85 °C to allow complete dissolution. When the solution is ready, it was put into polydimethylsiloxane (PDMS) molds at ambient temperature to cool down and to complete gelation. At this stage of fabrication, the already obtain gel was put in the fridge at -20 °C for 1 day before of the drying procedure.

At this point, the gel is ready to be put in the freeze dryer to remove the liquid part of the material, leaving the scaffold uncorrupted. The drying process is quite long: the chamber containing the sample was maintained at -50 °C for 1 or 2 days to ensure the cooling of all the sample, included the more internal section; after this time, the vacuum pump was switched on and a pressure of 0.001 mbar was reached. To reach a complete sublimation of all the liquid component, the sample was left for a week (the effective time depends on the dimension of the gel: bigger is the sample, longer is the required time) under these conditions. The polysaccharide aerogel is now ready to be transformed into a carbon material with good and controlled porosity.

The transformation is allowed thanks to the pyrolysis step: a thermal treatment at high temperature under argon flux. The high temperature causes the dehydration of the organic polymer, with the consequent release of water vapor, carbon monoxide and carbon dioxide; the nanocrystalline carbon is, instead, left in the structure. If the inert atmosphere is not maintained during the treatment, the carbon present in the material will simply burn.

Drying procedure and thermal treatment are critical steps for the final structure of the material: during these two treatments, in fact, the three-dimensional structure of the material can collapse, creating a dense film and destroying completely the porosity of the material.

The thermal process must be optimized to guarantee the carbonization and the partial graphitization together with a good aerogel structure; to do this, a thermo-gravimetric analysis (TGA) was performed on the material after the drying step, to understand which are the characteristic temperatures at which the evaporation of a component is present.

The resulting curve from the TGA is reported in Figure 34. From the graph, it is possible to appreciate two different steps at which a consistent loss of material occurs: the first one around 110 °C, is associated to water evaporation and to the burn of some low molecular weight components, and the other one from 200 °C to 500 °C approximately, attributed to the evaporation of volatile components and consequent carbonization of the organic aerogel.
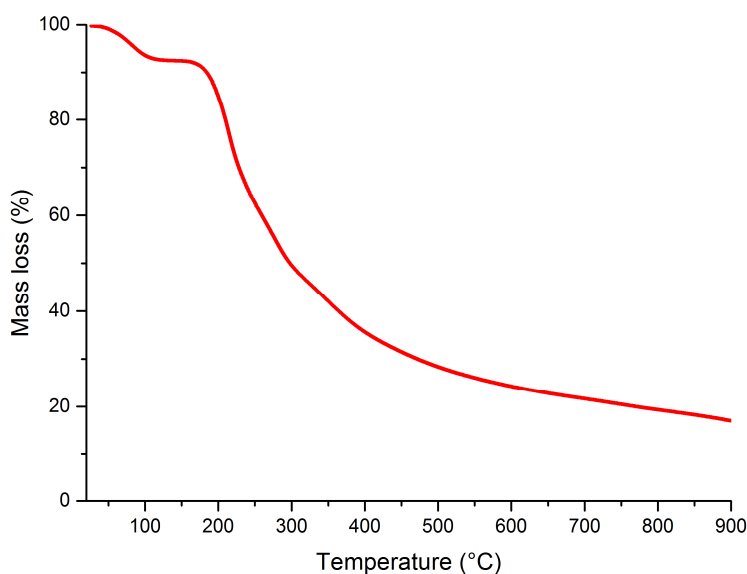
Figure 34 Thermo-Gravimetric analysis of polysaccharide based aerogel.

Based on the results obtained from TGA measurement, a properly temperature ramp for the pyrolysis process was set-up.

The aerogel was placed in a quartz tube, filled with argon flux (300 cc/min, 2 bar) to create inert atmosphere. The final temperature of the treatment was 900 °C, that is lower with respect to the ones proposed for graphitization [107] but it is a good compromise between the treatment temperature and the good properties of the material, to keep low production costs of the final material, to be competitive with commercial ones.

To obtain a graphitic material with a good electrical conductivity, the treatment temperature must be set between 600 and 2100 °C. The thermal treatment was divided into two steps: the first one up from room temperature to 110 °C with a heating rate of 2.5 °C/min for 1 hour, to allow evaporation of low molecular weight

components (water in particular), and the last one, from 110°C up to 900 °C, for 3 hours to perform the partial graphitization of the material.

After the high-temperature treatment of the material, some specific measurements were performed, to understand its main properties.

To deeply study graphitization level of the carbonized material, the Raman analysis is the most accurate technique. The carbon aerogel was analyzed with Raman spectroscopy in the range of 700-3500 cm^{-1} in order to study graphitization degree of the material, analyzing graphite bands.

The pure graphite, when analyzed with a Raman technique, presents two characteristic bands: the D-band (defects and disorder) and the G-band (graphitic) at 1355 cm^{-1} and 1575 cm^{-1}, respectively [107].
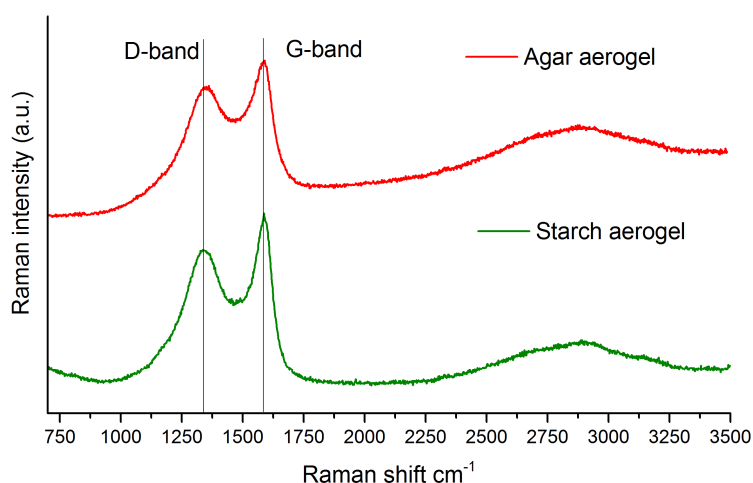
Figure 35 Raman spectra of agar with glucose (red curve) and starch with glucose (green curve) aerogels treated at 900°C under inert conditions

In Figure 35, Raman spectra of aerogels treated under Argon flux at 900°C are reported. Here, the two characteristic bands of graphite are present, meaning that the graphitization of the material occurred. The degree of graphitization is given by the position of peaks with respect to the nominal ones and their relative intensities.

Table 7 Parameters obtained from Raman Analysis

	D-band position	G-band position	I_D/I_G
Agar aerogel	1361 cm^{-1}	1591 cm^{-1}	0.87
Starch aerogel	1336 cm^{-1}	1587 cm^{-1}	0.86
Commercial Graphite [107]	1355 cm^{-1}	1575 cm^{-1}	≈0

In Table 7, the main output parameters of the Raman analysis are reported for both Agar and Starch aerogels.

Both the two materials present a shift in Raman peak position, but not significant. For simplicity, only the position of the G-peak, that is the one corresponding to graphitic properties, and the ratio I_D/I_G, demonstrating the extent of structural disorder, are considered.

A degree of graphitization can be also deduced from the intensity ratio of the peaks [108]: lower is this ratio, higher is the degree of graphitization. The D band of a carbon material is associated to defects and disorder of the crystalline planes; higher is the intensity of this band, lower is the quality of the material. Both materials present quite an identical value of the intensity ratio of the two peaks, and so can be considered to have the same graphitization degree, from Raman point of view.

To study morphological properties of carbon materials, a Scanning Electron Microscopy (SEM) analysis was performed. This is the best technique to evaluate the micro and nano porosity of the material, otherwise not appreciable using a classical optical microscope.

The morphological structure is maintained unmodified, but for what concerns the porosity, thanks to a statistical analysis on several different points over the whole sample, it is possible to say that the high temperature treatment made the porosity more regular, with better defined pores having a bigger mean diameter. Pores of different dimensions are present in the aerogel, starting from nanometric features to macrometric ones.

Depending on the final application, as anode or cathode, not all the porosities can be usable: if the aerogel is used as anode, considering that microorganism dimensions are of the order of some micrometers, the nanostructuration itself is useless, and pores bigger than few microns are needed in order to take advantage of the entire surface area.

As cathode materials, on the other hand, if small molecules, such as oxygen, are involved into the reduction reactions, the microporosity can be useful, as well, also preventing the biofilm formation inside the electrode.

To obtain a higher porosity in the range of meso and micro pores, a further treatment, after the pyrolysis was performed: the activation of the structure with a KOH thermal treatment.

The KOH activation treatment is one of the most known techniques to open the pore network in carbon materials. Operatively, the KOH activation was performed selecting a proper ratio of carbon material/activating agent, and following the wet impregnation method. Having fixed the ratio at 1:4, the carbon aerogel was immersed into the water solution containing the KOH, put in stirring and left overnight at 85°C until complete evaporation of the liquid.

After this, samples were pyrolyzed at 750°C, with a heating rate of 5°C/min, for 2 hours under an Argon flux. After a naturally convective cooling down of the samples, they were repeatedly washed with a 5M solution of HCl, followed by distilled water rinsing until pH 6 is reached.

Finally, the KOH treated samples were dried at 110°C overnight.

In Figure 36, a SEM analysis of the KOH treated samples compared with the non-treated ones is reported.

As it is possible to appreciate from SEM analysis, for both the two materials, agar and starch, the porosity is modified: dimensions of pores are bigger especially the more external ones.

Results
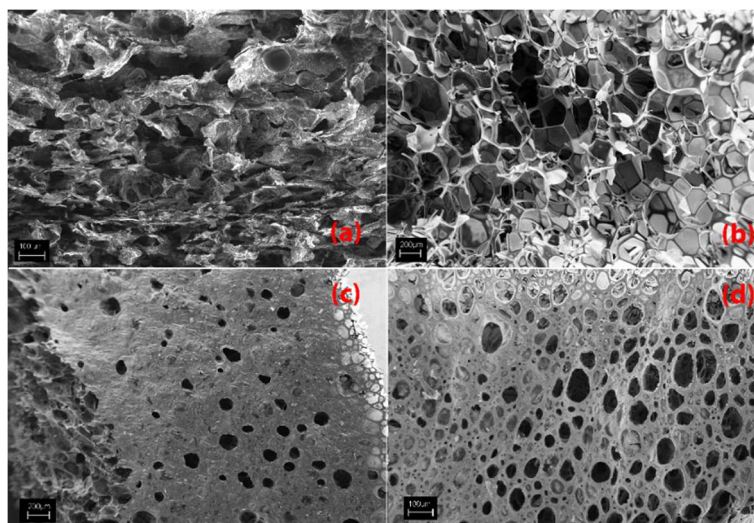
Figure 36 SEM imaging of post-pyrolyzed agar aerogel (a) and after KOH treatment (b). Starch aerogel after pyrolysis (c) and starch aerogel after KOH treatment (d)

The KOH thermal treatment (Figure 36-B and D) increased the porosity of the aerogel, creating holes on the external surface. In this way, the internal porosity of the material is made available and usable, otherwise hidden from the external dense and non-porous layer of material.

To numerical appreciate the porosity and the surface area of a structured material, the Brunauer-Emmett-Teller (BET) method was used. Performing the analysis of the amount of adsorbed gas (nitrogen) at 77.3 K, it is possible to evaluate the specific surface area of the material. During the same measurement, also the cumulative pore volume and the distribution of pores can be calculated. This last parameter was obtained using the BJH method evaluated at 0.9 p/p_0, where p/p_0 is the relative gas pressure (partial pressure over saturation pressure). For both the materials, specific surface areas are comparable and on the order of 400 m^2/g, in line with polysaccharides based aerogels [87]. In Figure 37 an isotherm curve, resulted from BET method, for a polysaccharide aerogel is reported. Porosity and surface area values can be extracted analyzing the reported curve.
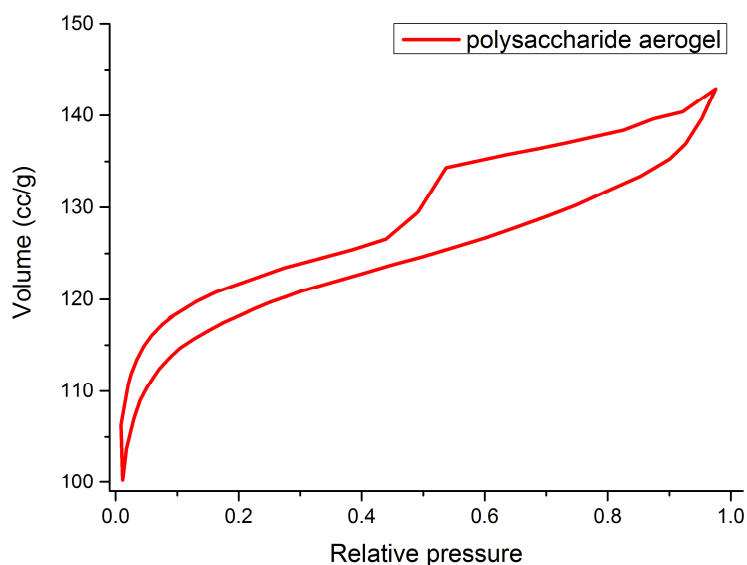
Figure 37 Isotherm curve of a polysaccharide aerogel obtained using BET method

Considering the aerogels described in the previous paragraph, in order to be used as anode in bio-electrochemical cells, some preliminary biological characterization must be performed: the two main used biological tests are the cytotoxicity test, and the aerogel-liquid interaction to study the colonization of the carbon material from biological colonies.

Cytotoxicity test were based on the inclusion of the material into a gel made of Agar (15 g/l), sodium acetate (1 g/l), peptone (1.25 g/l) and microorganisms (100 µl of inoculum diluted into 900 µl of sodium acetate solution). The plate was obtained from the gelification of the mixture at room temperature. After 2 hours, the amount of colonies generated in contact with the material was counted. Resulting plates are reported in Figure 38.
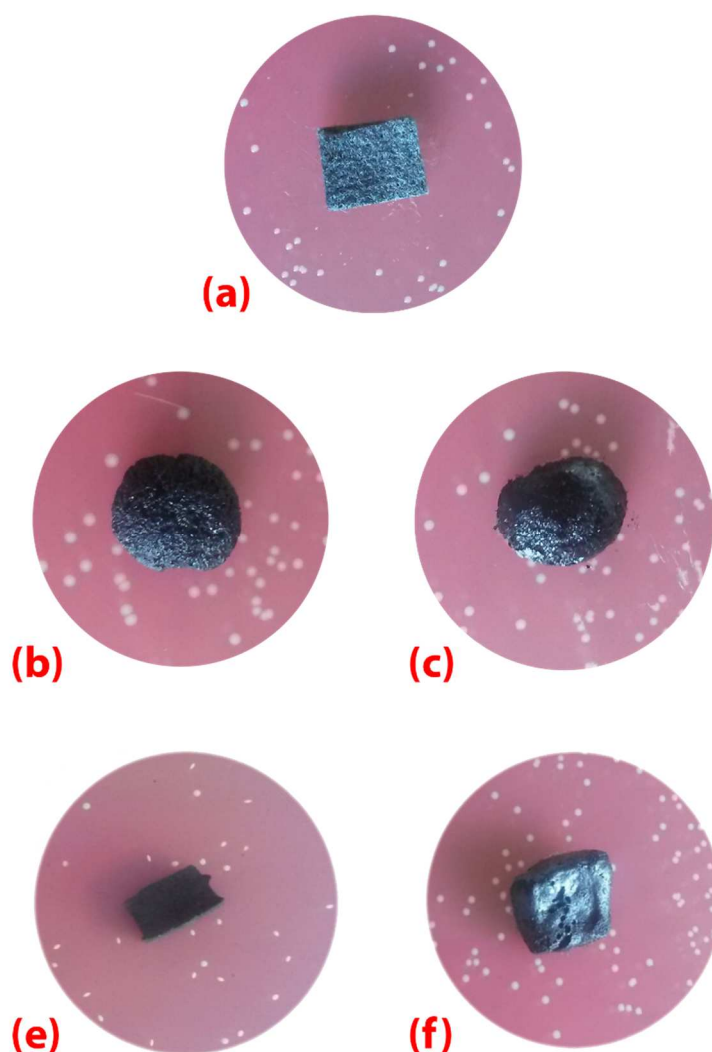
Figure 38 Cytotoxicity test on agar based aerogel. (a) Silver control, (b) agar aerogel, (c) agar and glucose aerogel, starch aerogel (e), starch with glucose aerogel (f)

In Figure 38-A, a piece of commercial carbon felt material was covered with a Silver layer as a control for the test, being Silver cytotoxic for bacteria. All around the material, in fact, a cytotoxicity ring, without any colony, was formed, validating the test. Agar and starch aerogels, instead, present normal colonization by the biofilm, without any cytotoxicity ring.
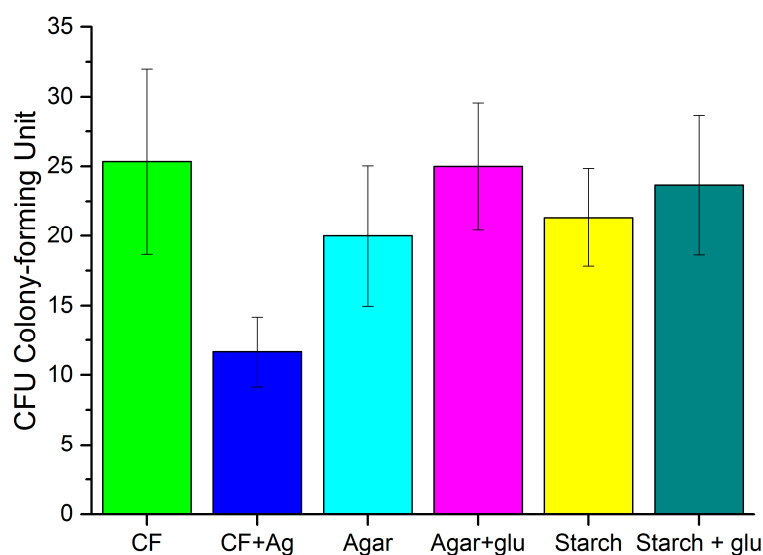
Figure 39 Plate count after 2 hours of commercial carbon felt (CF), carbon felt with Silver (CF+Ag), agar aerogel, agar with glucose aerogel, starch aerogel and starch with glucose samples

After 2 hours, the number of colonies was evaluated, and results are reported in the graph in Figure 39. Apart from the commercial material treated with silver, all the carbon materials present a comparable number of colonies. The addition of glucose both in agar aerogel, and in starch one, apart from structural advantages listed previously, seems to improve the interaction between the material and bacteria, making the aerogel a material with characteristics comparable to commercial ones as the colonization degree.

The second test to evaluate the interaction between the aerogel and the biofilm, is the liquid test. During this analysis, samples were put into a solution containing 2.5 g/l of sodium acetate and microorganisms for 1 month: both commercial carbon felt and carbon aerogels were tested. SEM analysis was used to morphologically characterize the interaction and the formation of the biofilm on materials: to do this, a standard fixation protocol was applied as reported in literature [109], [110].

Briefly, samples were left in a solution containing glutaraldehyde (2 %wt) in phosphate buffered saline (PBS) solution for 1 hour. After that time, there were performed three consecutive washes in a PBS buffer solution followed by a series of ethanol water dilutions, to dehydrate. To dry samples, a chemical process was applied, using a solution of hexamethyldisilazane (HDMS) and ethanol.
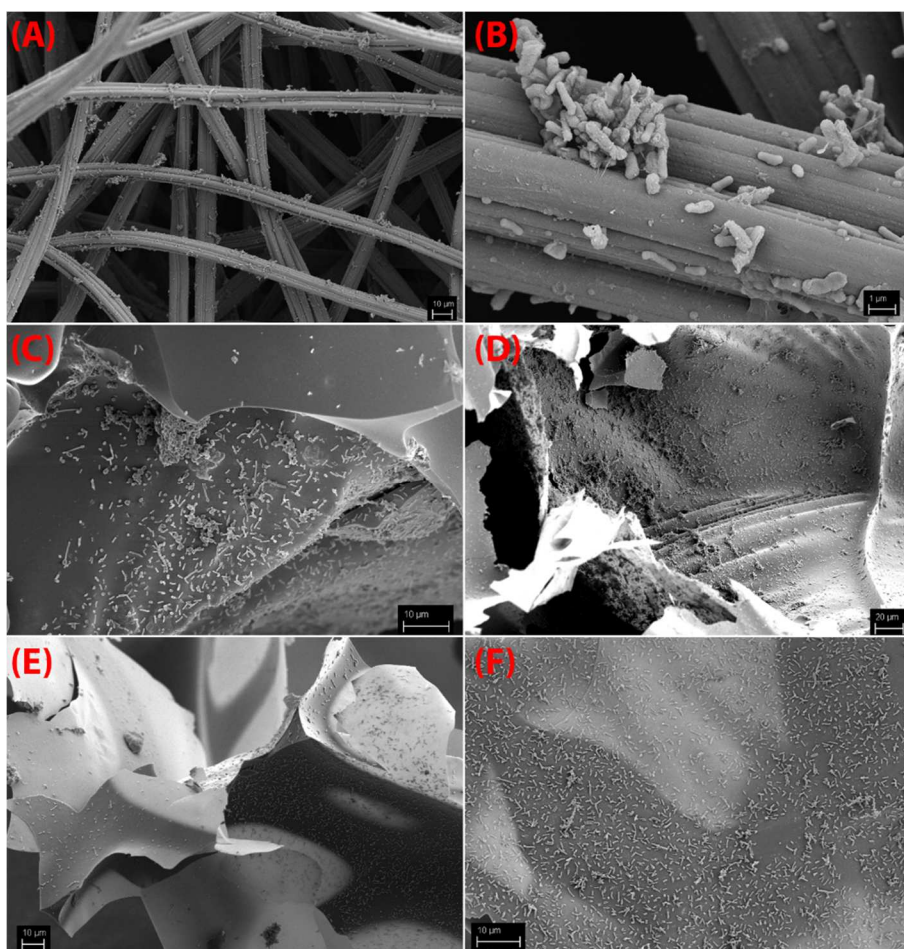
Figure 40 SEM analysis of liquid interaction tests on carbon felt (A) and (B) at different magnifications, agar aerogel (C), agar with glucose aerogel (D), starch aerogel (E) and starch with glucose aerogel (F)

Analyzing SEM images of carbon materials after exposure to the liquid solution containing bacteria, it is possible to observe that both the commercial material (Figure 40-A and B) and carbon aerogels (Figure 40-C, D, E and F) present a good interaction with the biofilm, showing and confirming previous results of a comparable degree of colonization. Considering only aerogels, both of them are uniformly populated by microorganisms, but the presence of glucose in the precursors of the synthesis (Figure 40-D and F) increases the colonization and the microorganisms' density on the surface of the material.

To be tested in the Single Chamber MFC as anode, only agar aerogel with the addition of glucose were chosen.

5.2.1 Agar aerogels as anode in SC-MFC

To ensure the electrical contact between the carbon aerogel and the external circuit, a carbon wire was inserted into the aerogel as the electrical collector.

Devices containing the carbon aerogel as anode were compared with two types of commercial materials: carbon felt and carbon paper.

Cells were operated in batch mode with a nutrient concentration (sodium acetate) of 1 g/L. Cell voltage was recorded during the entire experiment, conduced with an external load applied of 1 kΩ. Because aerogels have high surface area, very low density and also low weight, MFC performances cannot be analyzed considering the same area of the electrode for all the materials. The geometrical area of the electrode ($9cm^2$) is not appropriate because the porosity is neglected; considering the surface area obtained from BET analysis, instead, overestimates the effective area because also nanoporosity is taken into account. The best way to consider aerogel contribution is to evaluate performances as a function of the weight of the sample.

Current evaluation of the SC-MFCs is reported in Figure 41.
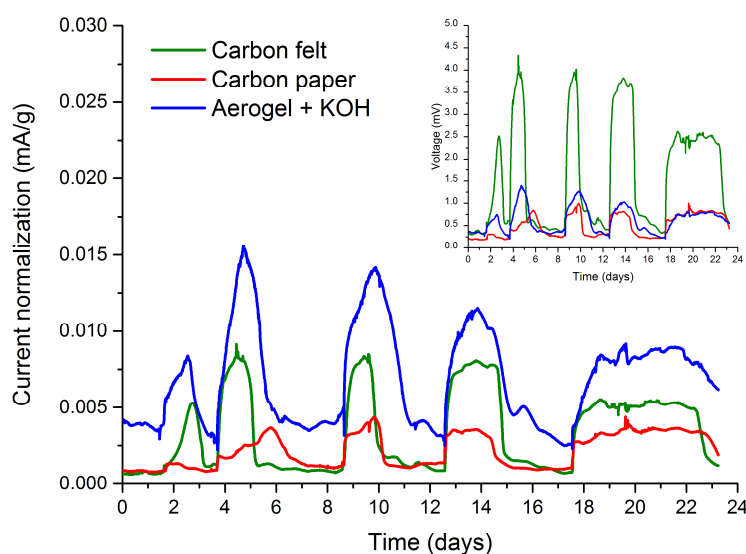
Figure 41 Current normalization versus time behavior of carbon-based aerogels SC-MFC compared with commercial ones. In the inset, the voltage without any normalization is reported

As it is possible to notice from the current normalization trend, carbon aerogel performances are higher with respect to the commercial materials. Behavior not similar if the voltage, without any normalization, is considered (inset of Figure 41).

Trends are very different due to a big difference in terms of amount of material really present in the reactor.

Further analysis useful to study MFC performance are Linear Sweep Voltammetry and Electrochemical Impedance Spectroscopy.

The polarization curve, that is the result of a Linear Sweep Voltammetry analysis, is the evaluation of the Power density as a function of the current density flowing in the reactor. From the curve trend, it is possible to compare performance of different materials and extract information about the maximum generated power. Results performed on the Agar aerogels compared with commercial carbon materials are reported in Figure 42.
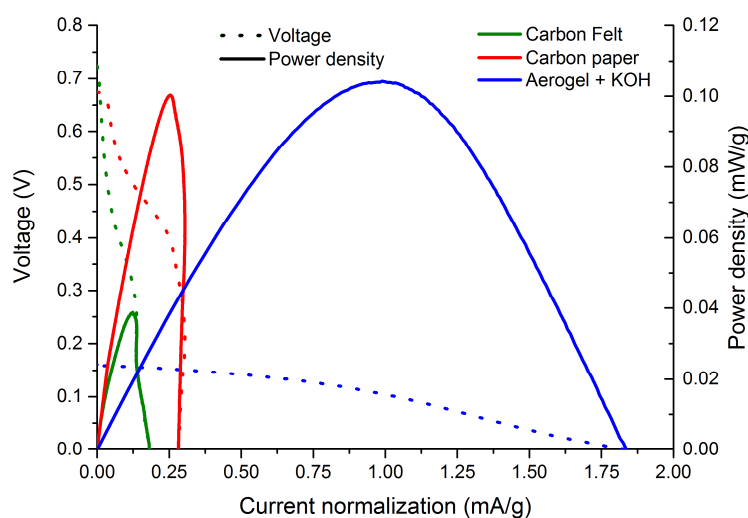
Figure 42 Power density curves and I-V characteristics obtained for Carbon aerogel compared with commercial materials

From the graph it is possible to notice that the carbon aerogel presents the highest power density production and the maximum short circuit current. Because of the power curve is symmetric, it is also possible, apart from the maximum power point, to extract also the resistance value that should be applied to the reactor to obtain the maximum power. Results are summarized in Table 8.

Results

Table 8 Output parameters of MFC obtained through Linear Sweep Voltammetry

	Maximum Power	Resistance value to apply to have maximum power
Carbon Felt	0.039 (mW/g) @ 0.314V	5347 Ω
Carbon paper	0.100 (mW/g) @ 0.398V	6581 Ω
Aerogel + KOH	0.105 (mW/g) @ 0.105V	1182 Ω

Considering internal resistances obtained from the power density curves, these values decrease significantly passing from commercial materials to carbon aerogels. The best result is that the internal resistance of the cell based on aerogel as anode is around 1 kΩ, value that is comparable to the one typically applied to simulate real life operation of the cell.

The last measurement performed on the device to evaluate electrochemical properties of the material used as anode, is the Electrochemical Impedance Spectroscopy. Results are reported in Figure 43.
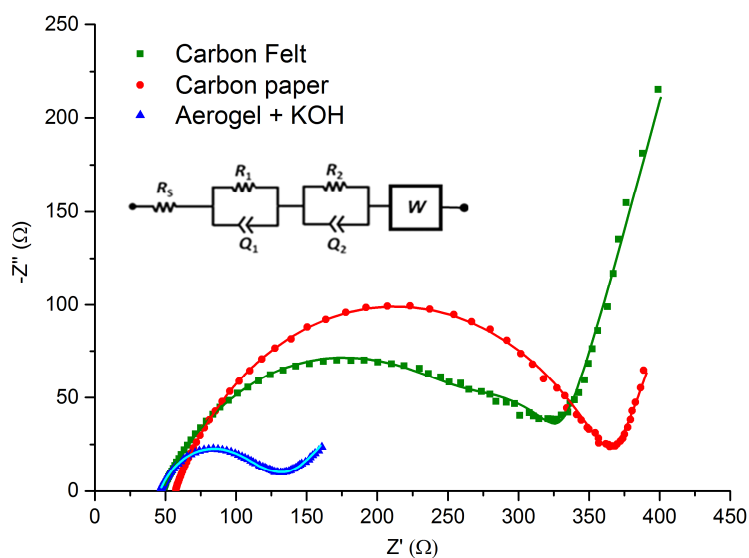
Figure 43 Nyquist plot comparing carbon aerogels with commercial carbon materials. Dots are experimental points, while straight lines are fitted ones. In the inset, the equivalent circuit used to fit EIS curves is reported

From the Nyquist plot, in which the imaginary part of the impedance is plotted as a function of its real part, the analysis of the internal resistance of the device can be conducted.

Experimental results were fitted using the equivalent circuit reported in the inset of Figure 43. In this way, internal resistances of the different devices can be calculated [111]. Between the three cells, a big difference emerged by the fitting: both the carbon felt and carbon paper based cells present a very large anodic resistance (modelled by the first parallel in the equivalent circuit) that hides the cathodic contribution, and the semicircle corresponding to the anode is overlapped to the cathodic one. In the aerogel based cell, this behavior is not present and both the interfaces are distinguishable. In Table 9, a summary of the obtained resistances is reported.

Table 9 Internal parameters obtained fitting experimental EIS data

	R_s	Anodic resistance	Cathodic resistance
Aerogel + KOH	45.96 Ω	62.74 Ω	30.78 Ω
Carbon felt	47.35 Ω	230.8 Ω	-
Carbon paper	56.82 Ω	309.3 Ω	-

A smaller anodic resistance of the cell when the aerogel is used as anode can be explained with some considerations regarding the properties of the material itself and its interaction with microorganisms: carbon based aerogels are more conductive with respect to commercial materials and present a better interaction with the biofilm. These properties result into a smaller internal resistance, leading higher performance of the total cell.

5.2.2 Nitrogen-doped carbon aerogels as cathode in SC-MFC

As introduced in Chapter 2, the most important reaction occurring at the cathode of an air-cathode MFC is the reduction of oxygen (ORR).

Despite of platinum has the better performance in directly reducing oxygen to water, it is expensive and little abundant. For these reasons, an alternative catalyst must be provided to the carbon aerogels.

To enhance catalytic activity of materials, several platinum alternatives are possible, ranging from the use of a variety of non-precious metals, or the addition of nitrogen source directly into the desired material. Recently, the development of N-doped materials with good electrocatalytic performances become an important category in ORR catalysis. Moreover, nitrogen doped carbon materials have also important advantages in addition to good catalytic properties: they are low costs materials, with good durability and environmental friendly [112].

Nitrogen is a good catalyst for ORR thanks to the strong electronic affinity of N atoms resulting in high positive charge density on the adjacent C atom that favors the adsorption of O_2. In other words, N, added to a carbon material, is a sort of *n-type* dopant, because it gives, to the graphite matrix, an extra electron that can be more easily donated [113].

In this work, carbon aerogels were doped by nitrogen using with amino acids as nitrogen source (glycine and lysine in particular) [112], in order to preserve the green approach to the synthesis for a green technology as MFC is.

Also in this case, the procedure followed for the synthesis of nitrogen doped aerogels is the sol-gel process, described in Chapter 3. The difference with respect to the aerogel used as anode is the addition of 0.07 mmol/l of glycine or lysine to the precursors as nitrogen source. After the mixing of all the precursors, water was added and the solution was boiled at 85 °C, and then mold for gelation.

The freeze drying process was followed by the pyrolysis one under inert gas flow at 900 °C for 3 hours in order to make the material graphitic as much as possible without losing a large amount of nitrogen.

To be able to quantitatively evaluate the presence of nitrogen inside the carbon aerogel, X-ray photoelectron spectroscopy (XPS) and Energy Dispersive X-ray Spectroscopy (EDS) analysis were performed.

The main difference between these two techniques is the depth of the measure: while EDS is able to analyze some micrometers in depth, XPS is a superficial technique able to detect only few nanometers of materials. In the graph in Figure 44, a comparison of atomic percentage of nitrogen between the two techniques, before and after the thermal treatment, is reported. It is possible to notice that both the methods show a common trend of the nitrogen content, with a partial loss of

nitrogen due to the thermal process. Measurements were also performed on agar aerogel without the addition of amino acids, to analyze the amount of nitrogen was contained in the precursor itself.
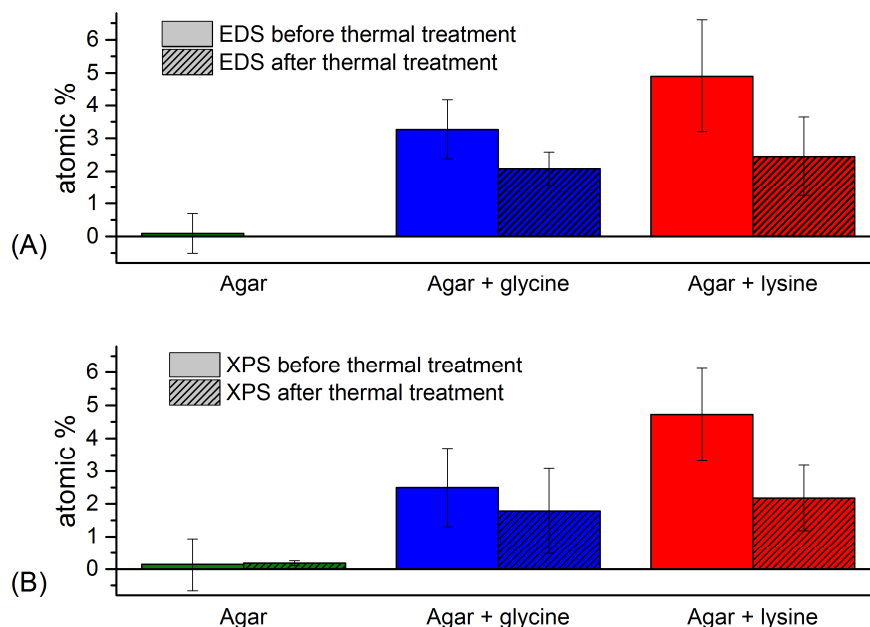
Figure 44 Relative atomic percentage of nitrogen extracted by EDS (A) and XPS (B) techniques. Filled bars represent the pre-pyrolysis sample, while patterned one, the post pyrolysis aerogel

N atoms can be substitutionally incorporated in the graphite matrix in three different forms: pyridinic nitrogen, pyrrolic nitrogen and graphitic nitrogen. Pyridinic atoms are located at the edges of the graphite plane, and bonded with two carbons; it is able to give one π-electron to the structure. Pyrrolic site, instead, is incorporated into five member heterocyclic rings, in which each N is bonded to two carbon atoms, and it is able to donate two π-electrons. Graphitic nitrogen, instead, is incorporated into the matrix and substitute carbon atoms. A summary of the three types of nitrogen, with their correspondent XPS peaks are reported in Figure 45.
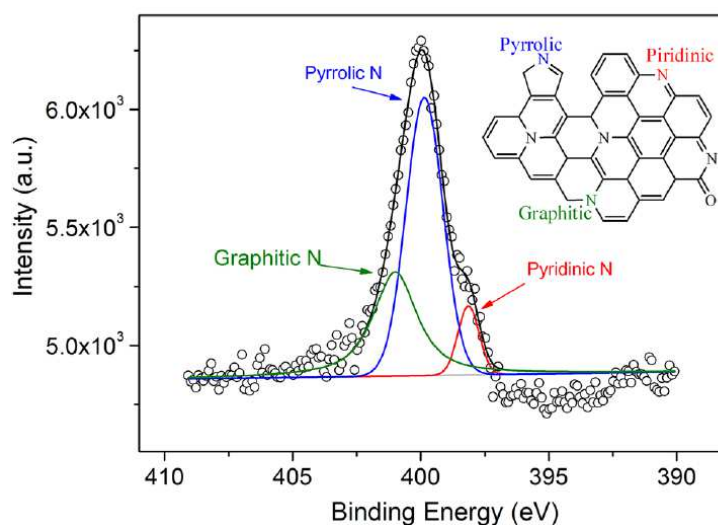
Figure 45 XPS high resolution nitrogen peak and, in the inset, different bonding configurations of nitrogen atoms

Focusing on the XPS technique, in Figure 46 a survey analysis is reported. It is able, like EDS, to identify the presence of nitrogen in the material, evaluating its atomic percentage.
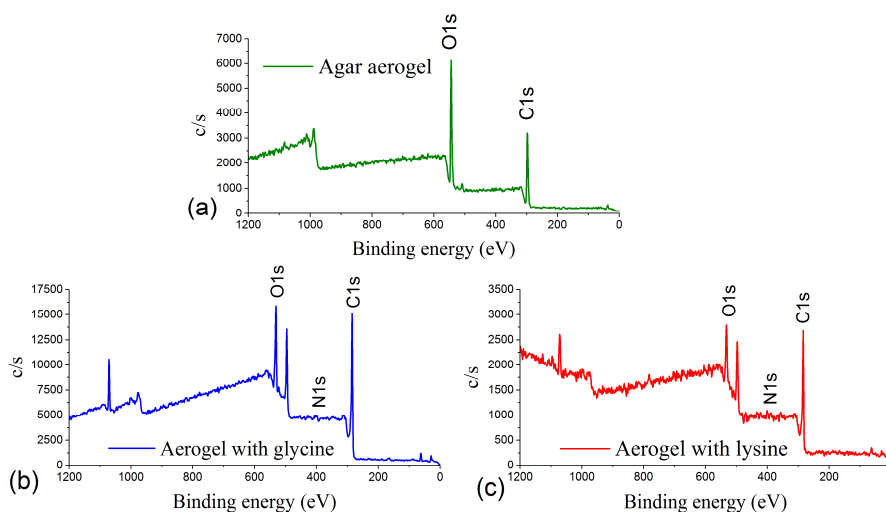
Figure 46 XPS survey analysis of carbon aerogels without addition of amino acid (a), containing glycine (b) and lysine (c)

Analyzing only on the nitrogen peak, located at around 400 eV as binding energy, XPS analysis has the possibility to perform a high resolution scan around that value,

in order to deeply understand the nature of nitrogen site, by fitting the obtained spectra.
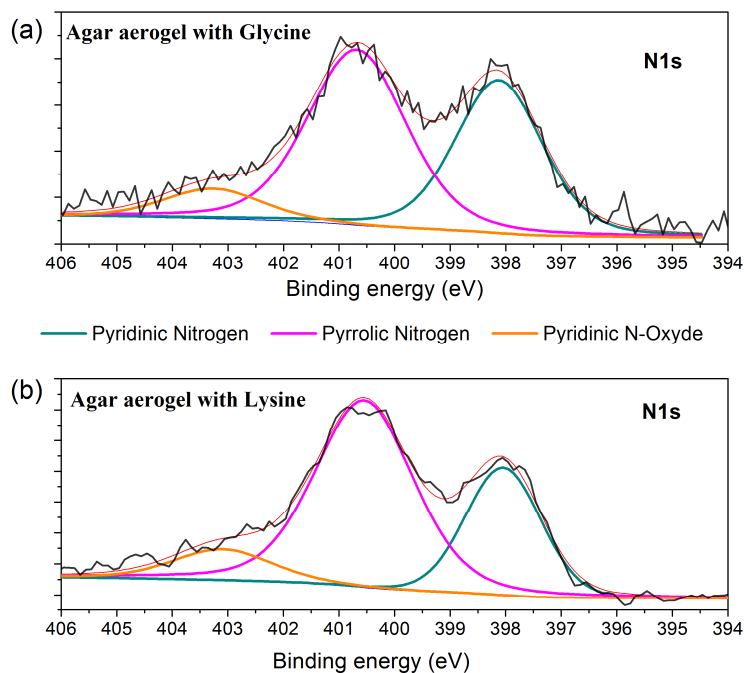
Figure 47 High Resolution XPS spectrum of Nitrogen peak of Aerogel with Glycine (a) and Lysine (b)

According to literature, the three types of nitrogen, described above, can be found thanks to a deconvolution of the Nitrogen peak into its sub-peaks: the pyridinic nitrogen located at 398.6 ± 0.3 eV, the pyrrolic one located at 400.5 ± 0.3 eV and the graphitic site corresponding to a binding energy of 401.3 ± 0.23 eV [114]. The graphitic nitrogen is a ORR site due to its reduced adsorption energy [112], but the active sites during the reduction reaction are the pyridinic and pyrrolic ones.

Atomic percentages of the pyridinic and pyrrolic nitrogen present in both the sample, are reported in Table 10.

Table 10 Percentage of different types on Nitrogen present in aerogels with amino acids

	Pyridinic Nitrogen	Pyrrolic Nitrogen	Other
Glycine	43.3 %	48.5 %	8.2 %
Lysine	32%	55.5 %	12.5%

As it is possible to see from the graph in Figure 47 and quantitatively appreciate in the above table, glycine based aerogel presents a higher value of pyridinic nitrogen, while aerogel containing lysine contains a higher value of pyrrolic nitrogen. To verify that nitrogen contained in carbon aerogels is really active for the catalysis of the ORR, some specific measurements on catalytic properties must be performed.

Catalytic performances of the nitrogen doped aerogels can be quantitatively evaluated using a rotating ring disk electrode (RRDE) analysis.
During this analysis, a paste containing carbon nitrogen doped aerogels (prepared following the procedure reported in [115]) was stimulated at different voltages, to understand the ability to produce electrons useful for the reduction of the oxygen. As introduced in Chapter 2, at the cathode of an air-cathode MFC the reduction of oxygen to water is needed: to do this, a 4 electrons reaction pathway has to be followed to prevent the formation of the hydrogen peroxide, toxic for microorganisms. Platinum, that is the best catalytic material, is able to give 3.9 electrons.

In Figure 48 catalytic activity of nitrogen doped aerogels is reported, compared with ones of platinum.

As explained in paragraph 5.4.3, during the RRDE analysis, applying a voltage scan, the current both of the disk (Figure 48-A) and of the ring (Figure 48-B) is measured; in particular, the current representing the catalytic activity following the four electrons mechanism is the one generated on the disk (Eqn. (**7**)). The current of the ring, in fact, is the one associated to the production of hydrogen peroxide. Higher is the ring current, lower are the catalytic performances of the material, because it means that the tested material is not able to produce all the four electrons needed for the complete reduction of oxygen.

Results
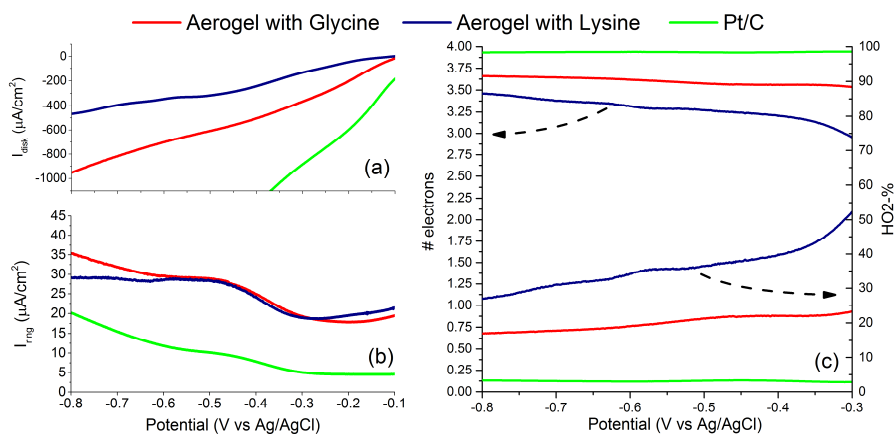
Figure 48 RRDE electrochemical results on nitrogen-doped carbon aerogels compared with Platinum on Carbon. Disk current corresponding to the four electrons mechanism (a), Ring current corresponding to the two electrons process (b) and number of electrons generated with the percentage of H_2O_2 produced (c)

Combining these two current contributions, using the Eqn. (31), the effective number of electrons that the material is able to give is extracted, together with the amount of hydrogen peroxide percentage produced by the two electrons process: results are reported in Figure 48-C.

It is possible to observe that for both the carbon aerogels obtained from the two amino acids, the ring current is more than one order of magnitude lower (as absolute value) with respect to the disk one: it means that during the operation of materials, the preferred mechanism occurring, is the one involving four electrons. This is also confirmed by the graph representing the number of electrons gave for the ORR (Figure 48-C). In comparison with commercial platinum on carbon, represented by the green curve in the graph, both the two aerogels are able to give an important number of electrons, even if a little less than the platinum-based one; they are able to favor the oxygen to water reaction, leaving a very small amount of H_2O_2 in the electrolyte. The number of supplied electrons, measured for potentials lower than -0.4V, is between 3.5 and 3.6 for glycine based aerogel, and between 3.2 and 3.5 for the lysine based one.

Catalytic properties of the materials were, then, tested directly in an open-air SC-MFC.

The performances of the resulting MFC was compared with that of a cell having a Pt on carbon-based cathode, and the current density trend is reported in Figure 49.
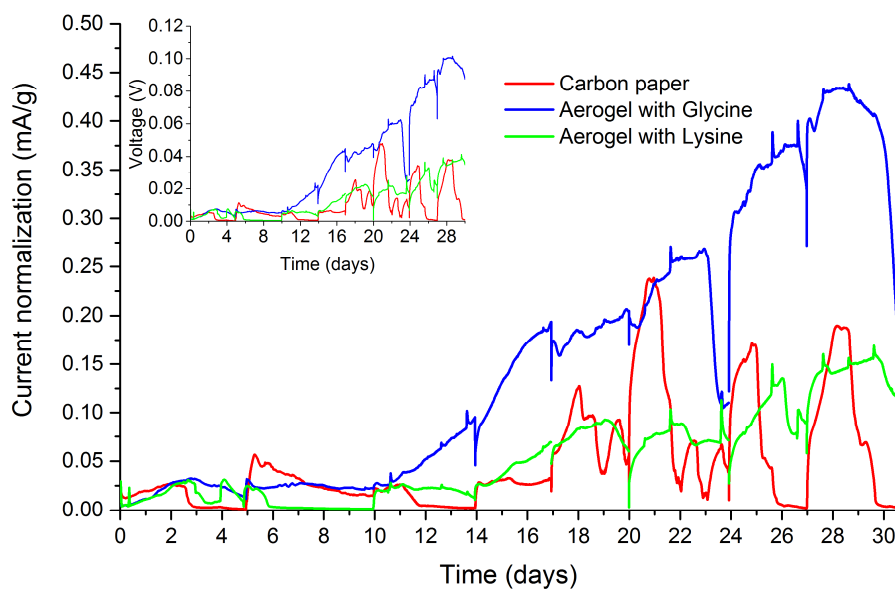
Figure 49 MFC performance of carbon aerogels doped with Glycine (blue curve) or Lysine (black curve) and compared with commercial materials with Platinum as catalyst

As it is possible to notice from the graph, cells containing the carbon aerogels doped by glycine present higher performance with respect to the commercial materials based on platinum. The one containing lysine, instead, presents lower performance, confirming the analysis performed on XPS. The glycine aerogel, in fact, presents a higher amount of pyridinic nitrogen, more active in oxygen reduction reaction, with respect to the lysine one [116], [117].

Generally, both the N-doped carbon based aerogels present good catalytic activities, as already demonstrated during measurements directly on the material itself. The main advantage of aerogels with respect to commercial materials, as support for catalyst, is the higher surface area and the good conductivity of the material itself, leading a higher number of active sites for the catalysis.

5.3 Manganese based aerogels for catalysis of Oxygen Reduction Reaction

Apart from nitrogen doped carbon based materials, a wide class of platinum alternative catalysts are present [112], [118]. Recently, two main classes of materials as ORR catalyst were investigated: the metal-free materials or non-precious metal compounds and the oxide based materials [119]. Among all the oxide based materials, manganese oxides are a promising choice, due to their low cost, high abundance, low environmental impact and good catalytic activity. Following this aim, aerogels based on manganese oxide were prepared [120]. As for nitrogen doped aerogels, described in Paragraph 5.2.2, also oxide based aerogels were synthetized starting from agar.

The material was synthetized using the already described sol-gel technique, adding to the polysaccharide precursor, manganese(II) acetate ($Mn(CH_3COO)_2 \cdot 4H_2O$) as the Mn source. Two different concentrations of precursor were tested: 0.05M (Mn1 sample) and 0.1M (Mn2 sample).

The obtained gel was dried with a freeze-drying procedure and then calcinated in air at 600 °C for 6h with a heating rate of 2.5 °C/min with the aim to transform the manganese acetate into manganese oxide, burning agar.

To characterize morphologically the material, SEM analysis coupled with a X-ray diffraction (XRD) were used.
Also in this case, the calcination step was optimized based on the thermogravimetric analysis (TGA), reported in Figure 34.

To consider the material an aerogel, an evaluation of the specific surface area (SSA) together with a quantitative analysis of the shrinkage of the sample must be performed. SSA was calculated using the BET method, in the 0.1-0.3 p/p$_0$ range. In this case the surface area is about 40 m^2/g, that is a little bit lower with respect to typical aerogels; considering, instead, the shrinkage during the calcination step, that was not so effective (around 15%), it can be consider effectively an aerogel.

From the SEM analysis (Figure 50), a big difference in morphology is present before and after the oxidation step: in the pre-pyrolysis sample, agar morphology is the predominant one, while after the thermal treatment, a grain structure with two grain sizes, is prevalent.
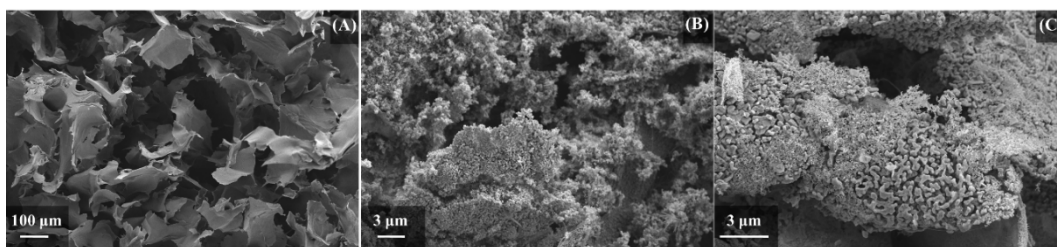
Figure 50 SEM images of aerogel containing manganese acetate before thermal step (A), and after with concentration Mn1 (B) and Mn2 (C)

The presence of grains with different sizes and shapes, suggests the co-existence of different types of oxide: hypothesis confirmed by X-Ray Diffraction (XRD) analysis.

In the Mn1 sample, the presence of peaks at 28.9°, 32.5° and 36.1° and 32.9°, 38.3° and 55.2° (2θ) confirms the presence of Mn_3O_4 and Mn_2O_3 phases, with a proportion of 1:4 ($Mn_3O_4 : Mn_2O_3$). These results, together with SEM analysis, permit to say that bigger grains with a dendritic shape are associated to Mn_2O_3; nanosized ones, instead, correspond to Mn_3O_4.

In the sample Mn2, the one with higher amount of manganese precursor, a different proportion between the two phases is present: in this case a ratio of 1:1 ($Mn_3O_4 : Mn_2O_3$) is present.
The difference is explained, considering the higher quantity of manganese acetate in the material, and the same calcination time for both the materials: not all the Mn_3O_4 present has had the time to convert in Mn_2O_3.

From the RRDE technique, it is possible to calculate the number of electron supplied during the ORR, applying Eqn. (31). Results are presented in Figure 51.

Results
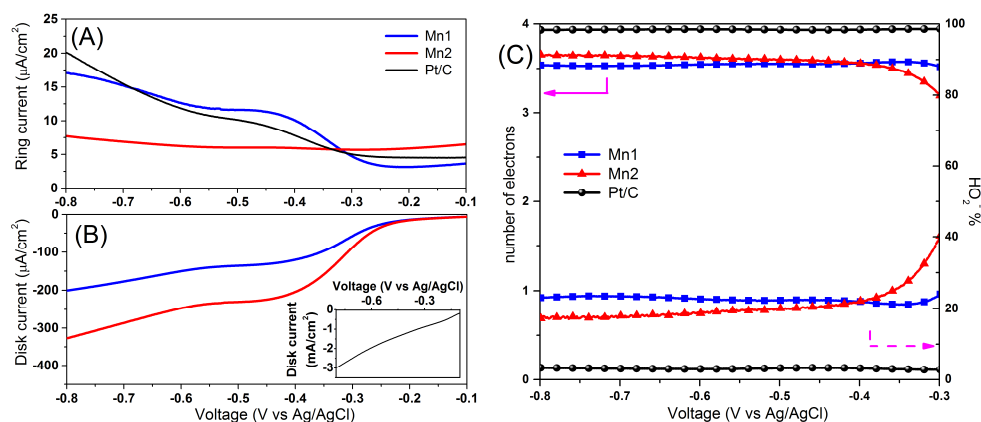
Figure 51 RRDE electrochemical analysis: Ring current (A) and Disk current (B) obtained from Mn oxide based aerogels compared with Pt/C reference. (C) Comparison of number of supplied electrons and amount of peroxide left during the ORR during the RRDE analysis

From Figure 51, it is possible to see that the number of electrons for both the two aerogels is comprised between 3.5 and 3.7, measured for potentials lower than -0.4V. For these values of potential, the corresponding amount of hydrogen peroxide left in the solution is lower than 25%, in line with other metal-free and low costs catalyst material proposed in literature [120]. These results are confirmed by a good disk current for both the materials, together with a low ring current.

The last analysis performed on the material to fully characterize it, is the EIS analysis. The main result, the Nyquist plot, is reported in Figure 52.
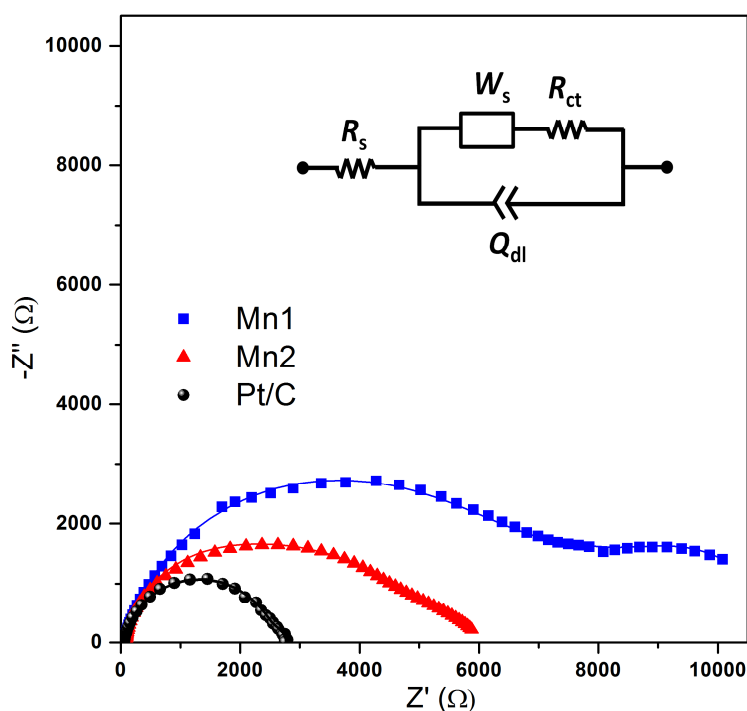
Figure 52 Nyquist plot of oxide based aerogels compared with Pt/C reference. in the inset, the equivalent circuit used to model the curve is reported

The Nyquist plot presents a typical high-frequency peak together with a low-frequency semicircle.

Observing qualitatively the graph, Mn1 sample presents a higher value of impedance with respect to Mn2. To better understand this difference, curves were fitted with the equivalent Randles' circuit [121] reported in the inset. With this fit, the series resistance R_S, correspondent to electrolyte conductivity, the charge transfer resistance R_{CT}, correspondent to electron transfer at the solid/liquid interface, the double layer capacitance Q_{dl} exploiting the charge accumulation at the same previous interface and the Warburg phase constant element W_S, modelling the diffusion of charges were evaluated.

As expected, Mn1 sample presented a higher value of R_{CT} (9850 Ω) with respect to Mn2 material (6082 Ω). Series resistance and double layer capacitance, instead, assumed comparable values (55 Ω and 11-13 μF, respectively): this is the explanation for a lower disk current value connected to a lower number of exchanged electrons.

Differently from nitrogen doped aerogels, oxide based ones were not tested in SC-MFC, but only a morphological and electrochemical study on the material was performed. Results showed that also oxide based aerogels are good competitors for platinum catalyst for ORR.

5.4 Materials and methods: Electrochemical characterization techniques

5.4.1 Power analysis

The most common techniques to evaluate power performances of a MFC are the *Polarization* and *Power density curves*.

Because of the Microbial Fuel Cell is a bio-electrochemical generator, it is important to maximize the power output obtaining so the highest current density at maximum potential. To do this, a polarization curve is used: it shows the current behavior of the generator as a function of the applied voltage, obtained by changing the external resistance applied to the system. The curve is so obtained as a sum of several point, each obtained with a different load applied; the current is than calculated with the first Ohm's law and the current density is reported on the independent variable axes. An example of polarization curve is reported in Figure 53.

$$I = \frac{E}{R_{ext}} \quad \Rightarrow \quad P = \frac{E^2}{R_{ext}} \tag{27}$$
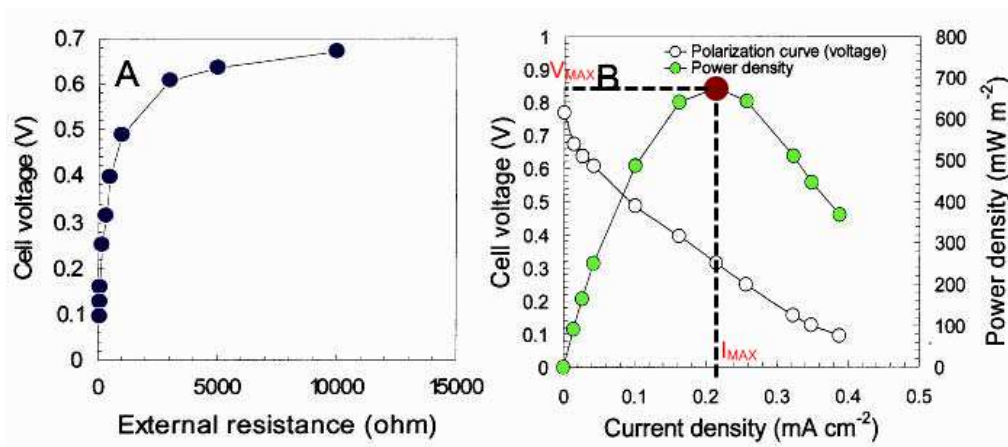
Figure 53 Polarization curve (A) and power density curve (B) in which the MPP is reported [27]

This characterization technique is useful to define the maximum power point of a MFC (MPP), appreciable in Figure 53-B. It is the maximum power that the device can produce during its operation: it occurs at a certain voltage E_{MAX} with a correspondent current I_{MAX}.

5.4.2 Electrochemical Impedance Spectroscopy (EIS)

As introduced before, the internal resistance of a MFC (R_{INT}) is the sum of all internal resistance losses, that affect the overall performance of the cell. Considering this contribution, the final voltage generated is:

$$E_{mfc} = OCV - IR_{int} \tag{28}$$

There are different methods usable to investigate the internal resistance of the reactor, but the most accurate one is the *electrochemical impedance spectroscopy (EIS)* analysis.

The *Electrochemical Impedance Spectroscopy (EIS)* is based on a superimposed sinusoidal signal with a small amplitude on the applied potential of the working electrode. The measurement consists into varying the frequency of the sinusoidal signal in a defined range: typically, from 10^6 to 10^{-2}; generally, to evaluate MFC internal parameters, a EIS measurement is conducted in Open Circuit Potential.

The main result obtaining from EIS is the Nyquist plot, reported in Figure 54, in which the opposite of the imaginary part of the impedance $(-Z_{imm})$ is plotted as a function of the real part (Z_{real}).
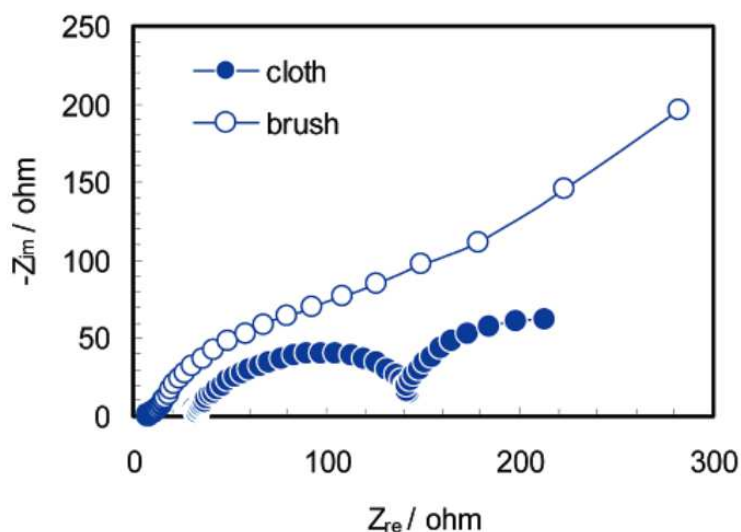
Figure 54 Nyquist plot of a typical 2C-MFC. Adapted from [122]

From this plot, three different information about the internal properties of the device can be extracted: the Ohmic resistance, that is defined as the interception between the first semi-arc of the graph and the x-axes; the charge transfer resistance represented by the length of the second semi-arc on the independent variable axis and the interface resistance between the electrolyte solution and the catalyst layer present on the cathode represented by the third semi-arc at lower frequencies; sometimes this arc is not complete and the result on the graph is a straight line.

These three parameters must be extracted from the Nyquist plot, by introducing an equivalent circuit modelling a MFC, and reported in Figure 55. Each block, constituted by a parallel between a resistance and a phase constant element, corresponds to a semi-arc in the graph and so to an interface of the device, while the Warburg contribution is the diffusion of charges in the electrolyte.
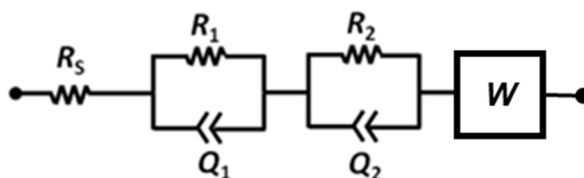
Figure 55 Equivalent circuit used to model the MFC in EIS analysis

5.4.3 RRDE technique

To study and understand catalytic activity of a material, Rotating Ring-Disk Electrode (RRDE) technique is the most powerful tool to detect, also, the intermediate such as hydrogen peroxide produced during the oxygen reduction reaction.

The RRDE setup consists of two electrodes: the disk electrode, surrounded by the ring electrode divided by an insulating ring. Both the electrodes, during the measurement, rotate at the same rate.

Using an electrochemical workstation (CH instrument 760D) and a RRDE apparatus (ALS RRDE-3A), currents at the two electrodes are collected. The catalyst material to be tested is transformed into powder and, using Nafion, water and isopropanol a paste is produced. It is deposited on the disk surface forming a uniform film and leaved for evaporation. Examples of RRDE working electrodes of different materials are reported in Figure 56.
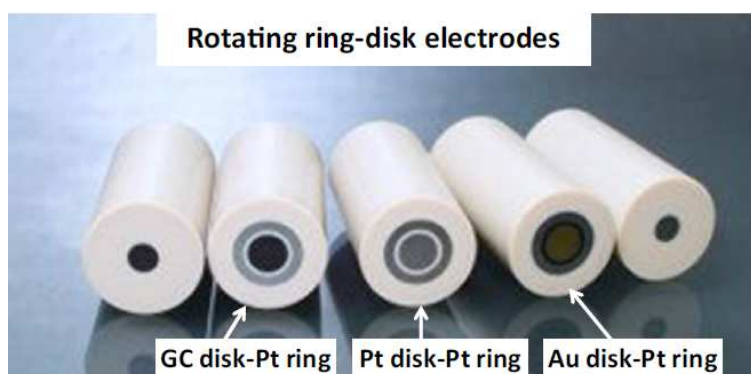
Figure 56 Commercially available RRDE working electrodes (GC represents the glassy carbon) [123]

The counter electrode is made of platinum and the reference electrode is Ag/AgCl one. All the electrodes are immersed into an electrolyte consisting of a 0.1 M KOH O_2 saturated aqueous solution.

The working electrode is scanned from 0.2 V to -0.8 V with a rate of 5 mV/s and different rotating speed, while the ring electrode is maintained at a fixed potential equal to 0.2 V

Results coming from this technique are governed by the Koutecky-Levich Equation (Eqn. (29)), expressing the current flowing through the disk electrode [115].

$$\frac{1}{J} = \frac{1}{J_k} + \frac{1}{J_{lev}} = \frac{1}{0.62nFD_{O_2}^{\frac{2}{3}} C_{O_2} v^{-\frac{1}{6}} \omega^{\frac{1}{2}}} + \frac{1}{J_{lev}} \tag{29}$$

where J is the measured current density, J_K is the kinetic current density, F is the Faraday constant, C_{O_2} is the oxygen bulk concentration, D_{O_2} is the oxygen diffusion coefficient, v is the kinematic viscosity of the electrolyte, and ω is the electrode rotation speed and n is the number of electrons transferred.

To calculate the number of electrons transferred and the amount of hydrogen peroxide produced, two equations must be applied:

$$HO_2^-\% = 200 \cdot \frac{\frac{I_D}{N}}{I_D + \frac{I_R}{N}} \tag{30}$$

$$n = 4 \cdot \frac{I_D}{I_D + \frac{I_R}{N}} \tag{31}$$

where I_D and I_R are the disk and the ring current, respectively, and N is the current collection efficiency of the Pt ring.

Chapter 6
Conclusions

The increasing number of inhabitants on the earth and a continuous economic development require a consistent amount of energy to satisfy human needs. Among all the produced energy in the world, fossil fuels remain the main resource exploited for this scope. This energy source has two main disadvantages: it is a non-infinite resource, and its processing leads to an increase in the amount of CO_2 in the atmosphere causing the greenhouse effect and a global increase of the temperature. Renewable energy sources are the emerging technology, able to produce energy in a green way. This topic, to be competitive with other possibilities on the market, still requires research. Renewable energy sources are based on sunlight, wind, flowing water and other resources already under investigation. A technology that uses one of these resources is represented by Fuel Cells, and in particular from Microbial Fuel Cell.

During my PhD work, the aim was the deep investigation of how a Microbial Fuel Cell really operates, using these results to optimize and improve the device.

A Microbial Fuel Cell is a bio-electrochemical reactor that, using exoelectrogens microorganisms, is able to convert chemical energy contained in the organic substrate into electrical energy. These microorganisms, in fact, can produce electrons that can be released outside the cell. Generated electrons are collected from the anode and then flow, through an external load to the cathode, where recombine with protons coming from the electrolyte, in order to close the circuit.

Different configurations and architecture were investigated in literature, from their birth to the present: MFCs can, in a general way, be classified in double chamber MFC and single chamber MFC.

Conclusions

While the setup with two separated compartment was deeply studies, the single chamber one is relatively new as technology.

Being an electrochemical cell, it is made by an anode and a cathode, physically separated by a membrane, if the double chamber setup is used, or sharing the same electrolyte solution if a single chamber MFC is chosen.

The single chamber assembly, having the cathode directly exposed to the air, exploits the possibility to use the oxygen naturally present in the atmosphere that, independently, diffuse through the electrode from the outside to the reactor chamber, as final electron acceptor. To allow this process, a diffusion layer on the air side is necessary, and it is realized with a polytetrafluoroethylene (PTFE) layer. This layer has two main functions: on one side, it must allow the oxygen flow from the air to the cell in a controlled way; on the other, it must guarantee the impermeability, not allowing the liquid electrolyte contained in the cell to go out.

Focusing the attention only on the single chamber MFC configuration, and, in particular, on architectural aspect, a modelling study to understand what happen, from a fluid-dynamic point of view, inside the cell during operation was performed. It was based on the application of equations from fluid-dynamics in order to study both the particle trajectories (using Navier-Stokes equations) and diffusion of substrate inside the reactor (using Fick's laws).

Three different architectures were analyzed, starting from the circular shape one, already used in the research group. The first upgrade, in geometry, consists into a square shaped reactor with an asymmetry between the inlet and the outlet, to increase the amount of exchanged area by the fluid movement.
Starting from particle trajectory inside the square-cell, an improved prototype with a new geometry was studied, in order to accommodate the flux distribution: the proposed geometry is a drop-shape one, that allows a significant increase of the percentage of exchanged area. Concerning the diffusion, instead, a study of the real concentration value present in the cell, evaluated in five different points was performed. Analyzing results, two different regimes can be underlined: the first, in which the contribution of the particle movement is dominant, leaving the diffusion as a secondary effect, and the other one, in which the diffusion of the nutrients inside the reactor is the most important one. These results lead to the use of the device for different applications, depending on the mechanism that should prevail over the other.

Conclusions

Improvements in architecture of MFC is not the only possibility to increase performances; also materials used as electrode play a fundamental role in operation efficiency of the device.

To be used as efficient electrode in a bio-electrochemical cell, a material must satisfy some important condition: biocompatibility, good electrically conductivity, resistance to electrolytic solutions and high surface area together with high porosity to allow the formation of the biofilm.

Carbon based aerogels can satisfy all these characteristics. Aerogel is a porous, ultralight material derived from a gel in which the liquid component has been substituted by air. In my work, aerogels derived from marine polysaccharides, starch and agar in particular, were studied and optimized to be used both as anode, both as cathode.

They were synthetized through a sol-gel technique, followed by a drying process, in order to remove the liquid component from the gel, and obtain an organic aerogel. To pass from organic aerogel to carbon aerogel, a thermal treatment at high temperature under inert gas flow was necessary.

Synthetized materials were analyzed both structurally and morphologically in order to understand if porosity, surface area and chemical composition were appropriate. In order to enhance some of these properties, a post synthesis treatment was performed: the surface of the aerogel was treated with a KOH solution to enlarge pores and increase the porosity of the overall material. The optimized aerogel was tested, as anode, into the square shape MFC and compared with commercial carbon material having the same function. Due to their high surface area, high porosity and good interaction with microorganisms, aerogels presented better performances of commercial materials if used as anode in MFC.

Starting form this material, the addition of amino acids as nitrogen source, allowed the use of carbon based aerogels also as cathode. Nitrogen is necessary in the cathode, because the single chamber MFC has the advantage of use directly the oxygen present in the air as final electron acceptor, leading the Oxygen Reduction Reaction (ORR). The drawback is that, ORR is a two-step reaction, in which the oxygen can be reduced to hydrogen peroxide, or, with a higher energy reaction, directly to water. In order to avoid the H_2O_2 production, that is toxic for

microorganisms, a catalyst material (typically platinum) is needed to guarantee the 4 electrons needed for the reduction of Oxygen to water.

Electrochemical characterizations performed on aerogels, confirm that carbon based materials with the addition of amino acids as carbon source, are good competitors of platinum for the catalysis of the ORR occurring at the cathode. As in the previous case, also these aerogels were tested in the squared MFC; the experiment showed comparable results between nitrogen-doped aerogels and platinum. Between the two amino acids tested, glycine presented better performances due to the nature of nitrogen contained within.

An alternative, both to platinum, both to nitrogen doped carbon materials, are the metal oxide aerogels. In this work, in particular, aerogels based on Mn_xO_y were tested. The synthesis of this material is similar to the previous one, with the difference of the addition of the manganese oxide precursor directly between initial precursors. The dried sample, were then thermally treated with a different process with respect to the carbon based ones: in this case the atmosphere was not inert, but oxygen is needed to activate the oxide precursor. Thanks to the thermal process, the organic part of the material is, in this case, burned, leaving an oxide structure that is active from a catalytic point of view. After the morphological, structural and chemical analysis of the sample, the catalytic activity of the material was tested, as in the previous case, using the Rotating Ring Disk Electrode (RRDE) technique, in order to investigate its catalytic properties. The metal oxide aerogel was not already tested in MFC device, but electrochemical characterizations presented good catalytic properties, that are comparable with the one of platinum.

All the obtained results demonstrate that the optimization of a MFC device is possible focusing the attention on different aspect of the device: on one side, the optimization of the architecture in terms of shape, dimensions and configurations; on the other side, the improvement of performances can be reached through an optimization of materials that are used as electrodes, both as anode both as cathode.

Chapter 7
References

[1]   European Commission Climate Action, "The roadmap for transforming the EU into a competitive, low-carbon economy by 2050."

[2]   J. Diefenderfer, M. assumptions Vipin Arora, and L. E. Singer, "International Energy Outlook 2016 Liquid fuels," vol. 484, no. May, pp. 202–586, 2016.

[3]   Enerdata, "Global Energy Statistical Yearbook 2016," *Enerdata Intelligence+Consulting, "https://yearbook.enerdata.net/world-electricity-production-map-graph-and-data.html*. 2016.

[4]   "U.S. Energy Information Administration, International Energy Outlook, November 2016, http://www.eia.gov." .

[5]   M. K. Nazeeruddin, E. Baranoff, and M. Grätzel, "Dye-sensitized solar cells: A brief overview," *Sol. Energy*, vol. 85, no. 6, pp. 1172–1178, 2011.

[6]   A. Sacco, A. Lamberti, M. Gerosa, C. Bisio, G. Gatti, F. Carniato, N. Shahzad, A. Chiodoni, E. Tresso, and L. Marchese, "Toward quasi-solid state Dye-sensitized Solar Cells: Effect of γ-Al2O3 nanoparticle dispersion into liquid electrolyte," *Sol. Energy*, vol. 111, pp. 125–134, Jan. 2015.

[7]   M. Gerosa, A. Sacco, A. Scalia, F. Bella, A. Chiodoni, M. Quaglio, E. Tresso, and S. Bianco, "Toward Totally Flexible Dye-Sensitized Solar Cells Based on Titanium Grids and Polymeric Electrolyte," *IEEE J. Photovoltaics*, vol. 6, no. 2, pp. 498–505, Mar. 2016.

[8]   A. Sacco, M. Gerosa, S. Bianco, L. Mercatelli, R. Fontana, L. Pezzati, M. Quaglio, C. F. Pirri, and A. O. M. Tucci, "Dye-sensitized solar cell for a solar concentrator system," *Sol. Energy*, vol. 125, pp. 307–313, 2016.

[9]   M. Grätzel, "Dye-sensitized solar cells," *J. Photochem. Photobiol. C*

Photochem. Rev., vol. 4, no. 2, pp. 145–153, 2003.

[10] M. C. Potter, "Electrical Effects Accompanying the Decomposition of Organic Compounds," *Proc. R. Soc. London*, vol. 84, no. 571, pp. 260–276, 1911.

[11] B. E. Logan, B. Hamelers, R. Rozendal, U. Schröder, J. Keller, S. Freguia, P. Aelterman, W. Verstraete, and K. Rabaey, "Microbial fuel cells: Methodology and technology," *Environ. Sci. Technol.*, vol. 40, no. 17, pp. 5181–5192, 2006.

[12] K. Rabaey, G. Lissens, and W. Verstraete, "Microbial fuel cells: performances and perspectives," *Biofuels fuel cells Renew. energy from biomass Ferment.*, pp. 377–399, 2005.

[13] K. Rabaey, W. Ossieur, M. Verhaege, and W. Verstraete, "Continuous microbial fuel cells convert carbohydrates to electricity," *Water Sci. Technol.*, vol. 52, no. 1–2, pp. 515–523, 2005.

[14] F. Davis and S. P. J. Higson, "Biofuel cells—Recent advances and applications," *Biosens. Bioelectron.*, vol. 22, no. 7, pp. 1224–1235, 2007.

[15] Z. Du, H. Li, and T. Gu, "A state of the art review on microbial fuel cells: A promising technology for wastewater treatment and bioenergy," *Biotechnol. Adv.*, vol. 25, no. 5, pp. 464–482, 2007.

[16] I. A. Ieropoulos, J. Greenman, C. Melhuish, and J. Hart, "Comparative study of three types of microbial fuel cell," *Enzyme Microb. Technol.*, vol. 37, no. 2, pp. 238–245, 2005.

[17] S. K. Chaudhuri and D. R. Lovley, "Electricity generation by direct oxidation of glucose in mediatorless microbial fuel cells," *Nat. Biotechnol.*, vol. 21, no. 10, pp. 1229–1232, Oct. 2003.

[18] A. Engdahl and B. Nelander, "The Vibrational Spectrum of Electrode-Reducing Microorganisms That Harvest Energy from Marine Sediments," *Science (80-.).*, vol. 295, no. January, pp. 482–483, 2002.

[19] M. Di Lorenzo, A. R. Thomson, K. Schneider, P. J. Cameron, and I. Ieropoulos, "A small-scale air-cathode microbial fuel cell for on-line monitoring of water quality," *Biosens. Bioelectron.*, vol. 62, pp. 182–188, 2014.

[20] S. Sevda, X. Dominguez-Benetton, K. Vanbroekhoven, H. De Wever, T. R.

Sreekrishnan, and D. Pant, "High strength wastewater treatment accompanied by power generation using air cathode microbial fuel cell," *Appl. Energy*, vol. 105, pp. 194–206, 2013.

[21] K.-Y. Kim, W. Yang, and B. E. Logan, "Impact of electrode configurations on retention time and domestic wastewater treatment efficiency using microbial fuel cells," *Water Res.*, vol. 80, pp. 41–46, 2015.

[22] C. Xia, M. Xu, J. Liu, J. Guo, and Y. Yang, "Sediment microbial fuel cell prefers to degrade organic chemicals with higher polarity," 2015.

[23] N. Habibul, Y. Hu, and G.-P. Sheng, "Microbial fuel cell driving electrokinetic remediation of toxic metal contaminated soils," *J. Hazard. Mater.*, vol. 318, pp. 9–14, 2016.

[24] B. Zhang and Z. He, "Improving water desalination by hydraulically coupling an osmotic microbial fuel cell with a microbial desalination cell," *J. Memb. Sci.*, vol. 441, pp. 18–24, 2013.

[25] C. M. Werner, B. E. Logan, P. E. Saikaly, and G. L. Amy, "Wastewater treatment, energy recovery and desalination using a forward osmosis membrane in an air-cathode microbial osmotic fuel cell," *J. Memb. Sci.*, vol. 428, pp. 116–122, 2013.

[26] A. Kaur, J. R. Kim, I. Michie, R. M. Dinsdale, A. J. Guwy, and G. C. Premier, "Microbial fuel cell type biosensor for specific volatile fatty acids using acclimated bacterial communities," *Biosens. Bioelectron.*, vol. 47, pp. 50–55, 2013.

[27] B. E. Logan, *Microbial Fuel Cells*. Hoboken, NJ, USA: John Wiley & Sons, Inc., 2007.

[28] B. Xiao, F. Yang, and J. Liu, "Enhancing simultaneous electricity production and reduction of sewage sludge in two-chamber MFC by aerobic sludge digestion and sludge pretreatments," *J. Hazard. Mater.*, vol. 189, no. 1–2, pp. 444–449, 2011.

[29] S. Hays, F. Zhang, and B. E. Logan, "Performance of two different types of anodes in membrane electrode assembly microbial fuel cells for power generation from domestic wastewater," *Journal of Power Sources*, 2011. .

[30] D. Pant, G. Van Bogaert, L. Diels, and K. Vanbroekhoven, "A review of the substrates used in microbial fuel cells (MFCs) for sustainable energy production," *Bioresour. Technol.*, vol. 101, no. 6, pp. 1533–1543, 2010.

References

[31] "standard hydrogen electrode," in *IUPAC Compendium of Chemical Terminology*, Research Triangle Park, NC: IUPAC.

[32] T. J. Gorby, YA and Beveridge, "Composition, Reactivity, and Regulation of Extracellular Metal-Reducing Structures (Nanowires) Produced by Dissimilatory Metal Reducing Bacteria," 2005.

[33] S. A. Patil, C. Hägerhäll, and L. Gorton, "Electron transfer mechanisms between microorganisms and electrodes in bioelectrochemical systems," *Bioanal. Rev.*, vol. 4, no. 2–4, pp. 159–192, Dec. 2012.

[34] J.-M. Monier, L. Niard, N. Haddour, B. Allard, and F. Buret, "Microbial Fuel Cells: From biomass (waste) to electricity," in *MELECON 2008 - The 14th IEEE Mediterranean Electrotechnical Conference*, 2008, pp. 663–668.

[35] H. Liu, S. Cheng, and B. E. Logan, "Production of electricity from acetate or butyrate using a single-chamber microbial fuel cell," *Environ. Sci. Technol.*, vol. 39, no. 2, pp. 658–662, Jan. 2005.

[36] S. Cheng, H. Liu, and B. E. Logan, "Increased performance of single-chamber microbial fuel cells using an improved cathode structure," *Electrochem. commun.*, vol. 8, no. 3, pp. 489–494, Mar. 2006.

[37] N. Bizon, "On tracking robustness in adaptive extremum seeking control of the fuel cell power plants," *Appl. Energy*, vol. 87, no. 10, pp. 3115–3130, 2010.

[38] L. M. Tender, S. A. Gray, E. Groveman, D. A. Lowy, P. Kauffman, J. Melhado, R. C. Tyce, D. Flynn, R. Petrecca, and J. Dobarro, "The first demonstration of a microbial fuel cell as a viable power supply: Powering a meteorological buoy," 2008.

[39] C. Donovan, A. Dewan, D. Heo, and H. Beyenal, "Batteryless, Wireless Sensor Powered by a Sediment Microbial Fuel Cell," *Environ. Sci. Technol.*, vol. 42, no. 22, pp. 8591–8596, Nov. 2008.

[40] I. Ieropoulos, C. Melhuish, J. Greenman, and I. Horsfield, "EcoBot-II: An artificial agent with a natural metabolism," *Int. J. Adv. Robot. Syst.*, vol. 2, no. 4, pp. 295–300, 2005.

[41] I. S. Chang, J. K. Jang, G. C. Gil, M. Kim, H. J. Kim, B. W. Cho, and B. H. Kim, "Continuous determination of biochemical oxygen demand using microbial fuel cell type biosensor," *Biosens. Bioelectron.*, vol. 19, no. 6, pp. 607–613, 2004.

[42] M. Di Lorenzo, T. P. Curtis, I. M. Head, and K. Scott, "A single-chamber microbial fuel cell as a biosensor for wastewaters," *Water Res.*, vol. 43, no. 13, pp. 3145–3154, 2009.

[43] B. H. Kim, I. S. Chang, G. Cheol Gil, H. S. Park, and H. J. Kim, "Novel BOD (biological oxygen demand) sensor using mediator-less microbial fuel cell," *Biotechnol. Lett.*, vol. 25, no. 7, pp. 541–545, 2003.

[44] M. Kim, M. Sik Hyun, G. M. Gadd, and H. Joo Kim, "A novel biomonitoring system using microbial fuel cells.," *J. Environ. Monit.*, vol. 9, no. 12, pp. 1323–1328, 2007.

[45] W. Habermann and E. H. Pommer, "Biological fuel cells with sulphide storage capacity," *Appl. Microbiol. Biotechnol.*, vol. 35, no. 1, pp. 128–133, Apr. 1991.

[46] M. Zhou, M. Chi, J. Luo, H. He, and T. Jin, "An overview of electrode materials in microbial fuel cells," *J. Power Sources*, vol. 196, no. 10, pp. 4427–4435, 2011.

[47] H. Liu, R. Ramnarayanan, and B. E. Logan, "Production of Electricity during Wastewater Treatment Using a Single Chamber Microbial Fuel Cell," *Environ. Sci. Technol.*, vol. 38, no. 7, pp. 2281–2285, Apr. 2004.

[48] Y. Ahn and B. E. Logan, "Effectiveness of domestic wastewater treatment using microbial fuel cells at ambient and mesophilic temperatures," *Bioresour. Technol.*, vol. 101, no. 2, pp. 469–475, 2010.

[49] F. J. Hernández-Fernández, A. Pérez de los Ríos, M. J. Salar-García, V. M. Ortiz-Martínez, L. J. Lozano-Blanco, C. Godínez, F. Tomás-Alonso, and J. Quesada-Medina, "Recent progress and perspectives in microbial fuel cells for bioenergy generation and wastewater treatment," *Fuel Process. Technol.*, vol. 138, pp. 284–297, Oct. 2015.

[50] J. R. Kim, S. H. Jung, J. M. Regan, and B. E. Logan, "Electricity generation and microbial community analysis of alcohol powered microbial fuel cells," *Bioresour. Technol.*, vol. 98, no. 13, pp. 2568–2577, 2007.

[51] X. Wang, Y. J. Feng, and H. Lee, "Electricity production from beer brewery wastewater using single chamber microbial fuel cell," *Water Sci. Technol.*, vol. 57, no. 7, pp. 1117–1121, 2008.

[52] S. Cheng, H. Liu, and B. E. Logan, "Power densities using different cathode catalysts (Pt and CoTMPP) and polymer binders (Nafion and PTFE) in single

chamber microbial fuel cells," *Environ. Sci. Technol.*, vol. 40, no. 1, pp. 364–369, Jan. 2006.

[53] M. Ghasemi, W. R. W. Daud, S. H. a. Hassan, S.-E. Oh, M. Ismail, M. Rahimnejad, and J. M. Jahim, "Nano-structured carbon as electrode material in microbial fuel cells: A comprehensive review," *J. Alloys Compd.*, vol. 580, pp. 245–255, Dec. 2013.

[54] T. Tommasi, A. Chiolerio, M. Crepaldi, and D. Demarchi, "A microbial fuel cell powering an all-digital piezoresistive wireless sensor system," *Microsyst. Technol.*, vol. 20, no. 4–5, pp. 1023–1033, Apr. 2014.

[55] M. Rahimnejad, A. A. Ghoreyshi, G. Najafpour, and T. Jafary, "Power generation from organic substrate in batch and continuous flow microbial fuel cell operations," *Appl. Energy*, vol. 88, no. 11, pp. 3999–4004, 2011.

[56] Z. Wang, T. Lee, B. Lim, C. Choi, and J. Park, "Microbial community structures differentiated in a single-chamber air-cathode microbial fuel cell fueled with rice straw hydrolysate.," *Biotechnol. Biofuels*, vol. 7, no. 1, p. 9, 2014.

[57] B. Rangarajan and C. T. Lira, "Interpretation of Aerogel Shrinkage During Drying.," *MRS Proc.*, vol. 271, p. 559, Jan. 1992.

[58] "Porosity," *IUPAC Compendium of Chemical Terminology*. [Online]. Available: http://goldbook.iupac.org/P04762.html.

[59] "micropore in catalysis," *IUPAC Compendium of Chemical Terminology*. [Online]. Available: http://goldbook.iupac.org/M03906.html.

[60] "mesopore in catalysis," *IUPAC Compendium of Chemical Terminology*. [Online]. Available: http://goldbook.iupac.org/M03853.html.

[61] "macropore in catalysis," *IUPAC Compendium of Chemical Terminology*. [Online]. Available: http://goldbook.iupac.org/M03672.html.

[62] S. S. Kistler, "Coherent Expanded Aerogels," *Rubber Chem. Technol.*, vol. 5, no. 4, pp. 600–603, May 1932.

[63] S. D. Bhagat and A. V. Rao, "Surface chemical modification of TEOS based silica aerogels synthesized by two step (acid–base) sol–gel process," *Appl. Surf. Sci.*, vol. 252, no. 12, pp. 4289–4297, 2006.

[64] R. E. Russo and A. J. Hunt, "Comparison of ethyl versus methyl sol-gels for

References

silica aerogels using polar nephelometry," *J. Non. Cryst. Solids*, vol. 86, no. 1, pp. 219–230, 1986.

[65] A. A. Pisal and A. V. Rao, "Comparative studies on the physical properties of TEOS, TMOS and Na2SiO3 based silica aerogels by ambient pressure drying method," *J. Porous Mater.*, vol. 23, no. 6, pp. 1547–1556, Dec. 2016.

[66] T. M. Tillotson and L. W. Hrubesh, "Transparent ultralow-density silica aerogels prepared by a two-step sol-gel process," *J. Non. Cryst. Solids*, vol. 145, pp. 44–50, Jan. 1992.

[67] R. W. Pekala, "Organic aerogels from the polycondensation of resorcinol with formaldehyde," *J. Mater. Sci.*, vol. 24, no. 9, pp. 3221–3227, Sep. 1989.

[68] D. M. Smith, R. Deshpande, and C. J. Brinker, "Preparation of low-density aerogels at ambient pressure," *Mater. Res. Soc. Symp. Proc.*, vol. 271, no. Better Ceramics through Chemistry V, pp. 567–572, Jan. 1992.

[69] J. L. Mohanan and S. L. Brock, "A new addition to the aerogel community: unsupported CdS aerogels with tunable optical properties," *J. Non. Cryst. Solids*, vol. 350, pp. 1–8, 2004.

[70] P. Lv, X.-W. Tan, K.-H. Yu, R.-L. Zheng, J.-J. Zheng, and W. Wei, "Super-elastic graphene/carbon nanotube aerogel: A novel thermal interface material with highly thermal transport properties," *Carbon N. Y.*, vol. 99, pp. 222–228, 2016.

[71] A. E. Gash, T. M. Tillotson, J. H. Satcher Jr, L. W. Hrubesh, and R. L. Simpson, "New sol–gel synthetic route to transition and main-group metal oxide aerogels using inorganic salt precursors," *J. Non. Cryst. Solids*, vol. 285, no. 1–3, pp. 22–28, Jun. 2001.

[72] N. Hüsing and U. Schubert, "Aerogels—airy materials: Chemistry, structure, and properties," *Angew. Chemie Int. Ed.*, vol. 37, no. 1/2, pp. 22–45, Feb. 1998.

[73] L. F. Su, L. Miao, S. Tanemura, and G. Xu, "Low-cost and fast synthesis of nanoporous silica cryogels for thermal insulation applications," *Sci. Technol. Adv. Mater.*, vol. 13, no. 3, p. 35003, Jun. 2012.

[74] L. Kocon, F. Despetis, and J. Phalippou, "Ultralow density silica aerogels by alcohol supercritical drying," *J. Non. Cryst. Solids*, vol. 225, pp. 96–100, 1998.

[75] B. E. Yoldas, M. J. Annen, and J. Bostaph, "Chemical engineering of aerogel morphology formed under nonsupercritical conditions for thermal insulation," *Chem. Mater.*, vol. 12, no. 8, pp. 2475–2484, 2000.

[76] M. A. Aegerter, N. Leventis, and M. M. Koebel, *Aerogels Handbook*. New York, NY: Springer New York, 2011.

[77] O. Barbieri, F. Ehrburger-Dolle, T. P. Rieker, G. M. Pajonk, N. Pinto, and A. Venkateswara Rao, "Small-angle X-ray scattering of a new series of organic aerogels," *J. Non. Cryst. Solids*, vol. 285, no. 1, pp. 109–115, 2001.

[78] R. Brandt, R. Petricevic, H. Pröbstle, and J. Fricke, "Acetic Acid Catalyzed Carbon Aerogels," *J. Porous Mater.*, vol. 10, no. 3, pp. 171–178, 2003.

[79] A. C. Pierre and G. M. Pajonk, "Chemistry of aerogels and their applications," *Chem. Rev.*, vol. 102, no. 11, pp. 4243–4265, 2002.

[80] B. M. Novak, D. Auerbach, and C. Verrier, "Low-Density, Mutually Interpenetrating Organic-Inorganic Composite Materials via Supercritical Drying Techniques," *Chem. Mater.*, vol. 6, no. 3, pp. 282–286, Mar. 1994.

[81] F. Schwertfeger, W. Glaubitt, and U. Schubert, "Hydrophobic aerogels from Si(OMe)4/MeSi(OMe)3 mixtures," *J. Non. Cryst. Solids*, vol. 145, no. C, pp. 85–89, 1992.

[82] F. Schwertfeger, N. Hüsing, and U. Schubert, "Influence of the nature of organic groups on the properties of organically modified silica aerogels," *J. Sol-Gel Sci. Technol.*, vol. 2, no. 1–3, pp. 103–108, 1994.

[83] E. J. A. Pope, M. Asami, and J. D. Mackenzi, "Transparent silica gel-PMMA composites," *J. Mater. Res.*, vol. 4, no. 4, pp. 1018–1026, Aug. 1989.

[84] G. Philipp and H. Schmidt, "New materials for contact lenses prepared from Si- and Ti-alkoxides by the sol-gel process," *J. Non. Cryst. Solids*, vol. 63, no. 1–2, pp. 283–292, 1984.

[85] J. Wen and G. L. Wilkes, "Organic/Inorganic Hybrid Network Materials by the Sol−Gel Approach," *Chem. Mater.*, vol. 8, no. 8, pp. 1667–1681, 1996.

[86] A. C. Pierre, *Introduction to Sol-Gel Processing*, vol. 1. Boston, MA: Springer US, 1998.

[87] C. A. García-González, M. Alnaief, and I. Smirnova, "Polysaccharide-based aerogels - Promising biodegradable carriers for drug delivery systems,"

Carbohydr. Polym., vol. 86, no. 4, pp. 1425–1438, 2011.

[88] L. W. Hrubesh, "Aerogel applications," *J. Non. Cryst. Solids*, vol. 225, no. 0, pp. 335–342, 1998.

[89] J. L. Kaschmitter, S. T. Mayer, and R. W. Pekala, "Process for producing carbon foams for energy storage devices," 1998.

[90] C. Lin and J. A. Ritter, "Carbonization and activation of sol-gel derived carbon xerogels," *Carbon N. Y.*, vol. 38, no. 6, pp. 849–861, 2000.

[91] "Aerogel Technologies, LLC." [Online]. Available: http://www.buyaerogel.com/product/rf-aerogel/.

[92] J. Wang and S. Kaskel, "KOH activation of carbon-based materials for energy storage," *J. Mater. Chem.*, vol. 22, no. 45, p. 23710, 2012.

[93] D. Lozano-Castelló, M. A. Lillo-Ródenas, D. Cazorla-Amorós, and A. Linares-Solano, "Preparation of activated carbons from Spanish anthracite: I. Activation by KOH," *Carbon N. Y.*, vol. 39, no. 5, pp. 741–749, 2001.

[94] L. Zubizarreta, A. Arenillas, J.-P. Pirard, J. J. Pis, and N. Job, "Tailoring the textural properties of activated carbon xerogels by chemical activation with KOH," *Microporous Mesoporous Mater.*, vol. 115, no. 3, pp. 480–490, 2008.

[95] P. B. Malafaya, G. A. Silva, and R. L. Reis, "Natural-origin polymers as carriers and scaffolds for biomolecules and cell delivery in tissue engineering applications," *Adv. Drug Deliv. Rev.*, vol. 59, no. 4–5, pp. 207–233, May 2007.

[96] K. S. Mikkonen, K. Parikka, A. Ghafar, and M. Tenkanen, "Prospects of polysaccharide aerogels as modern advanced food materials," *Trends Food Sci. Technol.*, vol. 34, no. 2, pp. 124–136, Dec. 2013.

[97] Y. Zeng, Y. F. Choo, B.-H. Kim, and P. Wu, "Modelling and simulation of two-chamber microbial fuel cell," *J. Power Sources*, vol. 195, no. April 2016, pp. 79–89, 2010.

[98] C. Picioreanu, M. C. M. van Loosdrecht, T. P. Curtis, and K. Scott, "Model based evaluation of the effect of pH and electrode geometry on microbial fuel cell performance," *Bioelectrochemistry*, vol. 78, no. 1, pp. 8–24, 2010.

[99] B. H. R. Merle C. Potter, David C. Wiggert, *Mechanics Of Fluids*. Cengage Learning, 2011.

References

[100] J. P. Holman, "Heat Transfer," p. 758, 2010.

[101] W. F. Robert, J. P. Philip, and A. T. McDonald, *Introduction to fluid mechanics*. Wiley India Pvt. Limited, 2009.

[102] J. F. Douglas, J. M. Gasiorek, and J. A. Swaffield, *Fluid Mechanics*. Cambridge: Cambridge University Press, 1995.

[103] D. R. Tobergte and S. Curtis, *Introduction to Climate Modelling*, vol. 53, no. 9. Berlin, Heidelberg: Springer Berlin Heidelberg, 2013.

[104] R. W. Holloway, R. Maltos, J. Vanneste, and T. Y. Cath, "Mixed draw solutions for improved forward osmosis performance," *J. Memb. Sci.*, vol. 491, pp. 121–131, 2015.

[105] M. Ruler and M. Ruler, "How to Make Cathodes with a Diffusion Layer for Single-Chamber Microbial Fuel Cells," *Glass*, no. Di, 2006.

[106] Z. K. Brown, P. J. Fryer, I. T. Norton, and R. H. Bridson, "Drying of agar gels using supercritical carbon dioxide," *J. Supercrit. Fluids*, vol. 54, no. 1, pp. 89–95, 2010.

[107] F. Tuinstra and J. L. Koenig, "Raman Spectrum of Graphite," *J. Chem. Phys.*, vol. 53, no. 3, p. 1126, 1970.

[108] Y. Wang, S. Serrano, and J. J. Santiago-Avilés, "Raman characterization of carbon nanofibers prepared using electrospinning," *Synth. Met.*, vol. 138, no. 3, pp. 423–427, 2003.

[109] M. Kaláb, A. Yang, and D. Chabot, "Conventional Scanning Electron Microscopy of Bacteria," *Infocus*, pp. 44–61, 2008.

[110] A. M. Kashi, K. Tahermanesh, S. Chaichian, and M. T. Joghataei, "How to Prepare Biological Samples and Live Tissues for Scanning Electron Microscopy (SEM)," vol. 3, no. 2, pp. 63–80, 2014.

[111] Z. He and F. Mansfeld, "Exploring the use of electrochemical impedance spectroscopy (EIS) in microbial fuel cell studies," *Energy Environ. Sci.*, vol. 2, no. 2, p. 215, 2009.

[112] Z. Yang, H. Nie, X. Chen, X. Chen, and S. Huang, "Recent progress in doped carbon nanomaterials as effective cathode catalysts for fuel cell oxygen reduction reaction," *J. Power Sources*, vol. 236, pp. 238–249, 2013.

[113] P. H. Matter, L. Zhang, and U. S. Ozkan, "The role of nanostructure in nitrogen-containing carbon catalysts for the oxygen reduction reaction," *J. Catal.*, vol. 239, no. 1, pp. 83–96, Apr. 2006.

[114] G. Liu, X. Li, P. Ganesan, and B. N. Popov, "Development of non-precious metal oxygen-reduction catalysts for PEM fuel cells based on N-doped ordered porous carbon," *Appl. Catal. B Environ.*, vol. 93, no. 1–2, pp. 156–165, 2009.

[115] N. Garino, A. Sacco, M. Castellino, J. A. Muñoz-Tabares, A. Chiodoni, V. Agostino, V. Margaria, M. Gerosa, G. Massaglia, and M. Quaglio, "Microwave-Assisted Synthesis of Reduced Graphene Oxide/SnO2 Nanocomposite for Oxygen Reduction Reaction in Microbial Fuel Cells," *ACS Appl. Mater. Interfaces*, vol. 8, no. 7, p. acsami.5b11198, Feb. 2016.

[116] D. S. Yang, S. Chaudhari, K. P. Rajesh, and J. S. Yu, "Preparation of nitrogen-doped porous carbon nanofibers and the effect of porosity, electrical conductivity, and nitrogen content on their oxygen reduction performance," *ChemCatChem*, vol. 6, no. 5, pp. 1236–1244, 2014.

[117] P. H. Matter, E. Wang, and U. S. Ozkan, "Preparation of nanostructured nitrogen-containing carbon catalysts for the oxygen reduction reaction from SiO2- and MgO-supported metal particles," *J. Catal.*, vol. 243, no. 2, pp. 395–403, 2006.

[118] H. A. Gasteiger, S. S. Kocha, B. Sompalli, and F. T. Wagner, "Activity benchmarks and requirements for Pt, Pt-alloy, and non-Pt oxygen reduction catalysts for PEMFCs," *Appl. Catal. B Environ.*, vol. 56, no. 1, pp. 9–35, 2005.

[119] Z.-Y. Zhou, N. Tian, J.-T. Li, I. Broadwell, and S.-G. Sun, "Nanomaterials of high surface energy with exceptional properties in catalysis and energy storage.," *Chem. Soc. Rev.*, vol. 40, no. 7, pp. 4167–4185, 2011.

[120] L. Delmondo, G. P. Salvador, J. A. Muñoz-Tabares, A. Sacco, N. Garino, M. Castellino, M. Gerosa, G. Massaglia, A. Chiodoni, and M. Quaglio, "Nanostructured MnxOy for oxygen reduction reaction (ORR) catalysts," *Appl. Surf. Sci.*, vol. 388, pp. 631–639, 2016.

[121] J. E. B. Randles, "Kinetics of rapid electrode reactions," *Discuss. Faraday Soc.*, vol. 48, no. 0, pp. 828–832, 1952.

[122] B. Logan, S. Cheng, V. Watson, and G. Estadt, "Graphite fiber brush anodes for increased power production in air-cathode microbial fuel cells," *Environ.*

Sci. Technol., vol. 41, no. 9, pp. 3341–3346, 2007.

[123] Z. Jia, G. Yin, and J. Zhang, *Rotating Ring-Disk Electrode Method.* Elsevier B.V., 2014.